Influence of a *Staphylococcus aureus* infection on human coronary artery endothelial cells regarding bacterial internalization, cellular migration and thrombogenicity

I n a u g u r a l d i s s e r t a t i o n

zur

Erlangung des akademischen Grades eines

Doktors der Naturwissenschaften (Dr. rer. nat.)

der

Mathematisch-Naturwissenschaftlichen Fakultät

der

Universität Greifswald

vorgelegt von

Lisa Maletzki

Greifswald, Februar 2022

Dean:	Prof. Dr. Gerald Kerth
First supervisor:	Prof. Dr. Katharina Riedel
Second supervisor:	Prof. Dr. Hubert Bahl
Date of defense:	08.11.2022

Dedicated to

my beloved family

Abstract

Staphylococcus aureus (*S. aureus*) endocarditis is still one of the most fatal heart diseases, with a mortality rate of 20-45%. In recent years, the importance of endothelial cells (ECs) in the context of endocarditis has become more evident. The vascular endothelium forms a selective barrier between blood and the adjacent tissue by maintaining an anti-inflammatory and anti-thrombogenic phenotype. However, in case of insertion of cardiac implants, an injury of the endothelium can occur which promotes platelet aggregation followed by *S. aureus* adherence to the platelets, especially in areas with low hemodynamic shear stress. This process is considered as a key event in the development of infective endocarditis (IE) and allows bacteria to colonize the heart valves. Despite extensive research, the pathogenesis of IE is still not completely understood. Therefore, further investigations are needed to enable an effective prevention of this life-threatening disease.

In order to study the infection process of *S. aureus*, internalization experiments with two different *S. aureus* strains, one control strain (HG001) and one strain isolated from an endocarditis patient (T-72949) were performed in human coronary artery endothelial cells (HCAEC). Subsequently, an extensive proteome analysis of the host cells was carried out. More specific analyses were performed using peptidoglycan (PGN), a cell wall component of Gram-positive bacteria, which causes a pro-inflammatory response in ECs. In this context, the focus remained on the analysis of cellular changes in terms of cell stiffness, wound healing, and additionally platelet aggregation.

The analysis of the HCAEC host proteome revealed a time-related difference depending on the infecting bacterial strain. Several proteins involved in host cell signaling pathways exhibited a higher abundance at earlier time points in host cells infected with endocarditis strain T-72949 compared to those infected with HG001. Further proteome analysis uncovered several adaptations on the cellular side that enable internalization and replication of both *S. aureus* strains as well as the activation of pathways that promote cellular recovery. Furthermore, it could be shown that PGN reduced cellular stiffness which could lead to an increased

bacterial uptake and would thereby promote the development of a chronic *S. aureus* infection. Additionally, PGN prevented effective wound healing which promotes a pro-thrombotic and pro-inflammatory condition. This status could facilitate the bacterial infection of further cells. Apart from that, PGN induced platelet aggregation which could ease bacterial adhesion to thrombotic surfaces (e.g., dysfunctional endothelium). The following formation of a mature vegetation might protect the bacteria from the immune system and antibiotics.

The results of the present work emphasize the central role of ECs in the context of IE. It could be demonstrated that a healthy monolayer of ECs enables a beneficial cell response and may prevent the development of vascular diseases. Moreover, the comprehensive proteome dataset which was generated in this project provides a valuable source of information for future studies to unravel further molecular mechanisms of endocarditis and possible therapeutic approaches.

Zusammenfassung

Endokarditis, die durch das Bakterium *Staphylococcus aureus* (*S. aureus*) ausgelöst wird, ist nach wie vor eine der tödlichsten Herzkrankheiten mit einer Mortalitätsrate von 20-45 %. In den vergangenen Jahren wurde die Bedeutung von Endothelzellen im Zusammenhang mit Endokarditis immer deutlicher. Das Gefäßendothel bildet eine selektive Barriere zwischen dem Blut und dem angrenzenden Gewebe, indem es einen anti-inflammatorischen und anti-thrombogenen Phänotyp aufrechterhält. Das Einbringen kardialer Implantate kann jedoch zu einer Verletzung des Endothels führen, was die Thrombozytenaggregation und anschließende Anlagerung von *S. aureus* an Thrombozyten fördert, insbesondere im Bereich mit einer niedrigen Hämodynamik. Dieser Prozess gilt als Schlüsselereignis bei der Entwicklung einer infektiösen Endokarditis und ermöglicht den Bakterien die Besiedlung der Herzklappen. Trotz umfangreicher Forschungsarbeiten ist die Pathogenese der infektiösen Endokarditis noch immer nicht vollständig geklärt. Daher sind weitere Untersuchungen erforderlich, um eine wirksame Vorbeugung gegen diese lebensbedrohliche Krankheit zu ermöglichen.

Um den Infektionsprozess von *S. aureus* zu untersuchen, wurden Internalisierungsexperimente mit zwei verschiedenen *S. aureus*-Stämmen, einem Laborstamm (HG001) und einem aus einem Endokarditis-Patienten isolierten Bakterienstamm (T-72949), in menschlichen Endothelzellen aus der Koronararterie (HCAEC) durchgeführt. Anschließend wurde eine umfassende Proteomanalyse der Wirtszellen vorgenommen. Spezifischere Analysen wurden mit Peptidoglykan (PGN) durchgeführt, einem Zellwandbestandteil Gram-positiver Bakterien, der in Endothelzellen eine pro-inflammatorische Reaktion hervorruft. In diesem Zusammenhang lag der Schwerpunkt der Analyse bezüglich der zellulären Veränderungen auf der Zellsteifigkeit, der Wundheilung und zusätzlich der Thrombozytenaggregation.

Die Analyse des Wirtsproteoms ergab einen zeitlichen Unterschied in Abhängigkeit von dem infizierenden Bakterienstamm. Signalwege von Zellen, die mit dem Endokarditisstamm T-72949 infiziert wurden, wiesen zu früheren Zeitpunkten eine höhere Abundanz von Proteinen auf als bei HG001.

Weitere Proteomanalysen offenbarten mehrere Anpassungen auf zellulärer Seite, die die Internalisierung und Replikation beider *S. aureus*-Stämme sowie die Aktivierung von Signalwegen, die den zellulären Wiederaufbau fördern, ermöglichen. Des Weiteren konnte gezeigt werden, dass PGN die zelluläre Steifigkeit reduzierte, was zu einer erhöhten Bakterienaufnahme und somit zur Entwicklung einer chronischen *S. aureus*-Infektion führen könnte. Darüber hinaus verhinderte PGN eine effektive Wundheilung, was einen pro-thrombotischen und pro-inflammatorischen Zustand fördert. Dieser Zustand kann die bakterielle Infektion weiterer Zellen begünstigen. Außerdem induziert PGN die Thrombozytenaggregation, was die bakterielle Adhäsion an thrombotischen Oberflächen (z. B. dysfunktionales Endothel) erleichtern könnte. Die anschließende Bildung einer reifen Vegetation könnte die Bakterien vor dem Immunsystem und Antibiotika schützen.

Die Ergebnisse der vorliegenden Arbeit verdeutlichen die zentrale Rolle der Endothelzellen bei der infektiösen Endokarditis. Es konnte gezeigt werden, dass eine gesunde Einzelschicht von Endothelzellen eine positive Zellantwort ermöglicht und die Entwicklung von Gefäßerkrankungen verhindern kann. Darüber hinaus stellt der umfassende Proteom-Datensatz, der in der vorliegenden Arbeit erstellt wurde, eine wertvolle Informationsquelle für zukünftige Studien dar, um weitere molekulare Mechanismen der Endokarditis und mögliche therapeutische Ansätze zu entschlüsseln.

List of contents

Abstract I

Zusammenfassung III

List of contents V

Introduction 1

1.1 Infective endocarditis 1

1.1.1 Complications of cardiovascular implants 1

1.1.2 The role of *S. aureus* in endocarditis 3

1.2 The endothelium 5

1.2.1 Structure and function of the endothelium 5

1.2.2 Hemodynamic forces in the cardiovascular system 6

1.2.3 Pathophysiological relevance of the endothelium 7

1.3 Inflammation 8

1.3.1 Stiffness of endothelial cells 9

1.3.2 Migration of endothelial cells 10

1.3.3 Anti-thrombotic role of endothelium 12

1.4 Objective 15

Materials and methods 17

2.1 Materials 17

2.1.1 Chemicals 17

2.1.2 Antibodies 18

2.1.3 Enzymes and inhibitors 19

2.1.4 Cell lines 19

2.1.5 Media 19

2.1.6 Bacteria 19

2.1.7 Plasmid 20

2.1.8 Assays and Kits 20

2.1.9 Marker 21

2.1.10 Buffers 21

2.1.11 Consumable materials 22

2.1.12 Devices 23
2.1.13 Software 25
2.2 Methods 27
2.2.1 Cell culture 27
2.2.2 Internalization experiments with *S. aureus* 28
2.2.3 Cytotoxicity assay 33
2.2.4 Cell proliferation 34
2.2.5 Cellular stiffness 36
2.2.6 Cellular migration 37
2.2.7 Gene expression analysis 41
2.2.8 Western Blot 45
2.2.9 ELISAs 47
2.2.10 Immunofluorescence microscopy of actin and eNOS 48
2.2.11 Platelet adhesion 49
2.2.12 Statistical analysis 50
Results 51
3.1 Influence of a *S. aureus* infection on HCAEC 51
3.1.1 Temporal development of host cells and *S. aureus* strains 51
3.1.2. Proteome adaptation of host cells to infection with two different *S. aureus* strains 54
3.2 Influence of PGN on HCAEC 58
3.2.1. Preliminary tests to evaluate the concentration and time period for PGN stimulation 58
3.2.2 Effect of PGN on cell stiffness 60
3.2.3 Effect of PGN on cell migration 61
3.2.4 Effect of PGN on wound healing 63
3.2.5 Effect of PGN on gene expression and protein expression 64
3.2.6 Effect of PGN on platelets 67
Discussion 71
4.1 Internalisation of *S. aureus* in HCAEC 71
4.1.1 *S. aureus* persists in human primary endothelial cells for at least 72 h p.i. 71

4.1.2 Proteome adaptation of host cells to infection with two different *S. aureus* strains....72

4.1.3 Analysis of specific pathways of host cells after an infection with two different *S. aureus* strains....75

4.2 Effect of *S. aureus*-derived PGN on HCAEC....77

4.2.1 Cell stiffness....77

4.2.2 Cell migration and wound healing....79

4.2.3 Gene and protein expression....80

4.2.4 Platelet aggregation....81

Conclusion and outlook....85

Appendix....87

I Supplemental data....87

II Literature index....91

III Index of figures....103

IV Index of tables....105

V List of abbreviations....117

VI Acknowledgements....121

Introduction

1.1 Infective endocarditis

In case of endocarditis, an inflammation of the endocardium, the inner lining of the heart chambers and heart valves, occurs [11]. Endocarditis can be classified as a disease of infectious or non-infectious origin. Infective endocarditis (IE) is most often caused by Gram-positive bacteria whose virulence factors determine the clinical course. Hence, this disease can be subdivided into an acute and more aggressive form and a subacute form [9, 12].

In general, IE is a rare but deadly disease if left untreated and is considered to affect 3–7.5 people per 100,000 person-years [13]. The incidence of IE seems to vary dramatically in different geographical regions, even within one country and continues to rise in some areas of the world. The exact incidence of IE is still widely unknown. Nevertheless, new risk factors could be identified (degenerative valvular heart disease, intracardiac electronic devices, diabetes mellitus, intravenous drug use, and human immunodeficiency virus infection), which are also involved in the progression of IE besides conventional risk factors (persistent bacteremia, central venous catheter, and prosthetic heart valve).

S. aureus is the number one cause of IE globally and has displaced viridans group streptococci in several parts of the world. Worldwide, IE is associated with a serious burden due to a high mortality rate (in-hospital mortality rates of 22% and a 5-year mortality rate of 45%) [13, 14]. Without any treatment, it is a fatal disease and even with an intensive therapy, mortality rates can be as high as 45%. The mortality rate and severity of the disease even worsened due to the emergence of bacterial strains which are resistant to antibiotics (e.g., methicillin-resistant *S. aureus*) [15]. Therefore, further research is necessary to lower the prevalence of this serious disease.

1.1.1 Complications of cardiovascular implants

The percentage of patients with cardiovascular implants is constantly rising. Those patients have an additional infection risk including the threat of early infection related to the procedure and the occurrence of artificial material that facilitates bacterial

adherence. The subsequent formation of a biofilm effectively prevents the elimination of bacteria which has severe consequences for the patient [16, 17]. Furthermore, endothelial repair is required after an injury of the endothelial monolayer, e.g., after transcatheter aortic valve implantation (TAVI) [18, 19]. After implantation adverse effects such as a delayed re-endothelialization and impaired endothelial function may be associated with thrombosis and detrimental effects on the clinical outcome [20].

Unfortunately, after TAVI the hemodynamic environment differs compared to native valves. Consequently, altered blood flow patterns occur through the valves and in the thoracic aorta [21]. In contrast to the surgical approach, TAVI preserves the native leaflets, which are expanded in the paravalvular space of the Valsalva sinuses. This manifestation causes local changes in the hemodynamic flow patterns [22]. A previous study showed that the implant significantly decreased the flow at the basis of the Valsalva sinuses, leading to areas with low shear stress. This contributes to platelet activation and thrombus formation as well as enhances the risk of bacterial infection [23]. In Figure 1.1 the simulation of the hemodynamic flow conditions after TAVI illustrates this problem. Areas with a low velocity are also characterized by a high residence time of the blood which represents thrombogenic areas. The interaction of *S. aureus* and platelets is a key event in the development of IE. The formation of platelet aggregates in combination with a bacterial infection may allow the adhesion to pro-thrombotic surfaces, e.g., to dysfunctional or injured endothelium which is present after implant surgery [24].

Taken together, insertion of cardiac implants bears the following risks: a) injury of the endothelium leading to an impaired endothelial function, b) platelet aggregation in areas with low shear stress, and c) bacterial infection.

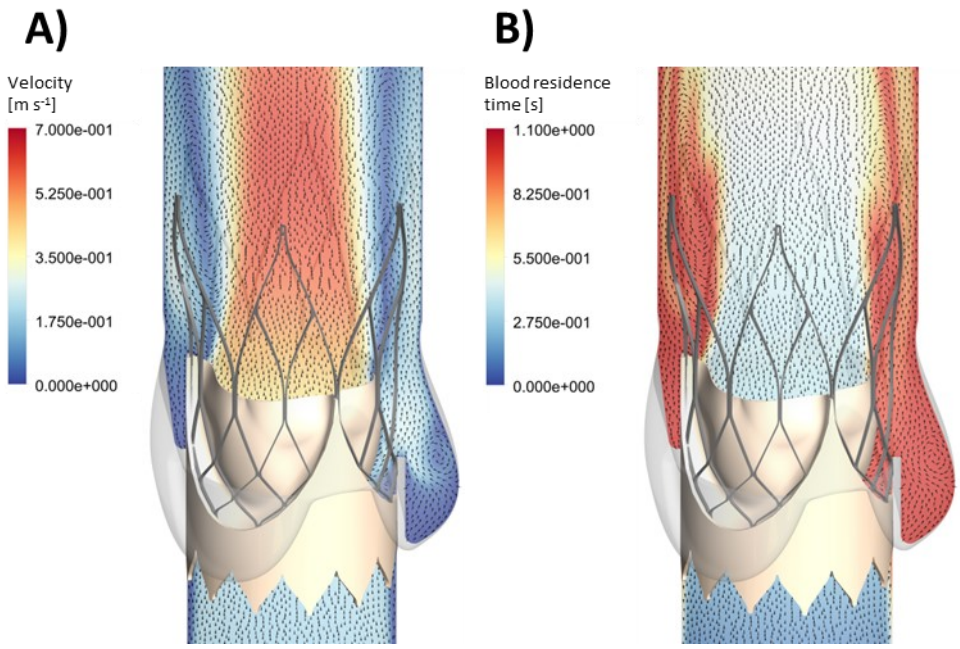

Figure 1.1: Hemodynamic flow conditions after transcatheter aortic valve implantation (TAVI): A) flow velocities and velocity vectors during systole, and B) blood residence time. Areas with a low velocity are also characterized by a high residence time of the blood [provided by Finja Borowski, Institute for ImplantTechnology and Biomaterials].

1.1.2 The role of *S. aureus* in endocarditis

Most of the knowledge about the pathogenesis of IE is based on studies of the virulence of *S. aureus* [9]. *S. aureus* is one of the main causes of life-threatening infections of the bloodstream, such as IE [25] and about 10-25% of IE cases are caused by a preceding bacteraemia of this pathogen [26]. The pathogenicity of *S. aureus* relies on a broad repertoire of virulence factors which are significantly influenced by genomic plasticity. The virulence factors, including e.g., adhesins, lytic toxins and proteins interfering with the immune system, are essential to enable the extracellular survival, cell internalization and survival within host cells [27, 28].

It has been shown that patients with a *S. aureus* bacteraemia and endocarditis possess higher serum concentrations of endothelial E-selectin and vascular cell adhesion molecule-1 (VCAM-1) compared to patients with a *S. aureus* bacteraemia but without endocarditis. This observation underlines the fact that endothelial cells (ECs) are activated to a higher extent during endocarditis [29]. Moreover, the attachment of bacteria to ECs or sites of injured endothelium on the heart valve is the initiating event of IE [30]. Numerous physiological adaptions are required for the interaction of cells

and bacteria. The pathogen attempts to receive nutrients from the host cell and tries to avoid elimination by the immune system. In response, the host cell produces oxygen-reactive and/or nitrogen-reactive species as a defence mechanism [31]. Previous studies have shown that the extent of bacterial infection largely depends on the type of host cell. Significant differences in terms of cytotoxicity, inflammatory response and persistence are evident [32, 33].

In general, the progression of endocarditis includes the following steps: 1) endocardial injury occurs (e.g., by implantation of a cardiac device), 2) thrombus formation is triggered, 3) transient bacteria adhere to the thrombus, 4) deposition of fibrin and bacterial proliferation leads to the formation of a mature vegetation which protects the bacteria from phagocytes and antibiotics (Figure 1.2) [9, 11].

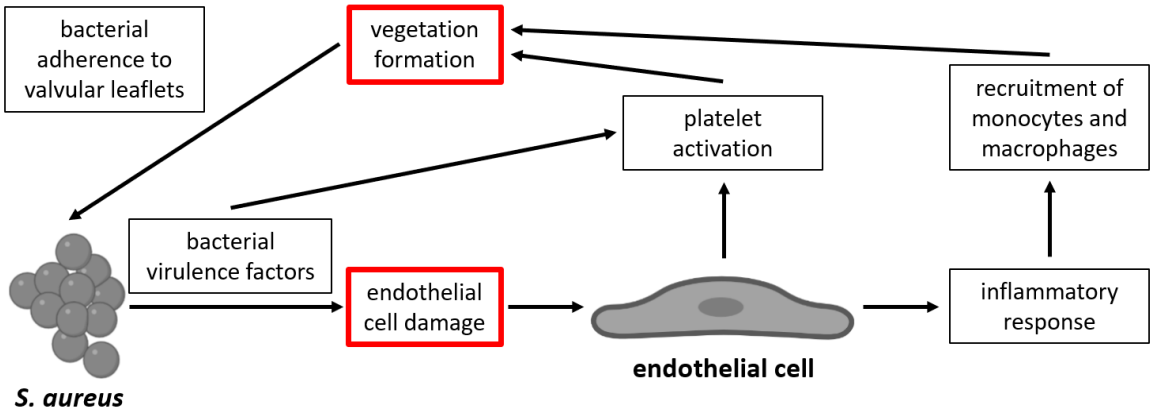

Figure 1.2: Pathophysiological role of endothelial cells (ECs) in endocarditis. Bacteria, circulating in the bloodstream, attach to ECs on the heart valve. Bacterial virulence factors subsequently cause endothelial cell damage. Thereupon, the damaged endothelial cells trigger an inflammatory response that leads to the recruitment of monocytes and macrophages. Furthermore, platelet activation is induced resulting in vegetation formation. The vegetation is then recolonized by further bacteria, which initiates an ongoing process (modified from [9]; created with BioRender.com).

The pathogenesis of IE is still not completely understood. Therefore, further research is needed to promote a successful prevention of this life-threatening disease [34].

1.2 The endothelium

ECs form the inner lining of blood vessels. The specific function can vary according to the localization and size of the associated blood vessel [35]. In general, ECs are flat cells which are about 30 µm long, 10 µm wide, 3 µm thick in the area of the nucleus and 0.2 µm or less thick in the periphery [36]. In a 70 kg adult 10^{12} ECs cover a surface area of more than 100 m^2 with a total weight of approximately 100 g [37, 38].

1.2.1 Structure and function of the endothelium

The vascular endothelium is a selective barrier between blood and the surrounding tissue. The most important function is a haemostatic balance between anticoagulation and thrombosis. Furthermore, the endothelium controls the vascular tone in order to provide an adequate perfusion pressure to target organs and also regulates wound healing, smooth muscle cell proliferation, angiogenesis, inflammation, and immune response. The endothelium interacts with most of the systems in the body and is involved in many diseases of numerous organs such as the neurologic, vascular, immunologic, dermatologic, and cardiac system. Typical cardiovascular risk factors, for instance: obesity, age, smoking, physical inactivity, hyperlipidemia, and hypertension adversely affect the endothelium. Additionally, numerous stimuli such as temperature, medication and shear stress influence the endothelium. In response to shear stress, nitric oxide (NO) is produced from L-arginine by endothelial nitric oxide synthase (eNOS) [39-41]. An imbalance in NO production and consumption occurs during endothelial dysfunction. This pathologic state provides a suitable condition for platelet activation and adhesion, leukocyte and vessel wall interaction, as well as an activation of cytokines which enhances the permeability of the vessel wall to oxidized lipoproteins and inflammation mediators. Thus, structural damage of the arterial wall with smooth muscle cell proliferation and atherosclerotic plaque formation can appear [40, 42]. Moreover, conditions such as heart failure reduce endothelial shear stress which can contribute to an alteration of the bioavailability of NO and changes the endothelial function [43, 44].

Since the function and phenotype of ECs in large vessels differ from those in the microvasculature, it is important to choose an appropriate cell culture model which is as close as possible to the examined system. Primary cells might vary between

different isolations but the primary endothelial characteristics are more present in contrast to immortalized cell lines [35].

1.2.2 Hemodynamic forces in the cardiovascular system

The product of blood velocity and shear rate determines shear stress which is defined as force per unit area (10 dyn/cm^2 = 1 Pa = 1 N/m). ECs are extremely sensitive to hemodynamic shear stress. The magnitude of shear stress ranges from 1-6 dyn/cm^2 in the venous system up to 10-70 dyn/cm^2 in arteries. In ECs, mechanotransduction is a flow-induced endothelial response which includes a cell-signaling repertoire [45, 46]. ECs are able to express mechanotransducers (integrins, ion channels, apical glycocalyx) that convert the physiological stress into biochemical signals [47]. A mechanical stimulus (blood flow) from the extracellular environment affects various properties of single and collective cells. Proliferation, migration, and alteration in cell adhesion are cellular responses that are influenced by mechanical signals [48]. In straight segments of the arteries the cells and their nuclei are orientated in the direction of the blood flow. This is not the case at bifurcations. Hence, an alignment of ECs according to the flow direction is a reversible process in response to hemodynamic shear stress [49]. Critical changes in hemodynamic forces affect the structure and function of ECs and modulate the expression of pathophysiologically relevant genes. At arterial bifurcations the vascular geometry induces a disturbance of the flow pattern with low shear stress (<4 dyn/cm^2). This process effects several characteristics of ECs including the morphology, wound repair, and expression of inflammatory genes (Figure 1.3). The resulting endothelial dysfunction might contribute to an elevated risk of cardiovascular diseases such as IE [7, 9].

high shear stress | disturbed flow/ low shear stress

morphology	elongated & aligned according to flow direction	polygonal, unaligned
expression of inflammatory genes	low	high
platelet aggregation	inhibition	promotion
wound repair	promotion	retardation
fibronectin/fibrinogen deposition	low	high

Figure1.3 Effects of different flow patterns and associated shear stresses on endothelial cells (ECs) (modified from [7]; created with BioRender.com).

1.2.3 Pathophysiological relevance of the endothelium

The endothelium is distributed everywhere in the body, it communicates with each tissue, and it is involved in several disease states. Therefore, it represents a key element in human health and disease [50].

The location of ECs in the inner layer of the vasculature in combination with a direct interaction with the blood flow involves the need to integrate biomechanical signals to maintain the endothelial barrier function which includes a selective permeability, vascular tone, and vascular formation [51]. Under physiological conditions non-activated ECs exhibit an anticoagulant, anti-inflammatory and vasodilatory phenotype [52, 53]. Persistent laminar shear stress induces alterations in cell shape, and cytoskeletal organization that trigger adaptive signaling pathways to minimize intracellular stress, and to maintain vascular homeostasis similar to lesion-resistant areas in the artery. In contrast, disturbed flow initiates alterations in cell shape, reorganization of the cytoskeleton, increases oxidative stress, and triggers the synthesis of molecules that act in an autocrine (ligand activates receptors on the cell of its origin), paracrine (ligand activates surrounding cells), or juxtacrine (membrane-anchored factor transmits signal to neighbouring cells) manner similar to lesion-prone areas in the artery [51, 54, 55]. Endothelial activation is caused in lesion-prone

areas by proinflammatory agonists (interleukins) as well as disturbed blood flow. The subsequent genetic modifications include the expression of chemokines (e.g., monocyte chemotractant protein-1), prothrombotic mediators (e.g., vonWillebrand factor (vWF)), and cell surface adhesion molecules (e.g., vascular cell adhesion molecule-1). This process promotes the recruitment of T lymphocytes and monocytes and results in the formation of a paracrine milieu of reactive oxygen species, growth factors and cytokines which maintains a chronic proinflammatory state and EC dysfunction [54]. This state is characterised by a procoagulant, pro-adhesive/pro-inflammatory and vasoconstrictive phenotype [53].

In addition, the attachment of bacteria to vascular ECs is considered as a triggering event for several intravascular infections [30]. During inflammation the activated endothelium produces chemotactically active cytokines and chemokines resulting in a recruitment of leukocytes. This process of leukocyte migration is essential in order to generate an effective inflammatory and immune response. Studying different types of ECs revealed a different expression pattern of chemokines which provides evidence for a site-specific recruitment of subtypes of leukocytes in the coronary artery [30, 56].

In general, it can be stated that a compromised endothelial function contributes to the disease progression of cardiovascular events. Therefore, an improved endothelial function should be the main target for therapeutic approaches in cardiovascular diseases [57].

1.3 Inflammation

An activation of the endothelium is a crucial event in the inflammatory process [56]. The vascular endothelium modulates the inflammatory and immune response and an activation of ECs triggers the expression of pro-inflammatory cytokines (e.g., Interleukin 6 (IL6)) [40]. ECs are able to control the attraction, trafficking and migration of leukocytes in the initial phase of inflammation. Consequently, an acute or chronic inflammatory response is triggered [56]. Tissue injury or an infection induce an inflammatory reaction. When ECs are exposed to inflammatory stimuli, they display modified characteristics including an enhanced permeability, increased procoagulant activity and an affected vascular tone which contributes to the

progression of vascular diseases. The specific investigation of EC responses to pathophysiological shear stress and inflammation provides an insight into the pathogenesis of cardiovascular disease and may reveal potential therapeutic approaches [51].

1.3.1 Stiffness of endothelial cells

Alterations of the mechanical properties of the vascular endothelium can be considered as the origin of cardiovascular diseases [58]. The stiffness of ECs is essential because it represents the crucial parameter between endothelial function and dysfunction [59]. Two compartments of the vascular endothelium in particular exhibit a close relationship between mechanics and function, namely the endothelial glycocalyx and endothelial cell cortex. The outer 150-200 nm of ECs modulate a multitude of vascular functions by regulating the release of vasoactive substances (e.g., NO) and by providing a dynamic scaffold for the expression of specific proteins. A persistent stiffening of the outer layer of endothelial cells is a critical development because it adds to the generation of endothelial dysfunction [60].

Atomic force microscopy can be used to sense the stiffness of ECs and to specifically assess the stiffness of the cell cortex which consists of cytoskeletal proteins [59, 61]. In this context, the degree of actin polymerization could influence the mechanical properties and consequently the function of the endothelium [59]. In the artery, an increase or decrease in the cell stiffness has a great relevance, because it determines the vascular tone and subsequently the arterial stiffness [62]. An enhanced arterial stiffness is a predictor of cardiovascular diseases. Inflammation plays a role in the development of arterial stiffness and clinical evidence also confirms the assumption that inflammation leads to an increased arterial stiffness [63]. Endothelial dysfunction is once again contributing to this process, because it can lead to an enhanced expression of proinflammatory cytokines which can consequently result in an increase of arterial stiffness [64].

Many factors are associated with cardiovascular events and, in addition, some of them also correlate with clinical outcome, namely endothelial dysfunction, and arterial stiffness. Endothelial dysfunction predisposes the vascular system to leukocyte adhesion, platelet activation, and thrombosis. Furthermore, it has been well known

for many years that inflammation causes endothelial dysfunction. Inflammatory cytokines affect vasodilatory responses by interfering with NO production, while reactive oxygen species generated by inflammatory processes further deplete existing NO [65]. The EC stiffness directly correlates with eNOS function. It could be demonstrated that stiff ECs release lower levels of NO in comparison to soft cells. Therefore, mechanics and cellular function are associated, and the EC stiffness can be applied as an indicator for endothelial function [59, 60, 66].

1.3.2 Migration of endothelial cells

Migration of ECs has a major impact on vascular regeneration and remodeling [67]. Chemotactic, haptotactic, and mechanotactic stimuli modulate this movement process which also involves the degradation of the extracellular matrix to allow the progression of migrating cells. An activation of multiple signaling pathways is involved in the remodeling of the cytoskeleton. For migration, three different types of movements are distinguished. Chemotaxis is the directional migration towards gradient of soluble chemoattractants (e.g., basic fibroblast growth factor or vascular endothelial growth factor). Haptotaxis describes the process of a directional migration towards a gradient of immobilized ligands (e.g., collagen type IV, fibronectin). The third option, the mechanotaxis is the directional migration which is generated by mechanical forces. EC migration is often based on a combination of these three types [67-69]. The involvement of dynamic changes in cell adhesion, signal transduction and cytoskeletal organization turns EC migration to a mechanically integrated molecular process. After sensing of motile stimuli by filopodia, the major steps of EC migration involve: (I) cellular elongation with the formation of protruding lamellipodia, (II) attachment of protrusions to focal adhesions of the extracellular matrix, (III) contraction of the cell via stress fibers which allows a forward progression, (IV) rear release of adhesive proteins which enables a forward progression of the cell movement, and (V) recycling of the involved adhesive and signaling components (Figure 1.4) [8, 68].

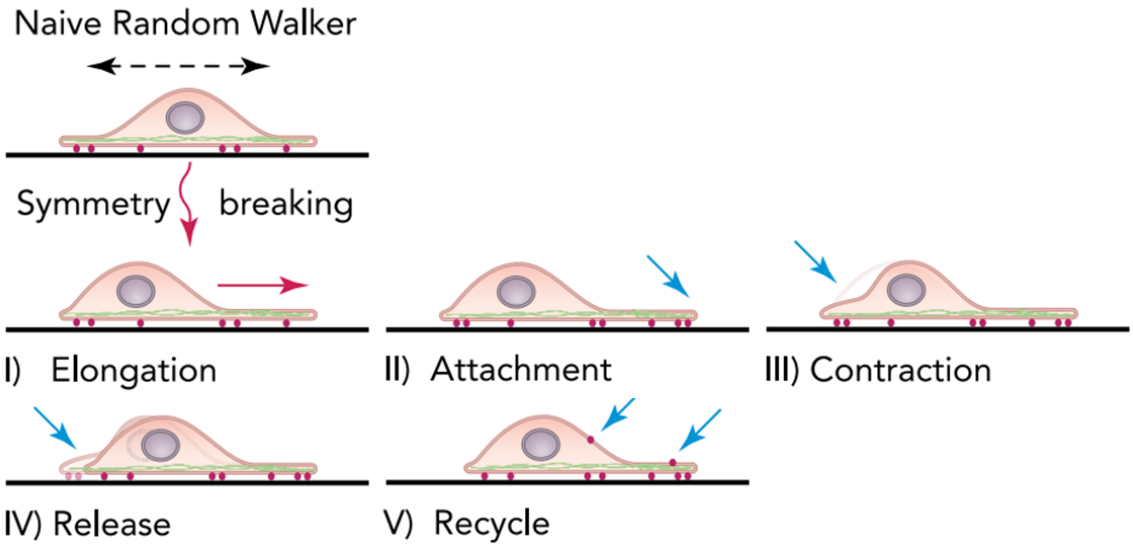

Figure1.4 Mechanism of single cell migration: Symmetry-breaking events (e.g., changes in blood flow) cause cell polarization and directed migration. I) elongation of the leading edge of the cell through actin-rich protrusions (lamellipodia), II) attachment of newly formed protrusion through adhesion proteins, III) contraction of the cell causes the posterior part of the cell to retract and the anterior part to move forward, IV) release of adhesive proteins allows progression of cell movement, V) recycling of migration components (modified from [8]).

In mechanotaxis, hemodynamic forces modulate stress fiber contraction, cell polarity, lamellipodia formation and the cytoskeletal structure. Laminar shear stress enhances tissue repair by promoting EC migration, whereas disturbed flow has a reverse impact on wound healing. Furthermore, shear stress promotes the interaction between ECs and the extracellular matrix, which may also ease EC migration under flow [51]. Specific transcription factors (e.g., dachshund family transcription factor 1) are important regulators in coronary artery development and are markedly upregulated in ECs under disturbed flow near arterial branches [70].

In general, the process of cell migration is involved in a variety of cellular events, namely: wound healing, tissue formation and immune response. Errors in this process may lead to tumor formation, metastasis, or cardiovascular disease. However, ECs possess the ability to repair areas damaged by toxic injury or detrimental mechanical stimuli, with EC proliferation and migration to restore wounded regions [51, 71]. Insertion of cardiac implants (e.g., TAVI) lead to damage of the endothelial monolayer which then requires endothelial migration and repair [18, 19]. Implantation exhibits detrimental effects such as delayed re-endothelialization and impaired endothelial

function which carries the risk of thrombosis and worsens the clinical outcome [20]. A compromised wound healing can also be postulated for *S. aureus* infections [72]. The incidence of an IE after TAVI is relatively low (~3.25%) and about 16.1% of the cases are associated with a *S. aureus* infection. Nevertheless, severe complications (e.g., heart failure) and a high mortality rate makes IE a serious medical indication [73].

All the listed points indicate the importance of promoting EC migration and wound healing to establish the endothelial barrier function [74].

1.3.3 Anti-thrombotic role of endothelium

The endothelium also regulates platelet function in response to hemodynamic stimuli. Under physiological conditions ECs maintain a non-thrombogenic condition [57]. ECs regulate the adhesiveness of platelets at the vessel wall by providing a negative charge which repels them from the vessel wall. A number of molecules are synthesized by ECs that inhibit platelet activation and subsequent thrombin generation [75]. Some of these known molecules are: NO [76], thrombomodulin [77], and prostacyclin [78].

Under regular circumstances, platelets circulate in the blood in an inactive state. Activation can occur in response to a vessel wall injury, changes in the blood flow or biomechanical stimuli. Platelet activation and recruitment includes platelet adhesion to the vessel wall and secretion of intracellular granule factors which leads to a recruitment and activation of further platelets, followed by platelet aggregation [79].

Activation or injury of ECs lead to secretion of vWF which temporarily remains on the endothelium. Additionally, multimers of vWF circulate in the blood and can accumulate in the subendothelial matrix (Figure 1.5). A shear stress-induced activation of vWF induces a conformational change which exposes the formerly hidden A1 domain to which platelets can attach via the GP1b receptor [10, 80, 81]. Binding of platelets to vWF enables the interaction with other molecules (e.g., collagen, fibrin, fibrinogen) [10]. The endocarditis-causing pathogen *S. aureus* synthesizes e.g., clumping factor A to bind to platelets followed by platelet activation and adhesion to the vessel wall. This process allows the bacteria to overcome shear stress [10, 82]. Furthermore, *S. aureus* has developed adhesion mechanisms to ECs

which are analogous to platelets (e.g., bacterial vWF-binding protein enables the binding to the A1 domain of vWF) [83, 84]. The ability of *S. aureus* to bind platelets and to adhere to ECs allows the bacterium to colonize cardiac valves with severe consequences for the patient [34].

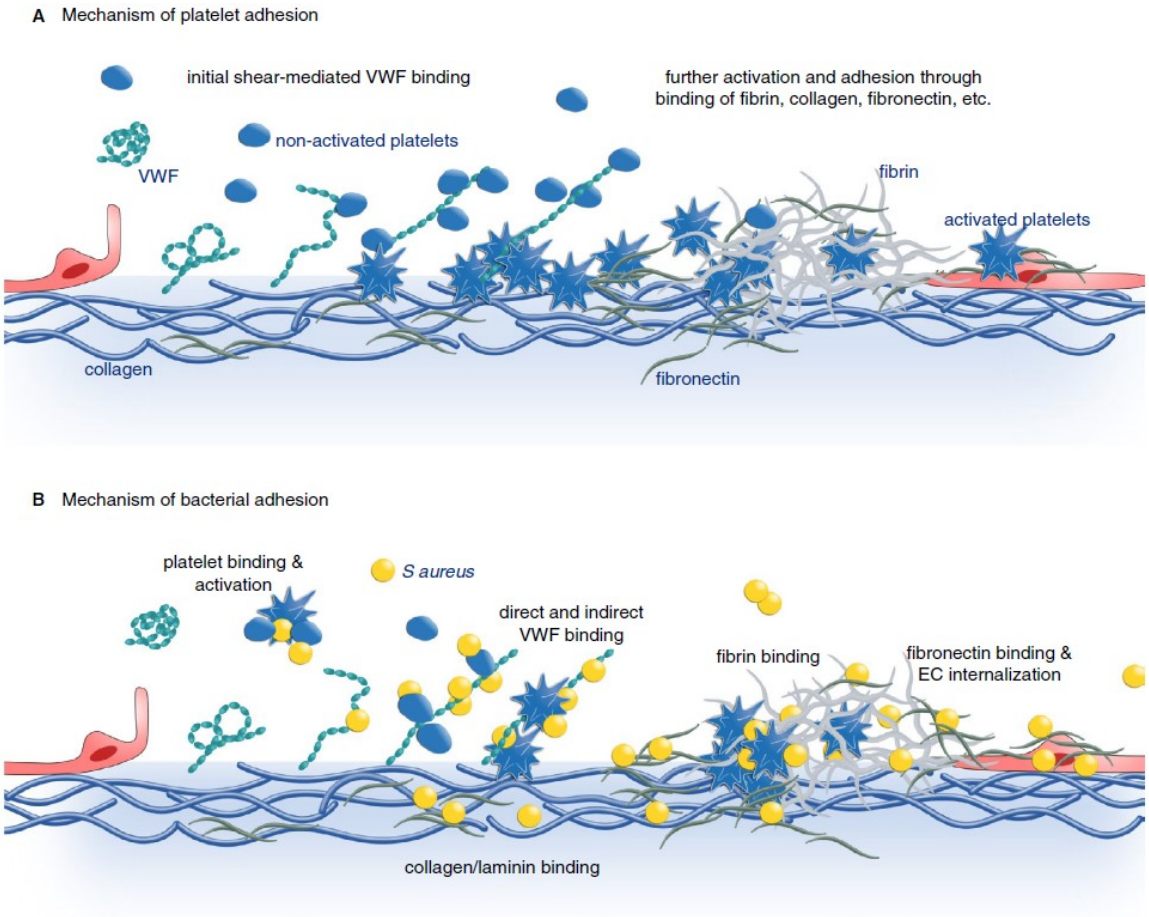

Figure1.5 Analogous mechanisms of platelet adhesion and bacterial adhesion to injured endothelium. A) Platelets bind to von Willebrand factor (vWF) and are thereby slowed down. Consequently, interactions with further matrix molecules (fibrin, collagen, fibronectin) are possible, which triggers platelet activation and aggregation. B) Initial adhesion of *S. aureus* to the endothelium is also mediated by vWF, either by direct binding of vWF or indirectly by binding platelets. This interaction also allows bacteria to interact with other matrix molecules and to initiate platelet activation and aggregation [10].

1.4 Objective

The inner lining of blood vessels is formed by ECs which provide an anti-thrombogenic barrier between the vessel wall and the blood. Additionally, they secret anti-inflammatory substances and are involved in the activation of the immune system. Nevertheless, EC injury, dysfunction or activation are key elements in the development of many pathophysiological conditions [85, 86]. Cardiac implants (e.g., TAVI) lead to changes in hemodynamics including areas with low shear stress at the basis of the Valsalva sinuses. This process facilitates platelet aggregation and enhances the risk of bacterial infection [23]. The resulting formation of a septic vegetation on the surface of the endothelium on heart valves causes a life-threatening disease, namely IE [87]. Although many studies address the issue of IE associated with *S. aureus* infection, surprisingly little is known about the particular role of the endothelium in the pathogenesis of endocarditis [9, 88]. In this context, the simultaneous analysis of the interacting host cells and bacteria is important to acquire a comprehensive knowledge which may provide new concepts for IE treatments [89].

The objective of this work was the analysis of the influence of a *S. aureus* infection on HCAEC regarding bacterial internalization, cellular migration and thrombogenicity. In this context, the following questions should be elaborated:

1) Can the endocarditis strain (T-72949) infect HCAEC more efficiently compared to the control strain (HG001)?
2) Are there specific differences in the proteomic data of the host cells after an infection with T-72949 and HG001 which might allow conclusions about the underlying mechanisms of bacterial internalization and cellular defense mechanisms?
3) Can PGN cause effects similar to those already known from *S. aureus* infection of ECs or platelets?
4) What is the effect of PGN on cell stiffness, wound healing and platelet aggregation and what conclusions can be drawn regarding bacterial infection of ECs?
5) Are the cellular characteristics accompanied by changes in gene and protein expression?

1.4 Objective

In a first approach, the present investigations concentrated on internalization experiments of two different *S. aureus* strains (T-72949: isolated from an endocarditis patient; HG001: control strain) in ECs of the coronary artery. For further analysis PGN, a cell wall component of Gram-positive bacteria, was used to determine its influence on more specific parameters (cell stiffness, wound healing, platelet aggregation).

Materials and methods

2.1 Materials

2.1.1 Chemicals

Product designation	Manufacturer
4',6-Diamidin-2-phenylindol (DAPI)	Carl Roth (Germany)
Acetic acid	Thermo Fisher Scientific Inc. (USA)
Acetonitril	Thermo Fisher Scientific Inc. (USA)
ActinGreen™ 488 ReadyProbes™ Reagent	Thermo Fisher Scientific Inc. (USA)
AlamarBlue®	Serotec (Germany)
Alexa Fluor™ 568 phalloidin	Thermo Fisher Scientific Inc. (USA)
β-Mercaptoethanol	Carl Roth (Germany)
Bovine serum albumin (BSA)	Sigma-Aldrich (USA)
Calcium chloride ($CaCl_2$)	Carl Roth (Germany)
Dako fluorescence mounting medium	Agilent Technologies (USA)
4′,6-diamidino-2-phenylindole (DAPI)	Thermo Fisher Scientific Inc. (USA)
Dimethylsulfoxid (DMSO)	Sigma-Aldrich (USA)
Dithiothreithol (DTT)	Thermo Fisher Scientific Inc. (USA)
Erythromycin	Sigma-Aldrich (USA)
Ethylendiamintetraessigsäure (EDTA)	Sigma-Aldrich (USA)
Ethanol ROTIPURAN® ≥99,8 %	Carl Roth (Germany)
Fetal Calf Serum (FCS)	Gibco® (USA), Biochrom AG (Germany)
Glutaraldehyde	Sigma-Aldrich (USA)
Glycerol	Sigma-Aldrich (USA)
Hank's Balanced Salt Solution (HBSS 1x)	Gibco® (USA)
HEPES	PAN-Biotech GmbH (Germany)
Hoechst 33258	Sigma-Aldrich (USA)
HPLC-grade water	Thermo Fisher Scientific Inc. (USA)
HRM peptides	Biognosys AG (Switzerland)
Iodoacetamide (IAA)	Sigma-Aldrich (USA)
Lysostaphin	AMBI Products LLC (USA)

Magnesium chloride ($MgCl_2$)	Sigma-Aldrich (USA)
Mounting medium	ibidi GmbH (Germany)
Paraformaldehyde	Sigma-Aldrich (USA)
Peptidoglycan (PGN)	Sigma-Aldrich (USA)
Phenylmethylsulfonyl fluoride (PMSF)	Sigma-Aldrich (USA)
Prostaglandin E_1	Abcam (UK)
RNAse-free water	Qiagen (Netherlands)
SG qPCR Master Mix (2x)	Roboklon GmbH (Germany)
Sodium dodecyl sulfate (SDS)	Carl Roth (Germany)
Sodium hydrogen carbonate (7.5%)	PAN-Biotech GmbH (Germany)
N,N,N',N'-Tetramethylethylendiamin (TEMED)	Bio-Rad Laboratories Inc. (USA)
Thiourea	Sigma-Aldrich (USA)
Tris-buffered saline with Tween20 (TBST)	Sigma-Aldrich (USA)
Tris(hydroxymethyl)aminomethan (Tris)	Carl Roth (Germany)
Triton X-102	Agilent Technologies (USA)
Trypan Blue Solution (0.4%)	Thermo Fisher Scientific Inc. (USA)
Tryptic Soy Broth (TSB)	Becton Dickinson (USA)
Tween20	Carl Roth (Germany)
Urea	Sigma-Aldrich (USA)

2.1.2 Antibodies

Specificity	**Organism**	**Dilution**	**Manufacturer**
α-Actinin 4	Rabbit	1:1,000	Cell Signaling Technology (USA)
Actin	Mouse	1:50	Santa Cruz (USA)
eNOS	Mouse	1:500	Abcam (England)
GAPDH	Mouse	1:10,000	HyTest (Finland)
ICAM1	Rabbit	1:500	Cell Signaling Technology (USA)
IL6	Rabbit	1:1,000	Abcam (England)
PECAM1	Mouse	1:500	Cell Signaling Technology (USA)
VCAM1	Mouse	1:1,000	Abcam (England)

2.1.3 Enzymes and inhibitors

Product designation	Manufacturer
Accutase®	BioWest (France)
cOmplete™ (protease inhibitor)	Sigma-Aldrich (USA)
Triton X-100	Sigma-Aldrich (USA)
Trypsin	Promega (USA)
Trypsin-EDTA (0.25%)	Gibco® (USA)

2.1.4 Cell lines

Product designation	Organism	Organ	Medium	Manufacturer
Human Coronary Artery Endothelial Cells (HCAEC); Lot: 03087	human	heart	VascuLife EnGS Medium	CellSystems GmbH (Germany)

2.1.5 Media

Product designation	Manufacturer/Ingredients
RPMI 1640 Medium	Gibco (USA)
VascuLife EnGS Endothelial Cell Culture Medium	CellSystems GmbH (Germany)
HCAEC cell culture medium	VascuLife EnGS with 10% FCS
HCAEC cell perfusion medium	VascuLife EnGS with 2% FCS
HCAEC infection medium (RPMI-Vascu medium)	RPMI 1640 medium supplemented with 20% VascuLife EnGS, 2% FCS, 2.5% HEPES (1 M), 0.112% Ammonium bicarbonate (7.5%)

2.1.6 Bacteria

Product designation	Publication
Staphylococcus aureus HG001 (CC8)	Herbert *et al*., 2010
Staphylococcus aureus T-72949 (CC5)	Grumann *et al*., 2011

2.1.7 Plasmid

Product designation	Characteristics
pJL-sar-GFP	constitutive production of green fluorescent protein (GFP) with 10 µg/ml erythromycin resistance (Liese *et al* 2013, additionally optimized by codon usage)

2.1.8 Assays and Kits

Product designation	Manufacturer
Bradford assay	Bio-Rad Laboratories, Inc. (USA)
Cell proliferation ELISA, BrdU colorimetric	Sigma-Aldrich (USA)
ChemiDoc™ MP System	Bio-Rad Laboratories, Inc. (USA)
dNTPs	Applied Biosystems™ (Germany)
Human IL-6 Quantikine® ELISA	R&D Systems® (USA)
Human sPECAM-1 Instant ELISA Kit	Thermo Fisher Scientific Inc. (USA)
Human sP-selectin ELISA Kit	Thermo Fisher Scientific Inc. (USA)
Multiscribe reverse Transcriptase	Applied Biosystems™ (Germany)
Pierce™ BCA Protein Assay Kit	Thermo Scientific Inc. (USA)
Random Hexamer Primer	Applied Biosystems™ (Germany)
RNase-free DNase Set	Qiagen (Netherlands)
RNase inhibitor	Applied Biosystems™ (Germany)
RNeasy® Mini Kit	Qiagen (Netherlands)
TaqMan® Gene Expression Assays	Applied Biosystems™ (Germany)
TGX Stain-Free™ FastCast™ Acrylamide Kit (7.5% und 12%)	Bio-Rad Laboratories, Inc. (USA)
Trans-Blot® Turbo™ Transfer System RTA Transfer Kit, Nitrocellulose	Bio-Rad Laboratories, Inc. (USA)

2.1.9 Marker

Product designation	Manufacturer
Precision Plus Protein™ Dual Color Standards	Bio-Rad Laboratories Inc. (USA)

2.1.10 Buffers

2.1.10.1 Manufactured buffers

Product designation	Manufacturer
Ammonium bicarbonate (ABC) buffer (7.5%)	PAN-Biotech GmbH (Germany)
Hank's Balanced Salt Solution (HBSS)	Gibco® (USA)
1x Phosphate buffered saline (PBS)	Gibco® (USA)
Dulbecco's Phosphate Buffered Saline (DPBS) (w/o: Ca and Mg)	PAN-Biotech GmbH (Germany)
DPBS (w: Ca and Mg)	PAN-Biotech GmbH (Germany)

2.1.10.2 Self-made buffers

Product designation	Ingredients
Blocking buffer	3% BSA diluted in TBST
Buffer A (2x)	4 % acetonitril, 0.2 % acetic acid and 1/50 Hyper Reaction Monitoring (HRM) peptides
Buffer A	2% ACN, 0.1% acetic acid diluted in HPLC-grade water
Buffer B	0.1% acetic acid diluted in acetonitril
Lysis buffer	1 ml 10% SDS, 0.1 ml 0.1 M Sodium orthovanadate, 0.1 ml 1 M Tris/HCL pH 7.4 → diluted in a total volume of 10 ml with A. dest → to 1 ml 40 µl cOmplete™, 10 µl 100 mM PMSF were added

Urea/thiourea (UT) buffer	8 M urea, 2 M thiourea in MS-grade water (Sigma-Aldrich (USA))

2.1.11 Consumable materials

Product designation	**Manufacturer**
Biosphere® SafeSeal tube (0.5 ml, 1.5 ml, 2 ml)	Sarstedt AG & Co. (Germany)
cantilevers (HQ:CSC38/tipless/Cr-Au)	MikroMasch® (Bulgaria)
cannula Microlance™ 3	BD Biosciences (USA)
C-Chip Neubauer Improved DHC-N01 (counting chamber)	NanoEnTek Inc. (South Korea)
cell culture flask (25 cm^2, 75 cm^2)	Greiner Bio-One GmbH (Germany)
cell culture multiwell plate (6-well, 96-well)	Sarstedt AG & Co. (Germany)
cell culture multiwell plate (12-well)	Greiner Bio-One GmbH (Germany)
Combitips advanced® (2.5 ml, 5 ml)	Eppendorf (Germany)
Cryotubes (1.8 ml)	Thermo Scientific Inc. (USA)
Culture-Inserts 2 Well	ibidi GmbH (Germany)
disposable syringe with Luer-Lok™ Tip (1 ml, 5 ml, 10 ml, 20 ml)	BD Biosciences (USA)
E-16 Plates	ACEA Bioscience Inc. (USA)
glass coverslips (round, 10 mm)	Roth (Germany)
glass coverslips (round, 18 mm)	Roth (Germany)
glass microscope slides	Thermo Scientific Inc. (USA)
low protein binding filter membrane (0.22 µm pore size)	Merck Millipore (USA)
Nalgene™ Rapid-Flow™ sterile filtration system	Thermo Scientific Inc. (USA)
needle (blunt fill, microlance™3)	BD Biosciences (USA)
NOA68T	Edmund Optics GmbH (Germany)
PCR Sealing Tape	Sarstedt AG & Co. (Germany)

PCR-Soft Tubes (0.2 ml)	Biozym Biotech Trading GmbH (Austria)
Perfusion Set white	ibidi GmbH (Germany)
pipette tips (10 µl)	Biozym Biotech Trading GmbH (Austria)
pipette tips (200 µl, 1 ml)	Sarstedt AG & Co. (Germany)
reaction tube (15 ml)	Sarstedt AG & Co. (Germany)
reaction tube (50 ml)	BD Biosciences (USA)
Rotilabo® (syringe filter) 0.22 µm	Carl Roth (Germany)
Rotilabo® (weighing pan) 41x41x8 mm	Carl Roth (Germany)
SafeSeal tips® professional (10 µ, 20 µl, 100 µl, 200 µl, 1000 µl)	Biozym Biotech Trading GmbH (Austria)
serological pipettes (2 ml, 5 ml, 10 ml, 20 ml)	Sarstedt AG & Co. (Germany)
silica bead Ø 4.77 µm, SD 0.20 µm	microParticles GmbH (Germany)
SP3 beads (hydrophobic: Sera-Mag Speedbeads carboxylated-modified particles; hydrophilic: Speedbead magnetic carboxylated modified particles)	hydrophobic: Thermo Fisher Scientific (USA) hydrophilic: GE Healthcare (United Kingdom)
sticky–Slide I $^{0.8}$ Luer	ibidi GmbH (Germany)
Thermo Scientific™ Nunc™ Thermanox™ (coverslips)	Thermo Scientific Inc. (USA)
µ–Slide I $^{0.8}$ Luer ibiTreat	ibidi GmbH (Germany)

2.1.12 Devices

Product designation	**Manufacturer**
Acclaim™ PepMap™ 100 C18 HPLC Columns	Thermo Fisher Scientific (USA)
Accucore™ C18 HPLC Columns	Thermo Fisher Scientific (USA)
Atomic Force Microscope NanoWizard 3	JPK Instruments AG (Germany)
AXIO Vert.A1 (microscope)	Zeiss (Germany)

2.1 Materials

BASE 120 (pump system for RT-DC)	Cetoni GmbH (Germany)
BioCell™ coverslip based liquid cell	JPK Instruments AG (Germany)
Biofuge fresco (table centrifuge)	Heraeus GmbH (Germany)
CFX96 Touch™ Real-Time PCR Detection System	Bio-Rad Laboratories Inc. (USA)
Cantilever Holder	JPK Instruments AG (Germany)
ChemiDoc™ MP System 170-8280	Bio-Rad Laboratories Inc. (USA)
Chrono-log Model 700	Chrono-Log Corporation (USA)
CO_2 Incubator	Binder GmbH (Germany); Heraeus GmbH (Germany)
Countess™ automated cell counter	Invitrogen AG (USA)
CPA324S (precision scale)	Sartorius (Germany)
Duomax 1030 (platform shaker)	Heidolph Instruments (Germany)
EVO LS10 scanning electron microscope	Carl Zeiss AG (Germany)
FACSAria IIIu cell sorter	Becton Dickinson Biosciences (USA)
Flow chamber system FCS1c	provitro AG (Germany)
Fluidic Unit	ibidi GmbH (Germany)
Fresco 17 (centrifuge)	Heraeus GmbH (Germany)
Gradient maker	Bio-Rad Laboratories, Inc. (USA)
Guava® easyCyte flow cytometer	Merck Millipore (USA)
Hera Safe (laminar flow box)	Heraeus GmbH (Germany)
ibidi Pump System	ibidi GmbH (Germany)
Infinite 200®Pro	Tecan Group Ltd. (Switzerland)
IPC 4 Microprocessor controlled dispensing pump	Ismatec® (Germany)
Isopropanol container (Mr. Frosty™)	Thermo Scientific Inc. (USA)
Keyence BZ-9000	Keyence (Japan)
JuLi™ (Br&FL) Life Cell Analyser	NanoEnTek Inc. (South Korea)
Mini Star silverline (mini-centrifuge)	VWR International GmbH (Germany)
Multipette HandyStep® S	Brand (Germany)
NanoDrop 2000 Spectrometer	Thermo Scientific Inc. (USA)
Pipetboy acu 2	INTEGRA Biosciences AG (Switzerland)

Pipette (2 µl, 10 µl, 20 µl, 100 µl, 200 µl, 1000 µl)	Eppendorf (Germany)
Q Exactive™ Plus mass spectrometer	Thermo Fisher Scientific (USA)
REAX 2000 (vortexer)	Heidolph Instruments (Germany)
Rotina 50 RS (centrifuge)	Hettich (Germany)
Shaking incubator	Eppendorf (Germany)
Shaking water bath SW22	Julabo GmbH (Germany)
Silicon pump tubing (1 mm)	provitro AG (Germany)
Synergy H1 Hybrid Multi-Mode Reader	BioTek Instruments, Inc. (USA)
T100™ Thermal Cycler	Bio-Rad Laboratories Inc. (USA)
UltiMate 3000 nano-LC system	Thermo Fisher Scientific (USA)
xCELLigence RTCA-DP Analyzer	ACEA Bioscience Inc. (USA)
TECAN infinite M200 PRO	TECAN Group AG (Switzerland)
TH 30 (incubation hood)	Edmund Bühler GmbH (Germany)
Ultrasonication bath	Sonorex (Germany)
UVGL-25 (ultraviolet lamp)	VWR International GmbH (Germany)

2.1.13 Software

Product designation	**Manufacturer**
Bio-Rad CFX-Manager, version 2.1	Bio-Rad Laboratories Inc. (USA)
BZ-II Analyzer, version 2.2	Keyence (Japan)
Chemotaxis and Migration Tool, version 2.0	ibidi GmbH (Germany)
Gen5™, version 2.0	BioTek Instruments, Inc. (USA)
GraphPad Prism 8.3.0	GraphPad Software Inc. (USA)
ibidi PumpControl, version 1.5.3	ibidi GmbH (Germany)
ImageJ	National Institute of Health (USA)
Image Lab, version 5.2.1	Bio-Rad Laboratories Inc. (USA)
Ingenuity Pathway Analysis (IPA)	Qiagen (Netherlands)
JPKSPM Data Processing, version spm-5.0.96	JPK Instruments AG (Germany)

2.1 Materials

LabView™ 2016, version 16.0 (temperature measurement for RT-DC)	National Instruments™ (USA)
Microsoft® Office 2010	Microsoft Corporation (USA)
NanoDrop 2000/2000c, version 1.5	Thermo Scientific Inc (USA)
Pump Control v 1.5.3	ibidi GmbH (Germany)
R, version 3.6.1	R Core Team
RTCA-Software, version 2.0	ACEA Bioscience Inc. (USA)
Spectronaut, version 14	Biognosys (Switzerland)
T100™ Thermal Cycler, version 1.197	Bio-Rad Laboratories Inc. (USA)

2.2 Methods

2.2.1 Cell culture

2.2.1.1 Freezing and thawing of cells

For the freezing of eukaryotic cells over longer periods of time, the medium of a cell culture flask with a confluent cell layer was removed and cells were washed twice with 5 ml HBSS. Subsequently, 500 µl accutase was added, followed by an incubation step for 10 min at 37 °C and 5% CO_2 in the incubator. Cells were resuspended in 5 ml medium and transferred into a 15 ml reaction tube. After centrifugation at 350x g for 5 min the supernatant was discarded. A solution with FCS and 3% DMSO was prepared. $5x10^5$ cells were resuspended in 1 ml of the solution and the suspension was transferred into a cryotube. The cell suspension was stored in a cryo freezing container with isopropanol at -80°C overnight and afterwards in liquid nitrogen until further usage.

For thawing cells, fresh cell medium was preheated at 37 °C and the cryotube with the cell suspension was incubated at 37 °C in a water bath until it was almost completely thawed. The cell suspension was diluted in 1 ml fresh cell culture medium and the cells were plated at a density of 2,500 – 5,000 cells/cm^2 in a t25 cell culture flask. 24 h later, the medium was removed, and fresh medium was added in order to remove cryopreservation reagents.

2.2.1.2 Passaging cells

First, medium was removed and cells were washed twice with 5 ml HBSS. After adding 500 µl accutase, cells were incubated for 10 min at 37 °C and 5% CO_2 in the incubator. Cells were then resuspended in 5 ml cell culture medium and transferred in a 15 ml reaction tube. After centrifugation at 350 g for 5 min, the supernatant was discarded and the cells were suspended in 5 ml cell culture medium. The cell number was determined with a Neubauer counting chamber and $5x10^5$ cells were seeded in a new t25 cell culture flask, or according to the planned experiment, in well plates, ibidi channel slides or Culture-Inserts 2 Well.

2.2.2 Internalization experiments with *S. aureus*

Internalization experiments were carried out in collaboration with Dr. Kristin Surmann, Department of Functional Genomics of the University Greifswald.

2.2.2.1 Bacterial strains and cultivation conditions

S. aureus strain HG001 (control strain) and clinical strain T-72949 isolated from an endocarditis patient were used. Both strains carried plasmid pJL-sar-GFP optimized for codon usage, provoking constitutive production of green fluorescent protein (GFP) with 10 µg/ml erythromycin resistance [90]. Bacteria were stored in aliquots of exponential cultures in tryptic soy broth (TSB) with 20% glycerol and 10 µg/ml erythromycin at -80 °C. Prior to infection experiments, bacteria were cultivated in TSB with 10 µg/ml erythromycin in serial dilutions overnight at 37 °C and 220 rpm. Using an exponential overnight culture (optical density at 600 nm (OD_{600}) 0.8 – 2.0), a pre-culture was inoculated in RPMI-Vascu medium to an OD_{600} of 0.05. To do so, an appropriate amount of overnight culture was centrifuged (8,000x g, 1 min) to remove TSB medium, resuspended in RPMI-Vascu and cultivated until exponential growth phase in a water bath at 37 °C linear shaking at 150 strokes/min. An exponential pre-culture (OD_{600} 0.15-0.35) was used to inoculate a main culture in RPMI-Vascu at OD_{600} 0.05 which was cultivated the same way and applied for HCAEC infection at OD_{600} 0.25. The same medium was used for eukaryotic cell culture during infection to avoid medium effects on the proteome. For each of the two strains, prior to infection, the bacterial number at OD_{600} 0.25 was determined in triplicates and the average value was used for calculation of the multiplicity of infection (MOI). Therefore, bacterial concentration was determined by flow cytometry with a Guava easyCyte™ flow cytometer (Merck-Millipore) using a 488 nm laser and detection at 510–540 nm taking advantage of GFP production of the bacteria [91].

2.2.2.2 Internalization experiment

In order to obtain a confluent cell layer, $1x10^5$ HCAEC cells/well were seeded in HCAEC cell culture medium on round Ø=22 mm Thermanox plastic coverslips in a 12-well plate four days before the internalization experiment started. Prior to infection, host cells from one well were detached from the plate with 0.25% trypsin-EDTA for 10 min at 37 °C, 1:1 stained with trypan blue 0.4% dye, and counted in an automatic

cell counter (Countess®). Remaining cells of this one well were subjected to cell sorting as described below, stored at -80°C for later proteomics preparation, and used as so called t0 mock control. The first bacterial control was comprised by 900 µl bacterial culture at OD_{600} 0.25, which was frozen with 10% DMSO in an isopropanol container at -80 °C until further use.

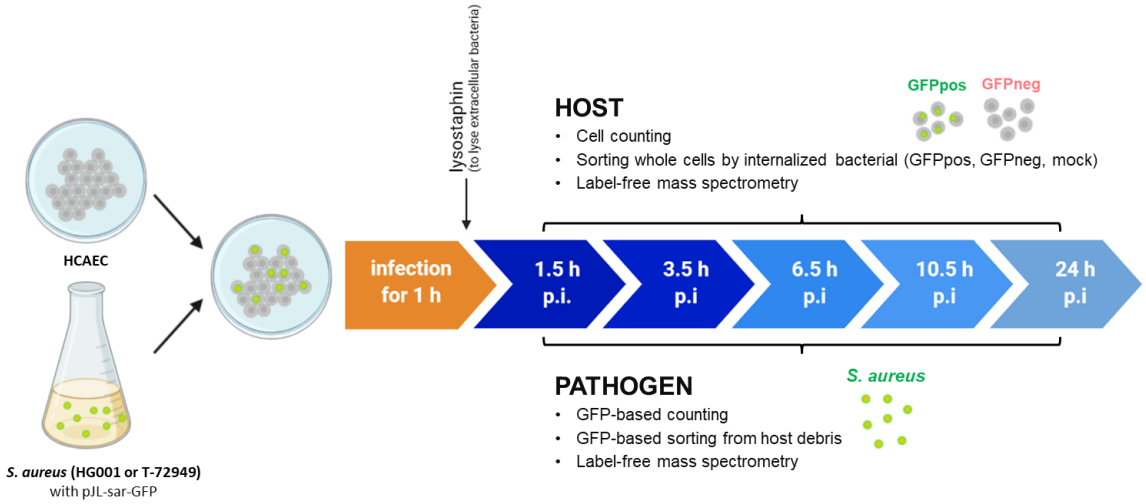

Figure 2.1 Experimental time-course for internalization experiments. Human coronary artery endothelial cells (HCAEC) were infected with *S. aureus* (HG001 or T-72949) for 1 h. Afterwards, lysostaphin was added to lyse extracellular bacteria and to avoid reinfections of the cells. Counting of host cells and bacteria were performed for all time points. Host cells were sorted in GFPpos and GFPneg cells and a mock control (infected with sterile medium) was also carried out. Proteome analyses of host and pathogen were performed up to 6.5 h p.i. (modified from [1]; created with BioRender.com).

The infection was performed at an MOI of 10 bacteria per host cell (Figure 2.1). To allow for equal infection of host cells, an infection master mix was prepared which contained the appropriate amount of exponential bacterial culture as described above, buffered with 2.9 µl sodium hydrogen carbonate per ml bacterial culture in RPMI Vascu. At the start of infection, cellular growth medium was replaced by the master mix followed by an incubation step for 1 h at 37 °C and 5% CO_2. 48 ml supernatant were collected (centrifuged at 10,000x g, 4 °C, 10 min, frozen in 1 ml phosphate buffered saline (PBS) containing 10% DMSO in the isopropanol container at -80 °C, as non-adherent control) and replaced with fresh RPMI Vascu medium containing 10 µg/ml lysostaphin to kill extracellular bacteria which allows the analysis of the replication of intracellular bacteria. At each time point (1.5 h, 3.5 h, 6.5 h, 10.5 h, 24 h, 48 h, 72 h) post infection (p.i.) the cells were washed and treated with 0.25% trypsin-EDTA per well for 10 min at 37 °C. The detached cells were

resuspended in PBS with 2% FCS. The aliquot which was determined for host cell proteomics (1.5 h – 6.5 h p.i.) was immediately applied for cell sorting. The second aliquot per time point (1.5 h – 6.5 h p.i.) was stored in 10% DMSO at -80 °C prior to bacterial sorting. At least five wells for host cell analysis and ten wells for pathogen analysis were detached at each time point (exact numbers are presented in Table S1). Additionally, at each time point (1.5 h – 72 h p.i.), the host cell concentration per well was counted using Countess® and intracellular bacterial concentration was assessed after 5 min host cell disruption with 0.05% aqueous sodium dodecyl sulfate (SDS) at 37 °C using a Guava® easyCyte, as described above.

In parallel, the non-infected mock control with HCAEC was cultivated and treated similarly to the infected cells including cell counting and cell sorting. This allows the analysis of the impact of pure contact to the bacteria, as well as internalization as described before [1, 89].

Five independent internalization experiments were performed to count the host cell and bacterial populations, as well as for proteome analyses by mass spectrometry.

2.2.2.3 Fluorescence activated cell sorting

All fluorescence activated cell sorting (FACS) analyses were performed by Dr. Petra Hildebrandt, Department of Functional Genomics, University Greifswald.

Whole eukaryotic cells were separated with the FACSAria IIIu (Becton Dickinson Biosciences) to discriminate between infected and non-infected cells taking advantage of GFP fluorescence of the internalized bacteria FITC-channel (Ex 488 nm/Em 530/30 nm). About $1x10^5$ infected GFP-positive and non-infected GFP-negative host cells were sorted into 15 ml reaction tubes, centrifuged at 500x g, 4 °C for 5 min, and pellets were immediately frozen in liquid nitrogen before storage at -80 °C. Non-infected mock control cells were also sorted in the FACSAria III with the same settings as the GFP-negative HCAEC cells to provide comparable stress conditions for infected samples and non-infected control samples.

GFP expressing bacteria were first assessed by quickly thawing the host cells, removal of DSMO-containing medium (500x g, 5 min, 4 °C) and a subsequent lysis using 1 ml 5% (v/v) SDS for 5 min at 37 °C. The volume was reduced by centrifugation (16,000x g, 10 min, 4 °C) to about 500 µl. Bacterial controls (OD_{600} 0.25 and

non-adherent bacteria) were treated similarly to allow for a comparison by avoiding methodological bias. About $5x10^5$-$1x10^6$ bacteria were sorted from each sample by excitation with a 488 nm laser and emission detection in the range of 515–545 nm in reaction tubes. From the non-infected controls, about $1x10^6$ bacteria were sorted to allow for exact normalization and comparison during data analysis of these low bacterial amounts. Bacteria were collected onto a low protein binding filter membrane. The liquid was removed constantly using vacuum (450-550 mbar). The bacteria containing filters were cut in four pieces, transferred into reaction tubes, and stored at -80 °C until sample preparation for proteome analysis.

2.2.2.4 Preparation of proteome samples

Bacteria on filters were prepared for proteome analysis as described recently with minor adaptations due to the very low bacterial numbers available [92]. In brief, bacteria were disrupted on filters first with 4 µl 0.05 µg/ml lysostaphin mixed with 30 µl 20 mmol/l aqueous ABC buffer followed by 30 µl 10 % SDS (v/v), bound to beads with 70% ACN, washed with 70% (v/v) ethanol and 100% ACN, digested with 15 ng trypsin and peptides were purified using 2 µl SP3 beads. Peptides, different to the published protocol, were washed only once with 100% ACN to avoid potential sample loss before resuspending in 2% (v/v) DMSO and equal amounts of double concentrated Buffer A.

Eukaryotic cells were solved in 30 µl aqueous buffer containing 8 mol/l urea and 2 mol/l thiourea. Cell disruption and protein extraction occurred during five cycles of freezing in liquid nitrogen and subsequent thawing at 30 °C, 2 min, and 1,400 rpm in a shaking incubator and supported subsequently by 5 min incubation in an ultrasonication bath. Soluble proteins were separated from further cellular components by centrifugation (16,000x g, 60 min, 22 °C). The protein concentration of the isolated supernatant was determined using a Bradford assay against bovine serum albumin as reference protein. Two µg protein of each sample were first diluted in 20 mmol/l ABC-buffer to a urea concentration of maximum 2 mol/l. Proteins were reduced with 2.5 mmol/l dithiothreithol for 30 min at 30 °C, and subsequently alkylated with 10 mmol/l iodoacetamide for 15 min at 30 °C after further dilution with 20 mmol/l ABC to a urea concentration of below 1 mol/l. Proteins were then bound to each 8 µl SP3 beads and digested with trypsin in protein : trypsin ratio of

25:1 as described in a recent publication [92]. Also host peptides were resuspended in 2% DMSO and 2x Buffer A with HRM-peptides similar to the pathogen samples.

2.2.2.5 Immunofluorescence microscopy

For immunofluorescence microscopy HCAEC were seeded on round high precision 18 mm glass coverslips and host cells were infected as described above. At three different time points (3 h p.i., 7.5 h p.i., and 24 h p.i.) coverslips were transferred into a new plate and fixed with 2% paraformaldehyde for 10 min at room temperature. All samples were stained simultaneously after finishing the experiment. The samples were treated with 0.1% Triton X-102 for 5 min at room temperature. The staining solution included 200 ng/ml Hoechst 33258 and 1 U/ml Alexa Fluor™ 568 phalloidin. After 10 min staining in the dark at room temperature, the samples were washed three times with distilled water. The coverslips were mounted on glass object slides with Dako fluorescence mounting medium and stored at room temperature. Fluorescence images were taken with a Keyence BZ-9000. The images acquired were taken with a 20x lens (CFI Plan Fluor ELWD, NA 0.45, WD 8.10 mm). GFP expressing bacteria were detected with an excitation wavelength (EW) of 480±15 nm and an absorption wavelength (AW) of 510 nm. Hoechst 33258-stained DNA was detected at an EW of 360±20 nm and an AW of 460±25 nm. The Alexa Fluor™ 568 phalloidin labeled F-Actin was excited at 560±20 nm and the AW was detected at 630±30 nm. The original images were processed with the BZ-II Analyzer software.

2.2.2.6 Data acquisition by mass spectrometry

Mass spectrometry analyses were performed by Dr. Manuela Gesell Salazar and Dr. Christian Hentschkter in the Department of Functional Genomics, University of Greifswald.

Peptides were separated in an UltiMate 3000 nano-LC system consisting of a combination of a pre-column (Acclaim™ PepMap™ 100 C18 HPLC Columns) and an analytical column (Accucore™ C18 HPLC Columns). A binary gradient of buffer and buffer B was applied at a flow rate of 300 nl/min. Subsequently, peptides were analysed with a Q Exactive™ Plus mass spectrometer in data independent acquisition (DIA) mode as described before [89].

Raw data were analysed using Spectronaut version 14 against a spectral library for *S. aureus* HG001 [89] or human proteins. Data normalization, statistical analysis, and visualization were accomplished with an R script. The script was set up by Dr. Stephan Michalik and the processed data was used for further analysis.

2.2.3 Cytotoxicity assay

2.2.3.1. alamarBlue®

Numerous methods exist to determine cell viability e.g., DNA synthesis, enzyme activity, plasma membrane integrity and cellular reducing conditions. Viable cells maintain a reducing environment in the cytosol. The resazurin-based alamarBlue® cell viability regent uses the reducing environment to quantitatively measure the cell viability. The non-toxic and active reagent resazurin is a cell permeable compound which is blue and non-fluorescent. After entering the cells, resazurin is reduced to the purple and highly fluorescent resofurin. After measuring the absorbance at 560 nm and 590 nm the values of absorbance can be used to quantify the number of metabolically active cells because they are proportional to the reduction of the substrate.

For each PGN experiment, 3 wells with cells grown on Thermanox (1 well for PGN stimulation, 1 well for medium control, 1 well for heat shock treatment for 5 min at 56 °C as a negative control) and 1 well without Thermanox (control) were prepared. After 2 days the cells were either treated with 10 µg/ml PGN or new medium was added to the cells for 12 h. In order to exclude the factor of heterogeneous growth, the cells were then detached, and the same number of cells was seeded in a 96-well plate in a total volume of 100 µl before adding 10 µl alamarBlue® reagent. Additionally, blank controls just with medium, or medium with 10 µg/ml PGN were prepared.

The plate was incubated for 2 h in the incubator. Subsequently, the absorbance was determined at 560 nm and 590 nm with the infinite® M200PRO to calculate the percentage of viable cells.

2.2.4 Cell proliferation

2.2.4.1 BrdU ELISA

The cell proliferation ELISA uses the reagent 5-bromo-2'-deoxyuridine (BrdU). During mitosis BrdU instead of thymidine is incorporated into the DNA of proliferating cells. BrdU can be detected by an antibody-mediated substrate reaction. A peroxidase is conjugated to the secondary antibody and allows a substrate conversion whereby light is emitted. Quantifying the luminescence allows the determination of the relative cell proliferation (Figure 2.2).

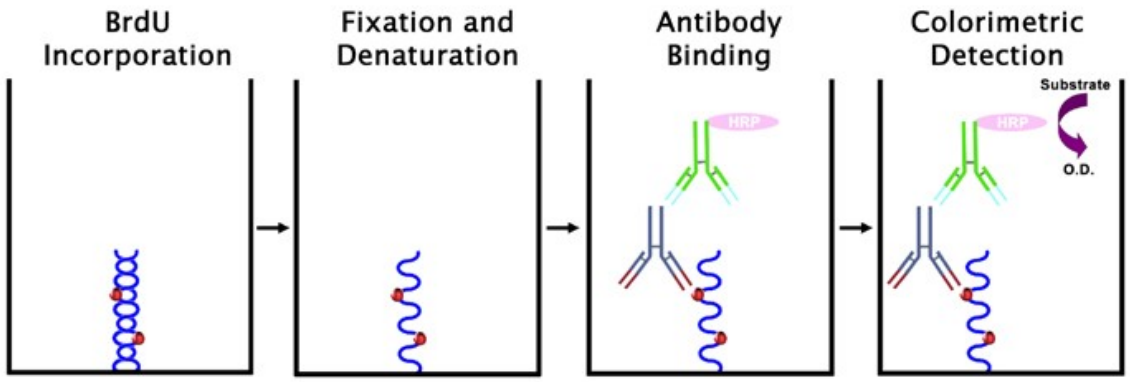

Figure 2.2 Principle of cell proliferation ELISA: BrdU instead of thymidine is incorporated into the DNA of proliferating cells during mitosis. BrdU can be detected by an antibody-mediated substrate reaction. A conjugated peroxidase allows a substrate conversion whereby light is emitted [5].

For PGN experiments, wells with cells grown on Thermanox (for PGN stimulation, medium control, with 0.5% FCS as a negative control, background control without the BrdU labelling solution) and wells with medium, or medium with 10 µg/ml PGN (blank) were prepared. 12,000 cells/well were seeded in a 96-well plate in a total volume of 100 µl and cultivated in the incubator for 2 days. The cell proliferation assay was performed according to the manufacturer's protocol (Cell Proliferation ELISA, BrdU, colorimetric). After 2 days 100 µl of the BrdU labelling solution (except the background samples) was added to each well for 24 h and the BrdU labelling solution including either 10 µg/ml PGN or new medium was added for 12 h.

The supernatant was then removed and 100 µl FixDenat solution was added to each well. After incubating the samples for 30 min at room temperature, supernatant was

removed and 100 µl anti-BrdU POD solution was added to each well. Samples were incubated for 90 min at room temperature, followed by three washing steps with 100 µl washing solution. The supernatant was removed, 100 µl substrate solution was added to each well and was incubated for 10 min at room temperature. The luminescence was then measured at 370 nm and 492 nm as a reference wavelength with the infinite® M200PRO to calculate the relative cell proliferation.

2.2.4.2 xCelligence

The xCelligence Real Time Cell Analyzer DP is able to measure cell proliferation in real-time via non-invasive electrical impedance monitoring (Figure 2.3). A set of gold microelectrodes is fused to the surface of the E-plates. When electrically conductive cell culture medium is applied, an electric potential across the electrodes is generated. By seeding adherent cells into the E-plates, the electron flow is impeded. The number of cells influences the magnitude of the impedance which is calculated as the unitless parameter cell index (CI). In comparison to the BrdU ELISA the cell proliferation can be determined in real-time and not just as an endpoint determination. Furthermore, cytotoxic effects could be determined via a reduction of the CI.

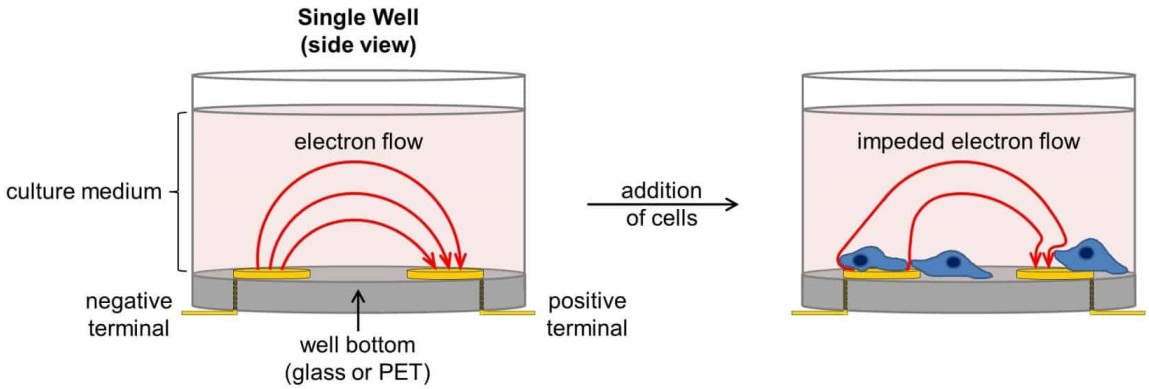

Figure 2.3 Principle of xCelligence to measure the cell index (CI): In the absence of cells an electric potential across the electrodes is generated. When cells attach and proliferate on the gold electrodes, the electron flow is impeded. The impedance is calculated as the CI [4].

The cytotoxicity of PGN was determined in preliminary tests with a concentration range (0, 2.5, 5, 10, 20 µg/ml). As a negative control, cells were incubated with 0.5% FCS over the duration of the experiment of 24 h. At the beginning of the experiment 3,000 cells/well were seeded in a total volume of 100 µl in each well.

After 30 min the development of the CI without any treatment was measured every 15 min for 4 h. During this time the cells were able to attach to the bottom. Afterwards, medium of all wells was removed, medium including PGN as well as the controls with medium and 0.5% FCS were added to the wells in a total volume of 200 µl. The CI was measured every 15 min for another 24 h. The results were analysed with the RTCA-Software.

2.2.5 Cellular stiffness

2.2.5.1 Atomic force microscopy (AFM)

Force distance curves were measured with the AFM (Figure 2.4) to determine the stiffness of the cells. A silica bead (Ø 4.77 µm) was glued to a soft tipless cantilever using a UV-curable liquid photopolymer (NOA 68T). The spring constant (k) of various prepared cantilevers was determined using the thermal noise method [93].

Force measurements were carried out on living HCAEC at 37 °C in cell culture medium using the JPK BioCell and the JPK Nano Wizzard 3. Each measured area had a size of 100 x 100 µm and 20 x 20 grids. The program JPKSPM Data Processing was used to analyse the force distance curves. The relative height and the stiffness of the samples were determined by using the hertz fit-model for the measured force distance curves. The results were further analysed with a MatLab code which was already published [94].

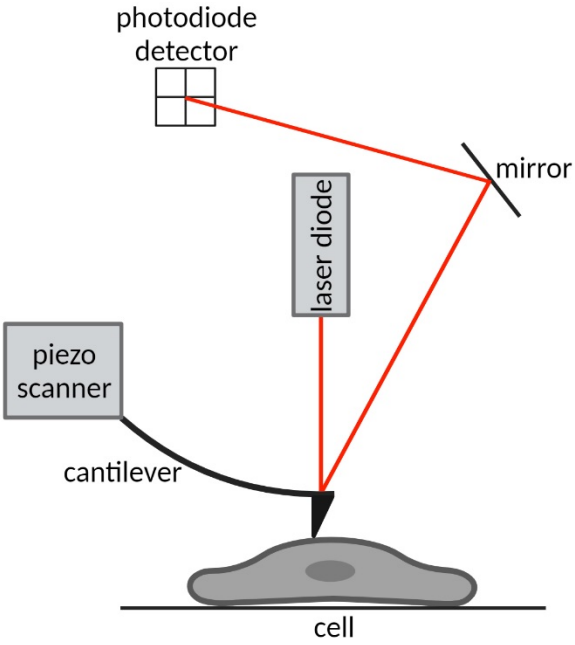

Figure 2.4 Detection scheme for atomic force microscopy (AFM): A cantilever is bent by a defined force, which is controlled by a piezo scanner. A laser diode generates a laser beam which is reflected from the cantilever and can be detected by a photodiode detector. The AFM generates a topographic image of the cell surface by plotting the laser beam deflection as the tip of the cantilever scans the surface (modified from [6]; created with BioRender.com).

2.2.6 Cellular migration

2.2.6.1 Wound healing assay

The implantation of a cardiac implant creates small wounds in the endothelium. In order to evaluate the initial cell growth, the Culture-Inserts 2 Well was applied on Thermanox. 70 µl of a cell suspension with $3x10^5$ cells/ml were seeded in each well. For PGN experiments, the stimulation was performed 12 h prior to the beginning of the experiment. After 24 h the insert was removed, and the cell movement was captured over 24 h with the JuLi™ Life Cell Analyser. Images were taken at a frequency of 1 frame/15 min and were analysed by Jan Oldenburg and Dr. Michael Stiehm (iib e.V., University of Rostock) with a newly developed method [95].

2.2.6.2 Cell perfusion experiments

Flow experiments were performed with two different cell perfusion systems: flow chamber system FCS^{1c} and ibidi pump system.

2.2.6.2.1 Flow chamber system FCS[1c]

In order to analyse the cellular stiffness with the AFM, the flow chamber system FSC[1c] was used. With this system, a defined shear stress can be applied to a cellular monolayer. HCAEC were seeded on Thermanox with a diameter of 22 mm in a 12-well plate with a density of $1x10^5$ cells/well in EnGS medium with 10% FCS. When a confluent cell layer was reached, the sample was inserted into the system (Figure 2.5).

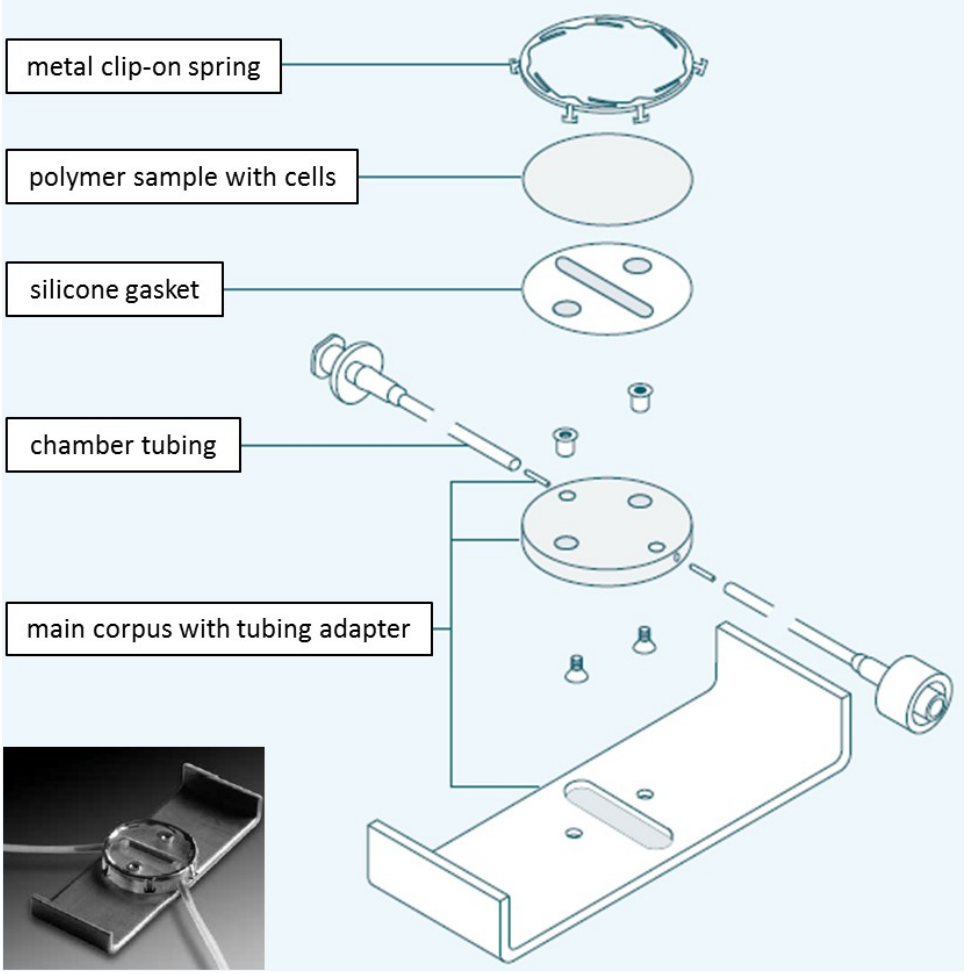

Figure 2.5 Assembly of the flow chamber system (provitro): On the main corpus the chamber tubing and the silicone gasket was placed. A longitudinal recess forms the flow channel which is covered with Thermanox with a confluent cell layer. The system is fixed by a metal clip-on spring (modified from [3]).

An external tube system was added to the tubing adapter which built the connection between the flow chamber system and a reservoir filled with cell medium. A peristaltic pump was used to circulate the medium from the reservoir to the flow channel. Shear stress (1.5 dyn/cm^2) in form of a laminar flow was applied for 3 h with

the flow chamber system. The experiment was performed under an incubation hood at 37 °C. Afterwards, the cellular stiffness was measured by AFM.

Technical data:

channel length [l]	1.5 cm
channel width [b]	0.2 cm
channel height [h]	0.05 cm
shear stress [T]	0-30 dyn/cm^2

The shear stress was calculated with the following formula: $T = \frac{3\mu Q}{2b^2h}$

T describes the shear stress [dyn/cm^2], μ the viscosity [g x cm^{-1} x s^{-1}] and Q the volume flowrate [ml/s].

The following applies: 1 dyn/cm^2 ≙ 0.1 Pa.

2.2.6.2.2 Ibidi pump system

As a second method, shear stress was applied to the cells using the ibidi pump system (Figure 2.6). The system allows shear stress experiments under defined flow conditions over a certain time period. Additionally, live cell imaging can be performed using the live cell analyser, JuLI™ FL. The advantage is that these experiments can be performed in an incubator under ideal cell culture conditions. A sticky–Slide I $^{0.8}$ Luer was connected to the perfusion system which consisted of silicone tubing, two syringe reservoirs which were filled with medium and covered with sterile air filters. This application was connected to a fluidic unit which was, in turn, connected to the pump. A drying bottle with silica beads eliminates excess water. Defined laminar flow conditions were software-controlled and maintained a shear stress of 1.5 dyn/cm^2 imitating venous shear stress or shear stress in recirculation areas of a cardiac implant.

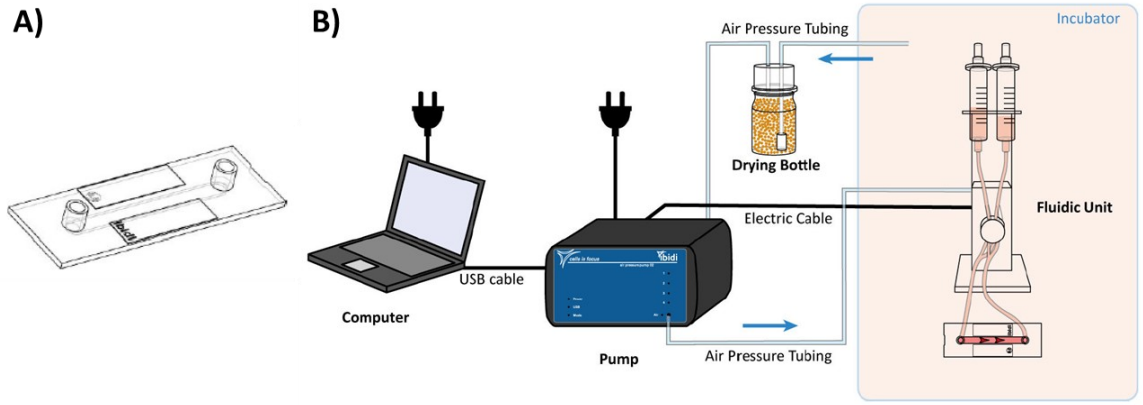

Figure 2.6 Ibidi perfusion set: A) schematic illustration of the µ-slide, B) schematic setup of the perfusion set including the computer, the pump, a drying bottle and the fluidic unit which is placed in an incubator [2].

For analysing the cellular migration, the samples were connected to two syringe reservoirs filled with EnGS medium with 2% FCS. The shear stress was then applied for 15.5 h before the cells were detached. The cell suspension was centrifuged for 5 min at 5,000 g, the supernatant was discarded, and the cells were resuspended in 1 ml PBS. After another centrifugation step the cell pellets were shock frozen with liquid nitrogen and then stored at –80 °C until further methods like RNA purification or Western Blot were performed.

2.2.6.3 Live cell imaging and tracking of endothelial cells

The application of sticky–Slide I $^{0.8}$ Luer in combination with the JuLi™ Life Cell Analyser, allowed a live cell imaging during cell perfusion experiments over 15 h. Images were taken at a frequency of 1 frame/15 min. All images were analysed by manual tracking using ImageJ. 20 cells per sample were analysed. The image was divided in four areas and five cells per quadrant were tracked. The results of the tracking analysis were further analysed with the Chemotaxis and Migration Tool. The directionality, velocity, accumulated distance, and Euclidean distance (length of straight line between cell start and end point) were determined. The directionality describes the ratio of Euclidean distance to accumulated distance where 1 represents a linear movement.

2.2.7 Gene expression analysis

2.2.7.1 Purification of total RNA

The RNeasy® Mini Kit was used for purification of total RNA. In order to lyse the cells 350 µl Buffer RLT containing beta-mercaptoethanol (β-ME) was applied. The reducing agent β-ME irreversibly denatures RNases by reducing disulfide bonds and therefore destroys the native conformation which is required for enzyme functionality. 350 µl of 70% ethanol was added to the cell lysate and the solution was mixed. The sample was transferred to a RNeasy Mini spin column placed in a 2 ml collection tube and centrifuged for 1 min at 10,000x g. The flow-through was discarded. In order to digest the DNA, 700 µl Buffer RW1 was added to the RNeasy column and centrifuged for 1 min at 10,000x g. The RNase-Free DNase Set was used to eliminate DNA which could negatively influence the gene expression analysis. A DNase I incubation mix with 10 µl DNase stock solution and 70 µl Buffer RDD was prepared, mixed gently by inverting the tube and was briefly centrifuged. The DNase I incubation mix was directly added to the RNeasy column membrane and incubated at room temperature for 15 min. 350 µl Buffer RW1 was added to the RNeasy column and the sample was centrifuged for 1 min at 10,000x g. The flow-through was discarded. 500 µl Buffer RPE was added to the RNeasy column and the sample was centrifuged for 3 min at 8,000x g. The RNeasy column was placed on a new 1.5 ml collection tube and then placed on ice before eluting the RNA. 20 µl RNase-free water was added directly to the column membrane and incubated for 3 min at room temperature. The sample was centrifuged for 1 min at 10,000x g to elute the RNA. The flow-through was pipetted once again on the RNeasy column and centrifuged for 1 min at 10,000x g to increase the amount of RNA.

2.2.7.2 Quantitative RNA analysis

The amount of RNA was determined with NanoDrop™ 2000 Spectrophotometer. The wave length at 260 nm (total amount of RNA) and at 280 nm (contamination with proteins) was measured. The quotient of 260/280 should be between 1.8 and 2.0. If a high contamination with proteins was present the quotient would decrease. Each sample was measured twice with a volume of 1.5 µl RNA solution.

2.2.7.3 cDNA synthesis

Via reverse transcription the synthesis of complementary DNA (cDNA) from the RNA template was performed with the TaqMan® Gene Expression Assays. A short primer which is complementary to the 3' end of the RNA is used for the synthesis of the cDNA. A 50 µl reaction was prepared (see table 2.2.1) with 400 ng RNA and the thermal cycler program which can be seen in table 2.2.2 was applied.

Table 2.2.1 Reagent volumes for a 50 µl cDNA reaction

Component	Volume
10X RT Buffer	5 µl
$MgCl_2$ (25 mM)	11 µl
dNTP mix (10 mM)	10 µl
Random hexamer primer (50 µM)	2.5 µl
RNase Inhibitor (20 U/µl)	1 µl
Reverse Transcriptase (50 U/µl)	1.25 µl
Template RNA (400 ng) in distilled H_20	19.25 µl

Table 2.2.2 Cycling parameters for cDNA synthesis

Step	Temperature	Time	Number of cycles
Annealing of primer	25 °C	10 min	1
Reverse Transcription	48 °C	30 min	1
Inactivation	95 °C	5 min	1
Hold	4 °C	indefinitely	
Storage	-20 °C		

Reverse transcriptases (RTs) use an RNA template and a short primer complementary to the 3' end of the RNA to direct the synthesis of the first strand cDNA. This cDNA can then directly be used as a template for the polymerase chain reaction (PCR). This combination of reverse transcription and PCR (RT-PCR) allows the detection of low abundance RNAs in a sample.

2.2.7.4 Real-time quantitative PCR using TaqMan®

A sensitive method to quantify nucleic acids is the real-time quantitative PCR. Traditional PCR enables the detection of PCR amplification at the endpoint of the PCR reaction. A high number of cycles can, however, lead to a saturation of the reaction. The advantage of real-time analysis is the detection of PCR amplification during early phases of the PCR.

In 1991 Holland *et al.* produced evidence of the thermostable DNA polymerase from the organism *Thermus aquaticus* which has a 5´ to 3´ exonuclease activity. During PCR the 5´ nuclease activity of the DNA polymerase allows a cleavage of the target probe which can be used to detect the amplification of a target-specific product [96]. The probe for the TaqMan® assay has a fluorescence reporter dye (FAM or VIC) which is attached to its 5´ end and a quencher dye (TAMRA) at its 3´ terminus. The proximity of the reporter and quencher dyes permit Förster resonance energy transfer (FRET) in an intact probe. The energy is transferred from the donor to the quencher and no fluorescence emission occurs.

When a complementary target sequence is present in the sample, the fluorogenic probe anneals and is cleaved by the 5' nuclease activity of the Taq polymerase enzyme during the extension phase of the PCR leading to a spatial separation of donor and quencher. The resulting fluorescence intensity is directly proportional to the amount of produced amplicons [97]. A duplication of the material in each PCR cycle is present in the exponential phase, allowing for a correct quantification of the produced amplicons. This number of amplicons, in turn, is proportional to the template quantity used for the experiment.

A list of applied TaqMan® primers is stated in table 2.2.3, the reagent volumes for a 10 µl RT-qPCR reaction in table 2.2.4 and the cycling parameters for a TaqMan®-RT-qPCR, which was performed with the CFX96 Touch™ Real-Time PCR Detection System, can be found in table 2.2.5. The $2^{-\Delta\Delta CT}$ method was used to determine the relative gene expression of the target gene. The threshold cycle (CT) is the cycle at which the fluorescence level reaches a certain amount (threshold). The calculation of the CT-value of a single probe was performed by calculating the mean of the duplicate determination. A housekeeping gene (GAPDH) was also measured to be able to

normalize the CT-values (ΔCT). Housekeeping genes are a ubiquitously expressed and are expected to maintain a stable expression level in all conditions because they are involved in the basic cell maintenance. The ΔΔCT-values were calculated by normalizing the ΔCT-values with an untreated control sample. For all genes a no template control (NTC) was performed. The Bio-Rad CFX-Manager was used to analyse the results.

Table 2.2.3 Applied TaqMan® primers

Gen	**Assay number**	**Manufacturer**
ACTA2	Hs00909449_m1	Thermo Fisher Scientific Inc. (USA)
ACTN4	Hs00245168_m1	Thermo Fisher Scientific Inc. (USA)
CALM1	Hs00300085_s1	Thermo Fisher Scientific Inc. (USA)
GAPDH	Hs02758991_g1	Thermo Fisher Scientific Inc. (USA)
ICAM1	Hs00164932_m1	Thermo Fisher Scientific Inc. (USA)
IL-6	Hs00985639_m1	Thermo Fisher Scientific Inc. (USA)
NOS3	Hs01574665_m1	Thermo Fisher Scientific Inc. (USA)
PECAM1	Hs00169777_m1	Thermo Fisher Scientific Inc. (USA)
VCAM1	Hs00365485_m1	Thermo Fisher Scientific Inc. (USA)

Table 2.2.4 Reagent volumes for a 10 µl RT-qPCR reaction

Component	**Volume**
2x Master Mix	5 µl
20xPrimer	0.5 µl
cDNA	2 µl
distilled H_20	2.5 µl

Table 2.2.5 Cycling parameters for TaqMan®-RT-qPCR

Step	Temperature	Time	Number of cycles
carry over digestion	50 °C	2 min	1
Activation of Taq-polymerase	95 °C	10 min	1
Denaturation of cDNA	95 °C	15 sec	40
Annealing and elongation	60 °C	1 min	40
Hold	4 °C	indefinitely	

2.2.8 Western Blot

2.2.8.1 Cell lysis, protein isolation and determination of protein content

For static experiments, cells of 1 12-well and for flow experiments, cells of 4 sticky–Slide I $^{0.8}$ Luer were detached and resuspended in 100 µl lysis buffer. The lysate was aspirated 10x with a cannula attached to a 1 ml syringe. The solution was incubated for 5 min at 95 °C and 500 rpm, and centrifuged for 5 min at 10,000 rpm. The protein-containing supernatant was transferred in a new tube which was stored at -20 °C until further usage.

The protein concentrations of prepared cell lysates were determined with the Pierce™ BCA Protein Assay Kit according to the manufacturer's protocol. The BCA standard was diluted in sterile water (0-400 µg/ml) and the sample was diluted 1:5. 10 µl of the standard and the protein sample was transferred twice in a 96-well plate in duplicates, and 200 µl staining reagent was added. After incubation for 30 min at 37 °C in the dark, the absorbance was measured at 562 nm with the Synergy H1 Hybrid Multi-Mode Reader and the software Gen5™ was used to calculate the protein content.

2.2.8.2 Sodium dodecyl sulphate polyacrylamide gel electrophoresis

Sodium dodecyl sulphate polyacrylamide gel electrophoresis (SDS-PAGE) is a frequently used method to separate proteins by their molecular mass. The separation of proteins is performed with a polyacrylamide gel, which contains a large-pored stacking gel and a small-pored separation gel. SDS destroys secondary and non-disulfide-linked tertiary structures. It is an anionic detergent and leads to negatively

charged molecules when it is dissolved. In an electric field these negative charges attract the molecules towards the anode.

The TGX Stain-Free™ FastCast™ Acrylamide Kit (7.5% and 12%) was applied to prepare a gradient gel. Two glass plates were assembled in a casting frame with 1.5 mm spacer. This was then placed in a casting stand before adding the gel components. TEMED (N,N,N',N'-tetramethylethylenediamine) and 10% APS (ammonium persulfate), which initiate the polymerization of the gel, were added to the separating gel (7.5% and 12%), which was then added in the gradient maker. The stacking gel was also prepared with TEMED and 10% APS, was directly added on top of the separation gel and the comb with 15 comb teeth. After 30 min the gel was polymerized.

Laemmli buffer was added to the protein samples with a final concentration of 10 µg. The samples were incubated at 95 °C for 5 min. The gels were transferred in a buffer tank which was filled with 10% running buffer. The gel pockets were rinsed and the marker as well as the protein samples were added. The protein samples were separated for 25 min and 300 Volt. Proteins are accumulated in a large-pored separation gel despite of the protein size. The small-pored separation gel is used to separate the proteins regarding to their molecular mass. Small molecules migrate faster than larger proteins in the small-pored separation gel. The protein size mainly depends on the molecular weight when complex structures are denatured. The determination of molecular masses was accomplished by comparing the protein bands to marker proteins with known sizes.

2.2.8.3 Blotting and staining of proteins

Western blotting is a technique where separated proteins are electrophoretically transferred to a nitrocellulose membrane. After blotting the gel, the proteins are accessible for specific antibodies, which are used to visualize the transferred proteins. In this work the semi-dry technique was applied using a Trans-Blot SD Semi-Dry Transfer Cell and the Trans-Blot® Turbo™ Transfer System RTA Transfer Kit, Nitrocellulose. The filter papers, the membrane and the separation gel were incubated in transfer buffer for 5 min before locating them in the blot chamber. To blot the separated proteins, the materials were arranged as following from the anode to the

cathode: filter paper, nitrocellulose membrane, SDS gel and filter paper. After removing the air bubbles, an electric field with 15 Volt was applied for 15 min. The gel and the nitrocellulose membrane were detected with the ChemiDoc™ MP System to check the blotting process.

Afterwards, the membrane was cut into strips regarding the different protein bands. The membrane strips were washed in distilled water. To prevent unspecific binding of the antibodies, the membrane was incubated in blocking buffer for 1 h at room temperature.

The primary antibody was diluted in 1% BSA/TBST and was added to the membrane which was incubated over night at 4 °C. The membrane was washed three times with TBST before adding the secondary antibody, which was diluted in TBST. After an incubation step for 1 h at room temperature, the membrane was washed three times with TBST. The Clarity™ Western ECL Substrate Kit was used to detect the proteins with the ChemiDoc™ MP System. Image Lab was used to quantify the intensities they were normalized to GAPDH.

2.2.9 ELISAs

2.2.9.1 IL-6 ELISA

For a confluent cell layer $0.5x10^5$ cells/well were seeded on round Ø=22 mm Thermanox plastic coverslips in a 12-well plate three days prior to the beginning of the experiment. For preliminary studies, different *S. aureus* PGN concentrations (2.5 µg/ml, 5 µg/ml, 10 µg/ml, 20 µg/ml) were tested with an incubation period of 24 h on a confluent HCAEC cell layer and additionally, a concentration of 10 µg/ml was tested in a time series (3 h, 6 h, 12 h and 24 h). After a specific time period, the supernatant was collected, centrifuged for 5 min at 1000 g and aliquots were stored at -20 °C. Supernatants were diluted 1:50 in calibrator diluent RD5T. The IL-6 ELISA was performed according to the manufacturer's protocol (Human IL-6 Quantikine® ELISA).

2.2.9.2 sPECAM-1 ELISA

The supernatant of the experiments of platelet adhesion were checked for sPECAM-1 concentrations. After the incubation step of platelets on Thermanox, the supernatant

was collected, centrifuged for 5 min at 5000 g and aliquots were stored at -20 °C. Supernatants were diluted 1:5 in sample diluent. The sPECAM-1 ELISA was performed according to the manufacturer's protocol (Human sPECAM-1 Instant ELISA Kit).

2.2.9.3 sP-selectin ELISA

The supernatant of the experiments of platelet adhesion were checked for sP-selectin concentrations. After the incubation step of platelets on Thermanox the supernatant was collected, centrifuged for 5 min at 5000 g and aliquots were stored at -20 °C. Supernatants were diluted 1:5 in sample diluent. The sP-selectin ELISA was performed according to the manufacturer's protocol (Human sP-selectin ELISA Kit).

2.2.10 Immunofluorescence microscopy of actin and eNOS

For immunofluorescence microscopy, HCAEC were seeded on round high precision 10 mm glass coverslips ($0{,}4x10^5$ cells per well) in a 48-well plate or on a glass slide which was previously attached to an ibidi slide (80,000 cells). After three days the samples were treated with 10 µg/ml PGN for 12 h or the medium was changed before starting the experiment under static or flow conditions (1.5 dyn/cm^2). The samples were fixed with 2% paraformaldehyde for 10 min at room temperature. Afterwards, they were washed three times with PBS+1% BSA. All samples were stained simultaneously after finishing all experiments. The samples were treated with 0.1% Triton X-100 for 5 min at room temperature. After washing the samples three times with PBS+1% BSA, they were blocked with PBS+1% BSA for 1 h. The staining solution included the primary antibody of eNOS (ab76198) diluted 1:200 and was incubated overnight on a shaker at 4°C. The following day, the samples were washed three times with PBS+1% BSA and then treated with the secondary antibody of eNOS (goat-anti-mouse Alexa 568, 1:200) and AlexaFluor™ 488 phalloidin. After an incubation step for 1 h in the dark, the samples were washed three times with PBS+1% BSA, incubated with DAPI (diluted 1:1000) for 10 min at room temperature, and again washed three times with PBS+1% BSA. All samples were fixed on a glass slide or glass cover slips with ibidi mounting medium and stored at room temperature. Fluorescence images were taken with a Keyence BZ-9000. The images were acquired with a 20x lens (CFI Plan Fluor ELWD, NA 0.45, WD 8.10 mm).

Actin (GFP) was detected with an excitation wavelength (EW) of 480±15 nm and an absorption wavelength (AW) of 510 nm. DAPI (nucleus) was detected at an EW of 360±20 nm and an AW of 460±25 nm. eNOS was excited at 560±20 nm and the AW was detected at 630±30 nm. The original images were processed with the BZ-II Analyzer software.

2.2.11 Platelet adhesion

2.2.11.1 Platelet isolation and sample preparation

Blood samples were taken in sterile citrate containers and were centrifuged for 15 min at 150x g. The platelet rich plasma (PRP) was collected, and the remaining blood sample was centrifuged for 15 min at 2,000x g. The platelet poor plasma (PPP) was collected to dilute the PRP and as a control for aggregometer measurements. The platelet aggregation and activation were determined with the Chrono-log Model 700 using ATP standard and collagen according to the manufacturer's protocol (Figure S 1). Platelet concentration was determined with a Neubauer counting chamber. A solution of $2x10^8$ platelets/ml was prepared and incubated with 2.5 mM $CaCl_2$ and 1 mM $MgCl_2$ for 30 min at 37 °C. For PGN experiments the incubation with PGN was included in this step. As negative controls unstimulated and PGN stimulated platelets were additionally treated with 1 µM Prostaglandin E_1. Thermanox was treated with PBS^+Mg^{++}/Ca^{++} for 30 min at room temperature. Afterwards, $2x10^8$ platelets/ml were added for 2 h at 37 °C and were washed three times with PBS Mg^{++}/Ca^{++} to remove non-adherent platelets. Samples were fixated with 2.5% glutaraldehyde for 1 h at room temperature. The samples were dehydrated in a graded series of acetone and critical-point dried. Subsequently, the samples were mounted on aluminium stubs and were sputtered with gold-palladium. The scanning electron microscopy (SEM) was performed with the EVO LS10 scanning electron microscope. The surface evaluation was acquired with 100x, 500x and 2000x magnification. Platelet adhesion on the 500x magnification was analysed and quantified using ImageJ software.

2.2.12 Statistical analysis

Analysis of all raw data was performed with Excel. Graphical representation and statistical analysis of the results was performed with Prism 5. Statistical analysis of AFM data was carried out with R. Statistical analysis of cell viability and proliferation was conducted using a one-way ANOVA with Dunnett's post hoc test for multiple comparisons, to compare all columns to a single control column. Gene expression and IL6 concentrations were analysed with a one-way ANOVA and a Dunnett analysis to compare all columns to a control column or followed by a Bonferroni analysis to compare selected pairs of columns for time lapse experiments. An unpaired t-test was performed for the results of cell migration, protein expression and platelet experiments. For normalized data (e.g., cell viability) the value 1 or 100 was defined for the control group. Graphical representations show the mean±SD (internalization experiments, viability, proliferation, migration, wound healing, gene expression, protein expression, IL-6 concentration, platelet aggregation), or mean±95% CI (AFM). Significant differences to control groups were marked with * for $p<0.05$, ** for $p<0.01$ and *** for $p<0.001$.

Results

3.1 Influence of a *S. aureus* infection on HCAEC

A cell culture model using HCAEC was applied to monitor potential interactions and adaptations of *S. aureus* similar as in endocarditis. Therefore, HCAEC were infected with the clinical strain T-72949 isolated from an endocarditis patient [98], or for comparison with a well-established control strain HG001 [99] at an MOI of 10. Both strains contained a plasmid pJL-sar-GFP optimized for codon usage**,** which ensured a constitutive GFP production. This characteristic was used for cell separation into infected and non-infected host cells, bacterial counting, separation of bacteria from lysed host cells, and for fluorescence microscopy.

3.1.1 Temporal development of host cells and *S. aureus* strains

Mock-infected control cells had higher cell numbers in the first 24 h p.i. compared to *S. aureus* infected cells and maintained up to 72 h p.i. an almost constant cell number. Bacterial and host cell counting at the indicated time points post infection (p.i.) revealed bacterial survival during the observation period (Figure 3.1). The numbers of host cells decreased over time (Figure 3.1 A). Additionally, the number of bacteria decreased almost steadily from ~$5x10^5$ (1.5 h p.i.: T-72949 $4.4x10^5 \pm 0.6x10^5$, HG001 $6.0x10^5 \pm 2.3x10^5$) to ~$2x10^5$ (72 h p.i.: T-72949 $1.7x10^5 \pm 0.8x10^5$, HG001 $2.5x10^5 \pm 1.0x10^5$) bacteria per well (Figure 3.1 A) or from ~ five (1.5 h p.i.: T-72949 4.5±0.98, HG001 5.4±1.55) to ~ two (72 h p.i.: T-72949 2.1±1.03, HG001 2.9±1.16) bacteria per host cell (Figure 3.1 B) with no distinct differences between both strains. At 10.5 h p.i. strain HG001 ($7.7x10^5 \pm 2.6x10^5$) was counted in higher amounts than endocarditis strain T-72949 ($3.7x10^5 \pm 0.8x10^5$). Live-cell imaging confirmed that both strains were able to replicate in HCAEC. In cells infected with T-72949, bacteria replicated faster and to a greater extent resulting in an earlier cell burst compared to cells infected with HG001 (Videos on the enclosed CD).

3.1 Influence of a S. aureus infection on HCAEC

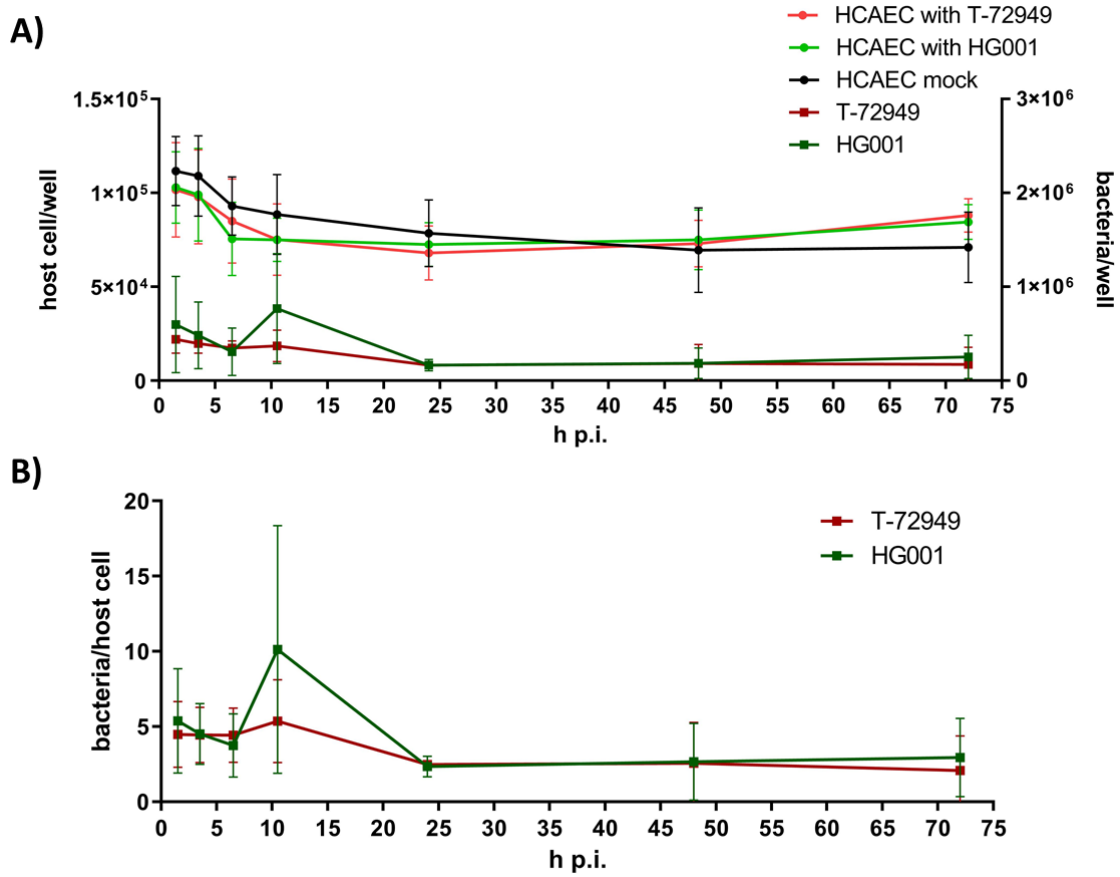

Figure 3.1 Effect of a *S. aureus* infection on human coronary artery endothelial cells (HCAEC): HCAEC were infected with *S. aureus* strain HG001 (control strain) and endocarditis strain T-72949. The number of host cells was determined with an automatic cell counter and the internalized bacteria were counted with the Guava® easyCyte. Presented are the mean values of A) host cells/bacteria per well and B) bacteria per host cell. The mean of five independent experiments ± SD is presented in the graphs.

Fluorescence microscopy at three selected time points (3 h, 7.5 h and 24 h p.i.) was performed to confirm the collected data of infected host cells and internalized bacteria. A constant bacterial number and distribution over the cells for both bacterial strains were detected with an infection rate of ~10% (Figure 3.2).

3.1 Influence of a S. aureus infection on HCAEC

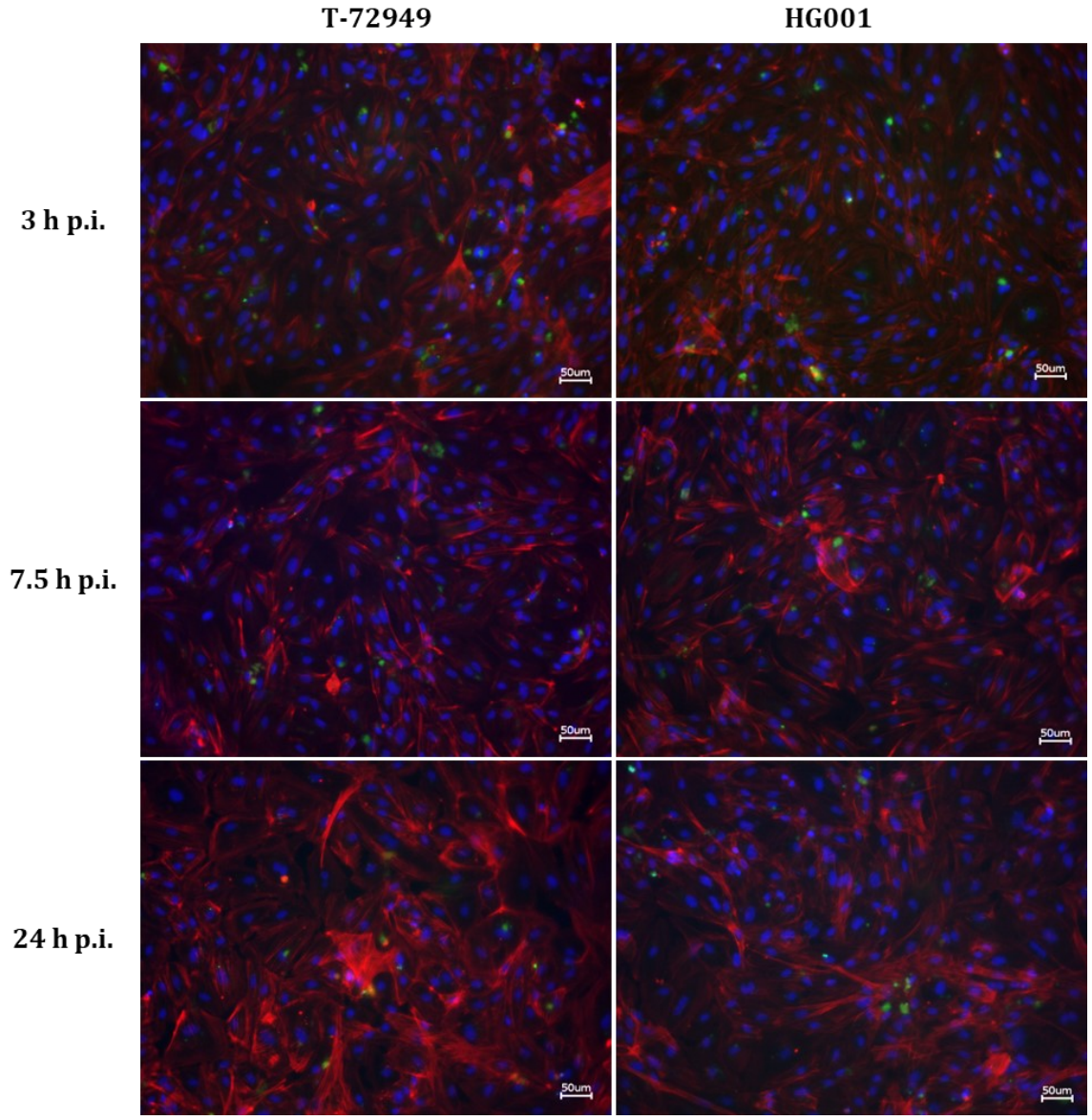

Figure 3.2 Fluorescence microscopy of human coronary artery endothelial cells (HCAEC) infected with *S. aureus* strain HG001 and endocarditis strain T-72949: The rate of infection (~10%) was determined for three different time points (3 h, 7.5 h and 24 h p.i.). F-Actin of HCAEC was stained with Alexa Fluor® 586 Phalloidin (red), the DNA of the nuclei was stained with Hoechst 33258 (blue) and the internalized *S. aureus* strains expressed GFP (green).

3.1.2. Proteome adaptation of host cells to infection with two different *S. aureus* strains

Furthermore, a proteome analysis was performed to potentially monitor varying pathogenic proteome patterns depending on the infecting strain. HCAEC were infected with HG001 or T-72949 with an MOI of 10 or treated with sterile medium as a mock control. The GFP expressing bacteria allowed a separation of host cells into GFP positive (GFP_{pos}) cells with intracellular bacteria and GFP negative (GFP_{neg}) cells without intracellular bacteria at each time point (1.5 h, 3.5 h and 6.5 h p.i.).

Differences in protein abundance between GFP_{pos}, GFP_{neg} and non-infected mock cells were analysed (Figure 3.3). In total, 2430 proteins were identified and quantified over the whole database. Out of these, 1082 proteins were significantly changed ($q < 0.05$, absolute fold change > 1.5) in HCAEC infected with T-72949 compared to non-infected mock cells and 916 proteins were significantly changed in HCAEC infected with HG001 compared to non-infected mock cells after 6.5 h p.i. (green circles, Figure 3.3). An overlap of 608 (43.7%) proteins showed significant differences to mock cells in the proteome profiles of HCAEC infected with T-72949 or HG001. A total of 474 proteins were exclusively altered in abundance in host cells infected with T-72949 and 308 proteins in host cells infected with HG001 each compared to mock cells. Higher numbers of proteins were significantly changed in level comparing GFP_{pos} HCAEC with non-infected mock cells (T-72949: 653 proteins with altered abundance; HG001: 758 proteins with altered abundance) compared to GFP_{neg} cells (white circles, Figure 3.3). In GFP_{neg} HCAEC compared with non-infected mock cells only 237 proteins were altered in abundance after infection with T-72949 and 78 proteins after infection with HG001 over all investigated time points. The overlap of proteins with significant differences to mock cells was higher in GFP_{pos} and GFP_{neg} host cells after an infection with strain T-72949 (192 proteins) compared to HG001 infected cells (80 proteins).

3.1 Influence of a S. aureus infection on HCAEC

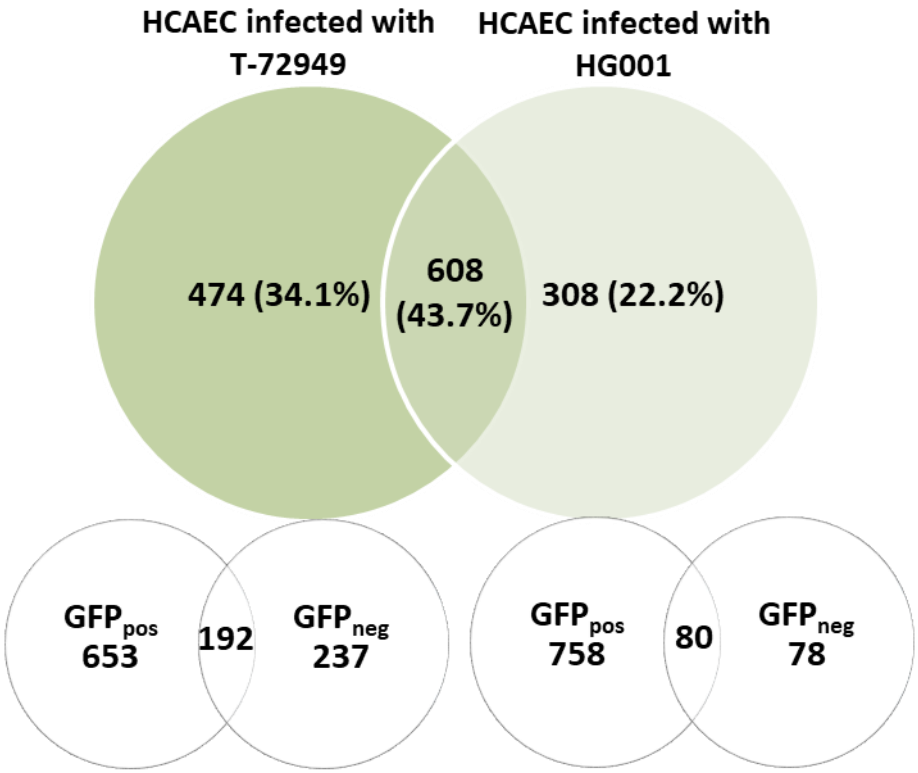

Figure 3.3 Classification of proteins expressed in human coronary artery endothelial cells (HCAEC) after bacterial infection: The Venn diagrams illustrate the number of proteins with significantly altered abundance ($q < 0.05$, absolute fold change > 1.5) over time in dependence of the infecting strain (green circle, endocarditis strain T-72949 left, control strain HG001 right) or in dependence of the infecting state (GFP_{pos} = host cells with intracellular bacteria, GFP_{neg} = host cells without intracellular bacteria). Numbers in the intersections refer to proteins significantly regulated in host cells by both bacterial strains within 6.5 h post infection, those at the outer edges indicate the number of proteins regulated only by the indicated strain within 6.5 h post infection or to proteins significantly changed in both GFP_{pos} and GFP_{neg} host cells.

Functional analysis with Ingenuity Pathway Analysis (IPA) revealed differences on pathway level during the time period in dependence of the infecting bacterium and the host's infection state (GFP_{pos}/GFP_{neg}) (Figure 3.4-3.5). Figure 3.4 shows a comparison of GFP_{pos} vs. GFP_{neg} host cells infected with the endocarditis strain T-72949 or control strain HG001. The five most regulated pathways in HCAEC after bacterial infection in GFP_{pos} host cells compared to GFP_{neg} host cells indicated a relevance of EIF2, EIF4, sirtuin, mTOR and RhoGDI signaling. In cells infected with T-72949, the canonical pathways altered significantly in comparison to GFP_{pos}/GFP_{neg} cells at the early time point of infection (1.5 h p.i.). After infection with strain HG001, the canonical pathways were modified to a higher extent after 6.5 h p.i. (Figure 3.4).

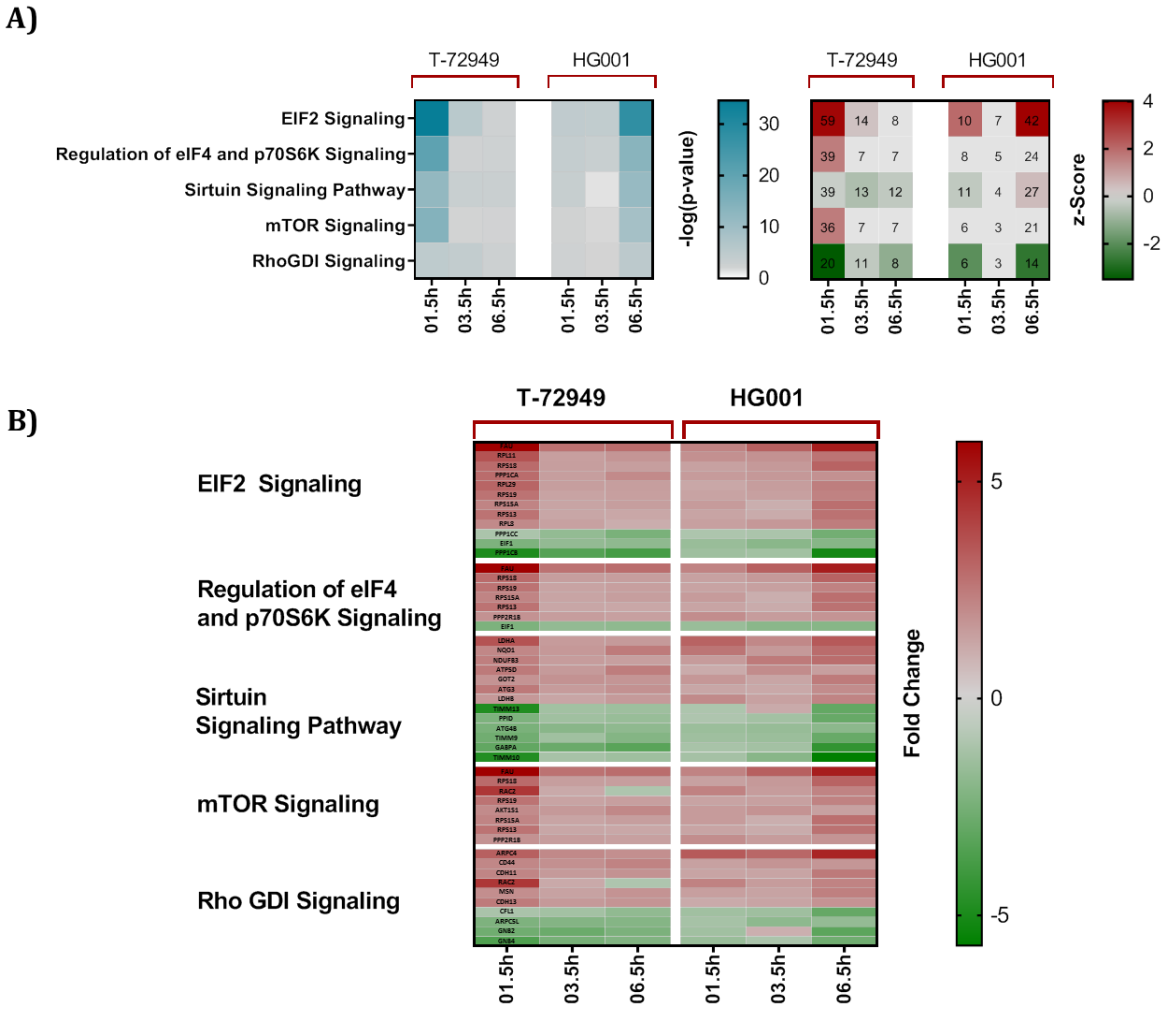

Figure 3.4 Regulated pathways in human coronary artery endothelial cells (HCAEC) after bacterial infection: (A) The heat map shows the five most extensively enriched canonical pathways in GFP_{pos} host cells compared to GFP_{neg} host cells based on all identified proteins. The negative log transformed significance value determined with Fisher's exact test is shown. Additionally, the activation z-Score indicates the direction of the regulation. The number of regulated proteins within the identified pathways is also given in the activation z-Score heat map. QV 0.05, FC |1.5|. (B) Specific proteins with a z-Score of >10/<-10 are significantly regulated (QV 0.05, FC |1.5|) in at least one of the six groups.

Additionally, selected pathways related to bacterial recognition, cytokine production, and infection-related cellular processes were analysed, where proteins displayed changes in abundance compared to non-infected mock cells (Figure 3.5). The intracellular fate of *S. aureus* can be retraced by analyzing the bacterial recognition/uptake, cytokines, which are important mediators of the inflammatory response, and specific cellular processes regarding the cytoskeleton, apoptosis, endocytosis, and phagosome [100-102]. Both bacterial strains caused higher levels of proteins involved in integrin signaling, ILK signaling, IL-8 signaling and actin cytoskeleton signaling and a decreased level of proteins

involved in apoptosis signaling compared to non-infected mock cells. In general, pathways were less affected in GFP_{neg} host cells than in GFP_{pos} host, each compared to mock cells (Figure 3.5).

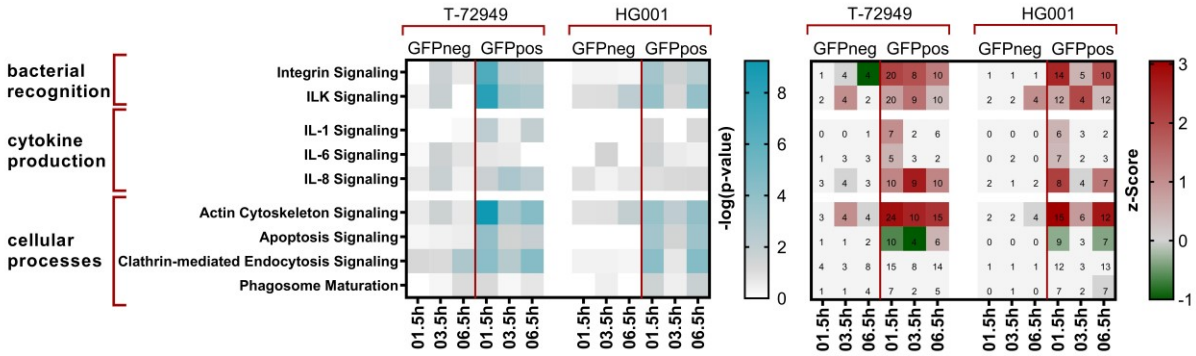

Figure 3.5 A selection of regulated pathways of proteins expressed in human coronary artery endothelial cells (HCAEC) after bacterial infection: The heat map on the right side shows the regulation of selected pathways relevant to recognition and signaling after *S. aureus* infection in infected host cells compared to non-infected host cells. The negative log transformed significance value determined with Fisher's exact test is shown. Additionally, the activation z-Score indicates the direction of the regulation. The number of regulated proteins within the identified pathways is also given in the activation z-Score heat map. QV 0.05, FC |1.5|.

3.2 Influence of PGN on HCAEC

PGN is a cell wall component of Gram-positive bacteria and can cause a pro-inflammatory response in different cell types, including ECs [103]. Hence, stimulation of HCAEC with PGN was used as an equivalent to bacterial internalization experiments.

3.2.1. Preliminary tests to evaluate the concentration and time period for PGN stimulation

A concentration series (2.5 µg/ml, 5 µg/ml, 10 µg/ml, 20 µg/ml) and a time series (3 h, 6 h, 12 h, 24 h) was tested for PGN (Figure 3.6-3.8). Regarding the cell viability no negative effect of PGN was detected (Figure 3.6 A). The cell proliferation decreased slightly in a concentration-dependent manner (Figure 3.6 B).

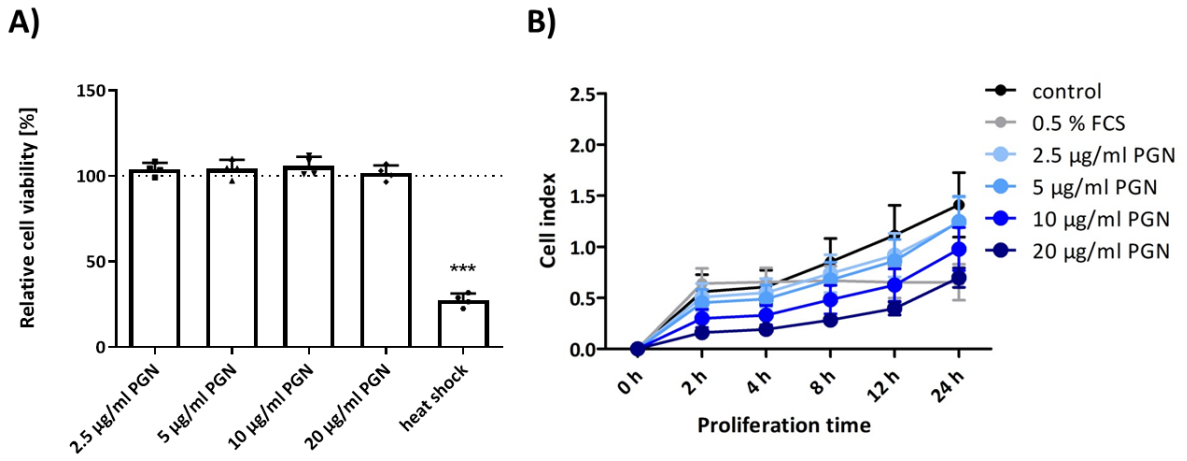

Figure 3.6 Cytotoxicity test of peptidoglycan (PGN): human coronary artery endothelial cells (HCAEC) were stimulated with a concentration range of PGN for 24 h. A) The cell viability was determined with the alamarBlue® assay and B) the cell proliferation was determined with the xCelligence Real Time Cell Analyzer DP. The mean of at least three independent experiments ± SD is presented in the graphs (***p<0.001).

A dose-dependent increase of IL-6 was detected on gene expression level (10 µg/ml PGN: 6,41±0.96) and in the supernatant (10 µg/ml PGN: 2848.81 pg/ml±847.31 pg/ml) (Figure 3.7). The time lapse experiment revealed a peak of IL6 on gene expression level after 3 h and the expression remained on nearly the same level up to 24 h (Figure 3.8 A). In the supernatant a time-dependent increase of IL-6 was detected (Figure 3.8 B). A stimulation with 10 µg/ml PGN for 12 h led to the following values on gene expression level 2.98±0.28 and in the supernatant 2537.85 pg/ml±388.34 pg/ml.

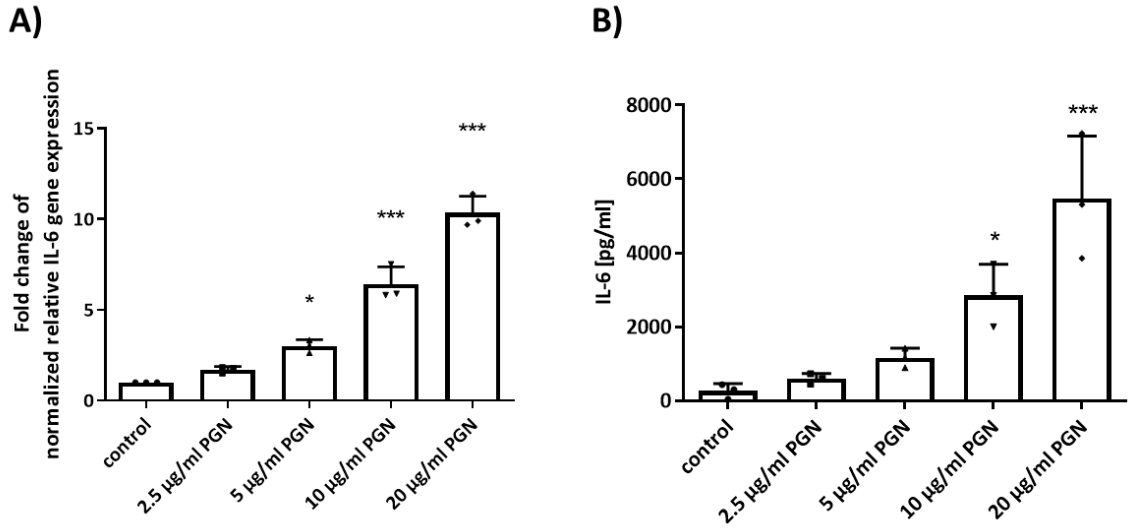

Figure 3.7 PGN stimulation and its effects on IL-6: human coronary artery endothelial cells (HCAEC) were stimulated with 10 µg/ml PGN for 24 h. A) The gene expression of IL-6 in the cell pellet and B) the IL-6 concentration in the supernatant was determined. The mean of three independent experiments ± SD is presented in the graphs (*p<0.05), (***p<0.001).

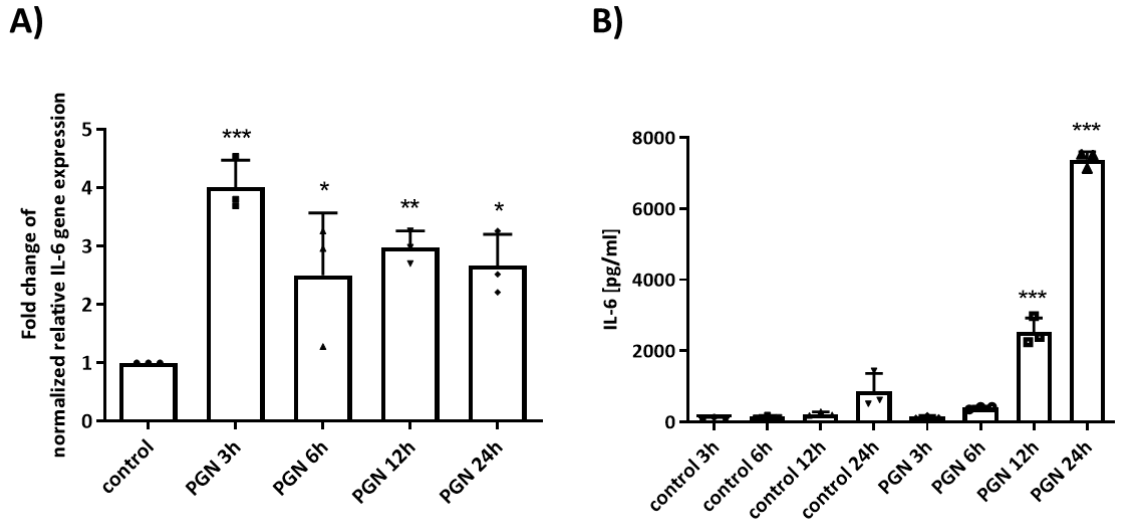

Figure 3.8 PGN stimulation and its effects on IL-6 in a time lapse experiment: human coronary artery endothelial cells (HCAEC) were stimulated with 10 µg/ml PGN. A) The gene expression of IL-6 in the cell pellet and B) the IL-6 concentration in the supernatant was determined. The mean of three independent experiments ± SD is presented in the graphs (*p<0.05), (**p<0.01), (***p<0.001).

The results of the preliminary tests of PGN on the cell viability, proliferation and IL-6 expression led to the conclusion that a PGN concentration of 10 µg/ml and a PGN stimulation period of 12 h should be performed. Therefore, prior to the beginning of all experiments, except for the platelet analysis, HCAEC were stimulated with 10 µg/ml PGN

for 12 h. A comparison of static cell samples and samples treated with a defined shear stress of 1.5 dyn/cm^2, corresponding to flow conditions in recirculation areas of a cardiac implant, was performed.

3.2.2 Effect of PGN on cell stiffness

As a first approach the cell stiffness was tested with AFM by measuring non-stimulated or PGN-stimulated cell samples under static conditions or treated with shear stress of 1.5 dyn/cm^2 for 3 h. Force measurements were carried out on living HCAEC at 37 °C in cell culture medium with or without 10 µg/ml PGN using the JPK BioCell and the JPK Nano Wizzard 3. The cell stiffness and cell height were determined by using the Hertz fit-model for all measured force distance curves. The results were further analysed with a MatLab code which was already used in previous studies [94, 104].

The Young´s Modulus (elastic modulus) increased significantly in control samples treated with shear stress (control static vs. control flow: 0.24 kPa vs. 0.42 kPa, p=0.001) which means that the cells became stiffer. This effect was attenuated after cellular stimulation with PGN (PGN static vs. PGN flow: 0.33 kPa vs. 0.34 kPa, p=0.907) (Figure 3.9 A). Cell height was measured as a second parameter to verify that the cells adapted to the shear stress by reducing the cell height in comparison to static cell samples. The reduction of cell height after shear stress could be confirmed for control (control static vs. control flow: 0.42 µm vs. 0.35 µm, p=0.003) and PGN samples (PGN static vs. PGN flow: 0.43 µm vs. 0.30 µm, p<0.0001) (Figure 3.9 B).

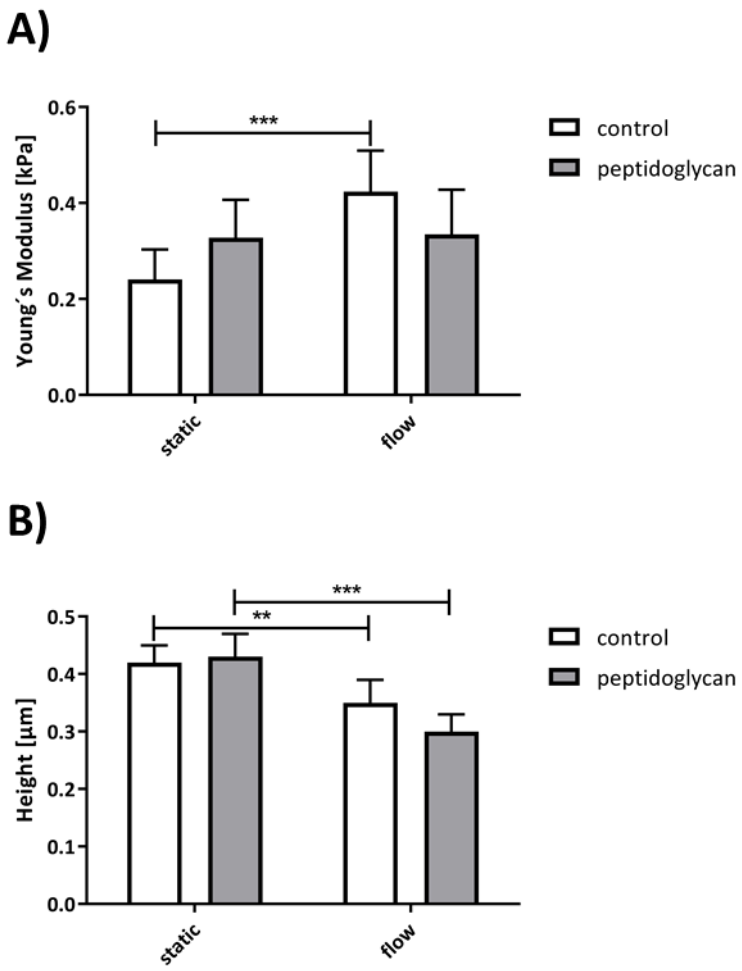

Figure 3.9 Effect of PGN on cell stiffness: human coronary artery endothelial cells (HCAEC) were stimulated with 10 µg/ml PGN for 12 h. Static samples and samples treated with shear stress of 1.5 dyn/cm² for 3 h (flow) were tested. The cell stiffness was determined with AFM measurements. Presented are the A) Young´s Modulus and B) height. The mean of at least four independent experiments ± 95% CI is presented in the graphs (**p<0.01, *** p<0.001).

3.2.3 Effect of PGN on cell migration

Cell migration and cell stiffness are closely related. A change of actin polymerization results in an increase of cellular stiffness which can inhibit cell migration [105]. The analysis of flow-induced migration was performed with the ibidi pump system in combination with live cell imaging using the live cell analyser JuLI™ FL over 15 h. The accumulated distance, and Euclidean distance, velocity, and directionality were determined (Figure 3.10 and Figure S2).

Stimulation with PGN had no effect on cell migration. The induced shear stress led to an increase of the Euclidean distance (control static vs. control flow: 100.6 µm±2.74 µm vs. 134.8 µm±12.93 µm, p=0.0146; PGN static vs. PGN flow: 96.6 µm±14.83 µm vs.

156.2 µm±9.41 µm, p=0.0221) and the directionality (control static vs. control flow: 0.35±0.025 vs. 0.52±0.036, p=0.0058; PGN static vs. PGN flow: 0.31±0.008 vs. 0.47±0.025, p=0.0003) (Figure 3.10). The time analysis revealed a slow decrease of the accumulated distance, Euclidean distance and velocity over time (Figure S2). Only the directionality increased slightly throughout the experiment and showed higher values for samples under flow conditions (control static vs. control flow: 0.58±0.005 vs. 0.68±0.015, p=0.0002; PGN static vs. PGN flow: 0.60±0.009 vs. 0.71±0.011, p<0.0001).

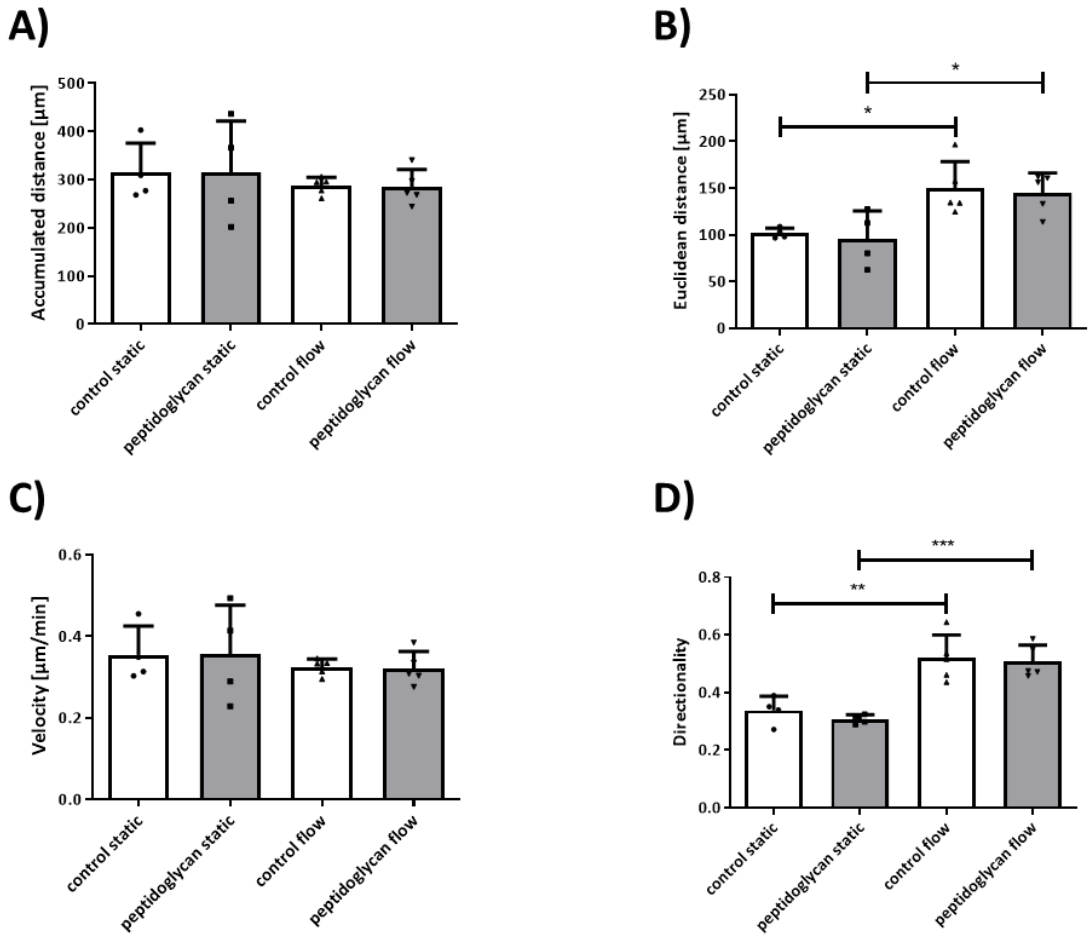

Figure 3.10 Effect of PGN on cell migration: human coronary artery endothelial cells (HCAEC) were stimulated with 10 µg/ml PGN for 12 h. The cell migration was determined with the ibidi pump system with 1.5 dyn/cm². Presented are the A) accumulated distance, B) Euclidean distance, C) velocity and D) directionality. The mean of five independent experiments ± SD is presented in the graphs.

3.2.4 Effect of PGN on wound healing

The implantation of a cardiac implant creates small wounds in the endothelium. In order to evaluate the initial cell growth, the Culture-Inserts 2 Well were applied. For PGN samples the stimulation was performed 12 h prior to the experiment. After 24 h the insert was removed and the cell movement was captured over 24 h with the JuLi™ Life Cell Analyser.

Two relevant parameters were examined for wound healing experiments A) the velocity and B) the change of gap width which is a quantitative measure for wound healing (Figure 3.11). Both parameters increased slightly in control samples under flow conditions in comparison to static control samples (velocity: control static vs control flow 0.28 µm/min±0.01 µm/min vs. 0.33 µm/min±0.05 µm/min, p=0.76; gap width: control static vs control flow 0.47 µm/min±0.10 µm/min vs. 0.66 µm/min ±0.06 µm/min, p=0.22). The effect vanished when the samples were treated with PGN samples (velocity: PGN static vs PGN flow 0.26 µm/min±0.03 µm/min vs. 0.25 µm/min±0.06 µm/min, p=0.76; gap width: PGN static vs PGN flow 0.60 µm/min±0.10 µm/min vs. 0.49 µm/min±0.06 µm/min, p=0.63).

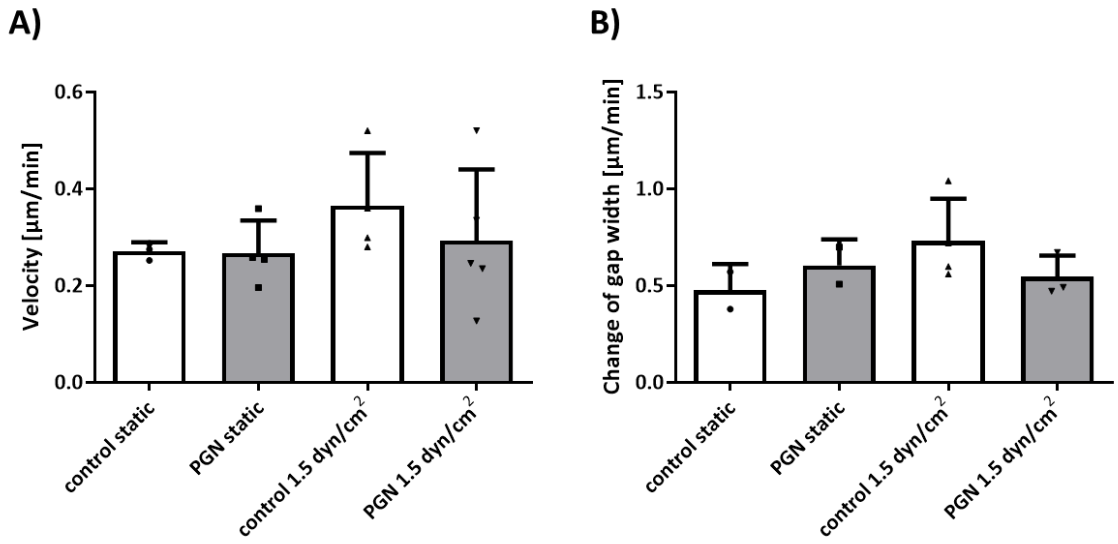

Figure 3.11 Effect of PGN on wound healing: human coronary artery endothelial cells (HCAEC) were seeded in an ibidi 2-well insert and were stimulated with 10 µg/ml PGN for 12 h. The parameters velocity (A) and gap width (B) were determined under static conditions and under flow conditions with 1.5 dyn/cm². The mean of at least three independent experiments ± SD is presented in the graphs.

3.2.5 Effect of PGN on gene expression and protein expression

Additionally, gene and protein expression analyses were performed to assess why cell stiffness and cell migration is influenced by PGN. The analyses focused on interleukin 6 (IL6) which is induced by PGN, stimulates an immune response [103], and increases cell permeability [106]. Furthermore, endothelial nitric oxide synthase (eNOS/NOS3), a marker of endothelial homeostasis [107], α-actinin 4 (ACTN4), which is able to inhibit eNOS activation and is also a component of the actin cytoskeleton [108], and actin (ACTA2), which determines cell shape [109] were assessed.

On gene expression level, PGN led to an increase of IL6 in static samples (control static vs. PGN static: 1.03±0.13 vs. 3.36±0.65, p=0.008) (Figure 3.12). Additionally, IL6-samples showed a flow-induced increase in non-stimulated (control static vs. control flow: 1.03±0.13 vs. 46.7±15.27, p=0.017) and PGN-stimulated samples (PGN static vs. PGN flow 3.4±0.65 vs. 41.2±15.54, p=0.041). On protein level, an opposite effect was examined for control samples, where shear stress led to a significant reduction of IL6 (control static vs. control flow: 0.62±0.06, p=0038). Therefore, an IL6-ELISA with samples of the cell supernatant was performed (Figure 3.13). The results confirmed the effects of the gene expression analysis. In static samples PGN induced an increase of IL6 (control static vs. PGN static: 141.4 pg/ml±84.7 pg/ml vs. 590.0 pg/ml±430.1 pg/ml, p=0.0139). Furthermore, the flow-induced increase of the IL6-concentration could be shown in non-stimulated (control static vs. control flow: 141.4 pg/ml±84.7 pg/ml vs. 812.6 pg/ml±229.7 pg/ml, p=0.0002) and PGN-stimulated samples (PGN static vs. PGN flow 590.0 pg/ml±430.1 pg/ml vs. 1733.3 pg/ml±781.1 pg/ml, p=0.0304).

On gene expression level NOS3 showed a PGN-induced reduction for static samples in comparison to non-stimulated static samples (control static vs. PGN static: 1.03±0.12 vs. 0.60±0.10, p=0.025) and a shear stress- induced reduction (control static vs. control flow: 1.03±0.12 vs. 0.34±0.07, p=0.001; PGN static vs. PGN flow 0.60±0.10 vs. 0.19±0.09, p=0.018). The shear stress-induced decrease could be confirmed on protein level (control static vs. control flow: 0.38±0.04, p<0.0001; PGN static vs. PGN flow 0.38±0.06, p=0.0005).

For ACTN4, a shear stress-induced reduction was analysed (control static vs. control flow: 1.01±0.07 vs. 0.63±0.12, p=0.028; PGN static vs. PGN flow 0.85±0.16 vs. 0.34±0.12, p=0.031).

3.2 Influence of PGN on HCAEC

No significant differences were observed for ACTA2 (Figure 3.12).

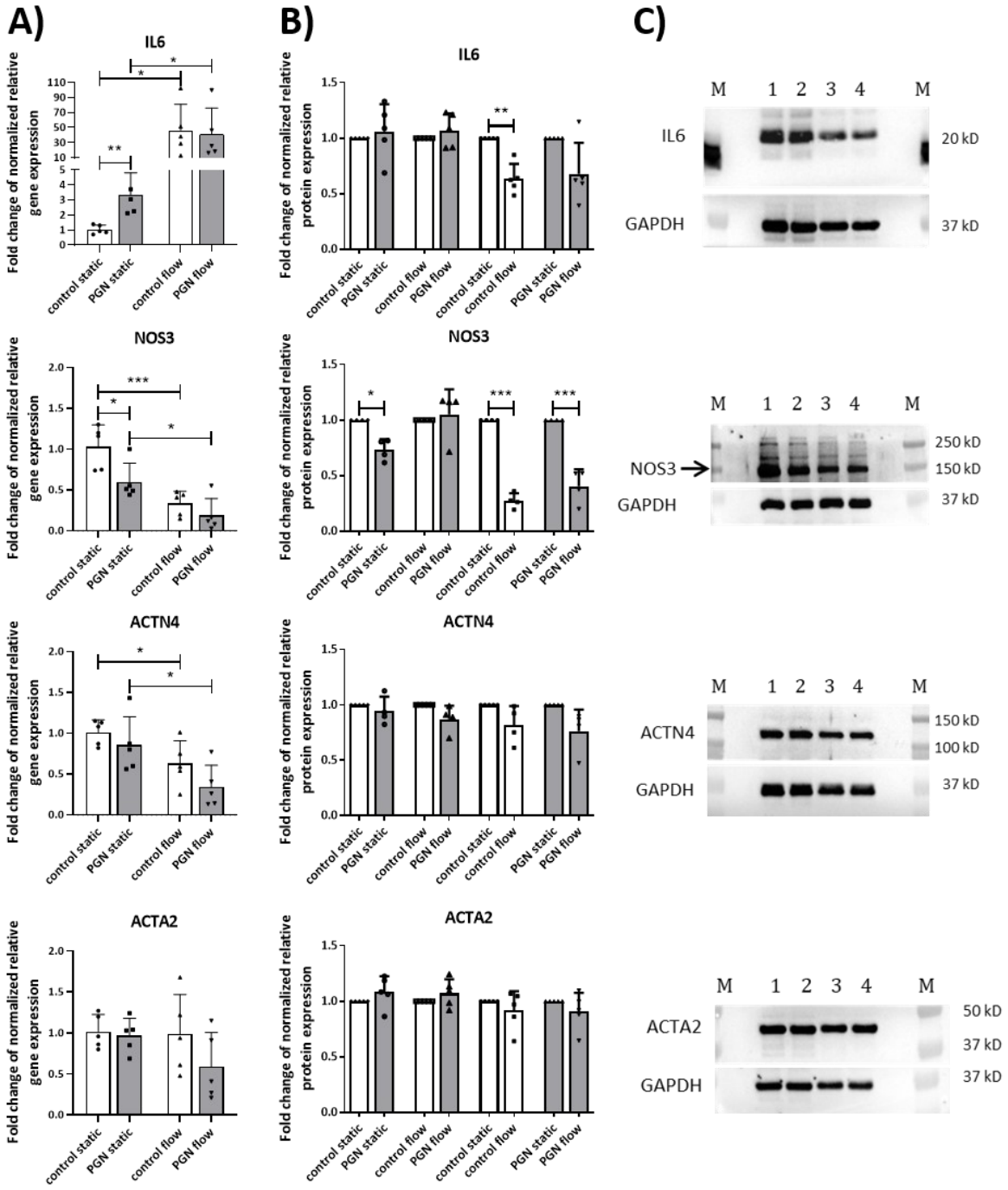

Figure 3.12 Effect of PGN on gene expression and protein expression: human coronary artery endothelial cells (HCAEC) were stimulated with 10 µg/ml PGN for 12 h. Presented are the A) gene expression, B) protein expression and C) representative Western Blot results (M: colorimetric marker, 1: control static, 2: PGN static, 3: control flow, 4: PGN flow). The mean of at least four independent experiments ± SD is presented in the graphs (*p<0.05, **p<0.01, *** p<0.001).

3.2 Influence of PGN on HCAEC

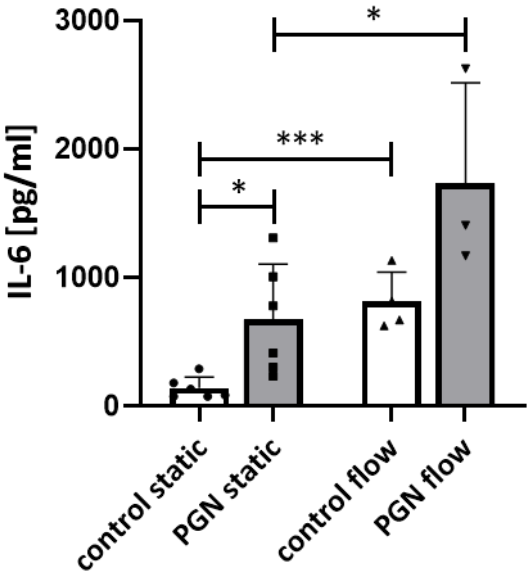

Figure 3.13 Effect of PGN on IL6-concentration in cell supernatant: human coronary artery endothelial cells (HCAEC) were stimulated with 10 µg/ml PGN for 12 h. Presented is the IL6-concentration in the cell supernatant of non-stimulated and PGN-stimulated samples under static and flow conditions. The mean of at least four independent experiments ± SD is presented in the graphs (*p<0.05, *** p<0.001).

Actin was further analysed with fluorescence microscopy (Figure 3.14). In static samples actin showed an unstructured arrangement. Under flow conditions actin exhibits a more ordered structure and appeared to be more evenly distributed around the cell nucleus.

A quantification of actin was not possible because especially in static samples the actin cytoskeleton of individual cells overlaps with the one of neighboring cells.

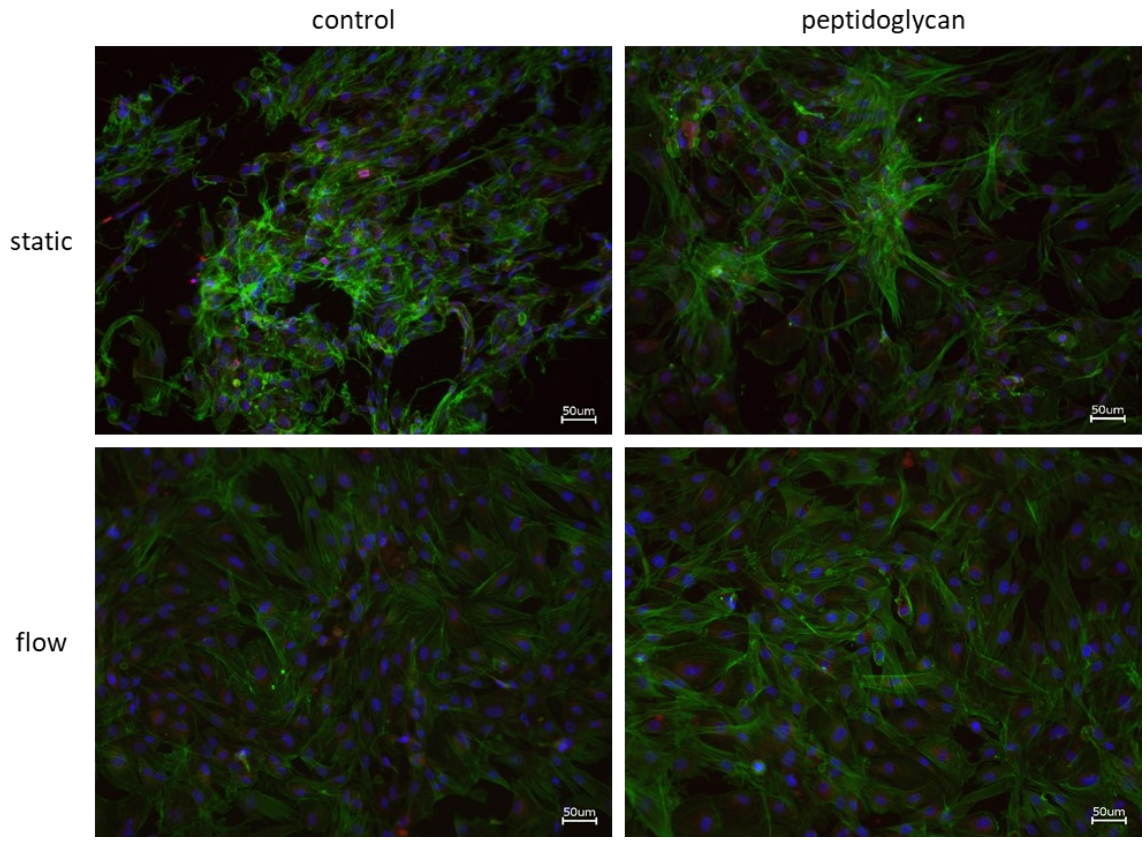

Figure 3.14 Fluorescence microscopy of human coronary artery endothelial cells (HCAEC) under static and flow conditions (1.5 dyn/cm²): Actin of HCAEC was stained with AlexaFluor™ 488 phalloidin (green), the DNA of the nuclei was stained with DAPI (blue) and eNOS was stained with Alexa 568 as a secondary antibody (red).

3.2.6 Effect of PGN on platelets

The interaction of *S. aureus* and platelets plays an essential role in the pathogenesis of IE [24]. Various proteins of *S. aureus* can bind to platelets and induce platelet aggregation, such as vWF-binding protein which binds prothrombin. After a conformational change, a staphylothrombin complex is generated which converts fibrinogen into fibrin. The initiated platelet aggregation and activation then facilitate the interaction of *S. aureus* and platelets [24, 110, 111].

Isolated platelets were either non-stimulated or stimulated with 10 µg/ml PGN for 2.5 h. The according negative controls were treated with 1 µM Prostaglandin E_1. Scanning electron microscopy (SEM) was applied to determine platelet adhesion and aggregation. Quantification (amount of platelets, platelet size, area covered with platelets) was performed with ImageJ software.

3.2 Influence of PGN on HCAEC

On non-stimulated samples single platelets occurred, whereas PGN-stimulated samples had a high number of platelet aggregates. Only a few single platelets were present on the negative controls (Figure 3.15).

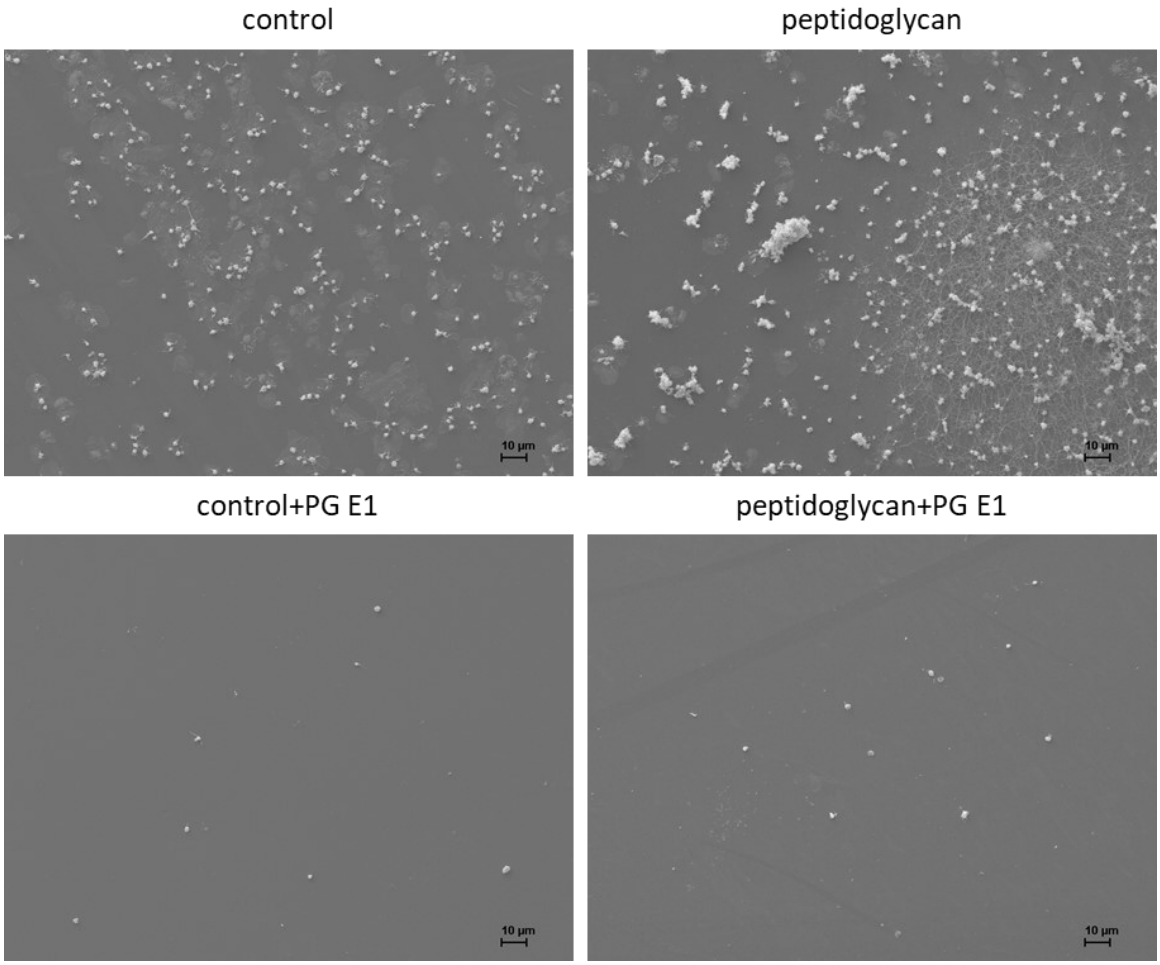

Figure 3.15 Effect of PGN on platelets: Isolated platelets were stimulated with 10 µg/ml PGN for 2.5 h and the according negative controls were treated with 1 µM Prostaglandin E_1. The platelet adhesion and aggregation were determined with SEM. Presented are representative images of a non-stimulated sample, a PGN-stimulated sample and the according negative controls which were treated with 1 µM Prostaglandin E_1.

The quantification (Figure 3.16) revealed that PGN-stimulated samples had a significant increase in platelet size (control vs. PGN: 3.84 µm±0.54 µm vs. 7.20 µm±0.46 µm, p=0.002) due to platelet aggregation and a larger percentage of the area was covered with adherent platelets (control vs. PGN: 1.35%±0.40% vs. 5.06%±1.47%, p=0.040). The additional treatment with Prostaglandin E_1 significantly reduced the amount of platelets (control vs. control+PG E_1: 130±51.62 vs. 26.5±6.59, p=0.040; PGN vs. PGN+PG E_1: 290±64.92 vs. 42±25.33, p=0.016), the platelet size in PGN-stimulated platelets (PGN vs. PGN+PG E_1: 7.2 µm±0.46 µm vs. 4.0 µm±0.16 µm, p=0.0004) and the area covered with

platelets (control vs. control+PG E_1: 1.35%±0.40% vs. 0.24%±0.08%, p=0.025; PGN vs. PGN+PG E_1: 5.06%±1.47% vs. 0.42%±0.29%, p=0.018) (Figure 3.16).

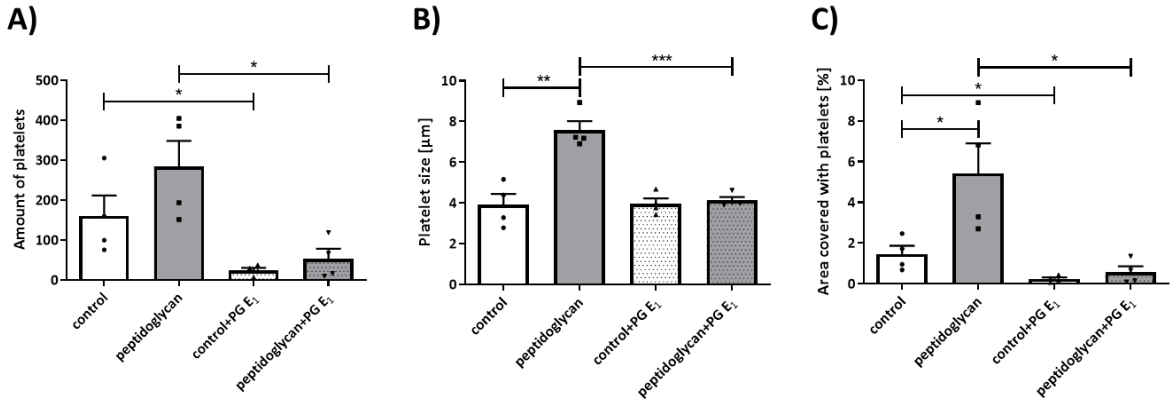

Figure 3.16 Quantitative analysis of the effect of PGN on platelets: Isolated platelets were stimulated with 10 µg/ml PGN for 2.5 h and the according negative controls were treated with 1 µM Prostaglandin E_1. The platelet adhesion and aggregation were determined with SEM and quantified using ImageJ software. Presented are A) the amount of platelets, B) the platelet size and C) the area covered with platelets. The mean of four independent experiments ± SD is presented in the graphs (*p<0.05; **p<0.01; ***p<0.001).

Discussion

S. aureus endocarditis is, with a mortality rate of up to 45%, still one of the most deadly heart diseases [10]. This pathogen can persist in human cells for long time periods and its pathogenesis is still not completely understood [10, 112]. The interface between tissues and inflammatory cells is formed by vascular ECs. This localization allows a targeted inflammatory reaction to infection sites and the protection of adjacent healthy tissue [113]. Therefore, internalization experiments of two different *S. aureus* strains, one control strain (HG001) and one strain isolated from an endocarditis patient (T-72949), were performed in HCAEC.

4.1 Internalisation of *S. aureus* in HCAEC

4.1.1 *S. aureus* persists in human primary endothelial cells for at least 72 h p.i.

In the present study, the two examined *S. aureus* strains were able to survive within HCAEC over the observation period of 72 h. However, an almost steady decrease of bacteria was detected with no significant differences between both bacterial strains (Figure 3.1). Additionally, live-cell imaging confirmed that both bacterial strains can replicate in HCAEC. These observations indicate that *S. aureus* is able to replicate in HCAEC, followed by bacterial clearance and may than persist for long periods within the cell.

Host cell invasion is an essential characteristic of *S. aureus*. Besides ECs, epithelial cells and fibroblasts are major host cells of *S. aureus*. The intracellular persistence requires diverse molecular mechanisms of bacterial invasion. Once the bacteria are internalized, they can activate host cells, can lead to cell death or can persist for long periods of time within the cell [32]. Previous studies with the specific *S. aureus* strain HG001 demonstrated that bacterial replication is apparently cell line dependent inside respiratory epithelial cells such as 16HBE14o- or CFT-1 cells [114, 115]. Moreover, long-term *in vitro* and *in vivo* infection models with *S. aureus* showed that bacteria can also persist in host cells or tissues for several weeks. In this context, intracellular persistence correlates with phenotypical changes in virulence factor expression or small colony variant phenotypes. Recovered small colony variants are

able to return to the virulent wild type form and infect other cells [116]. A study with bovine ECs provides evidence that *S. aureus* replicates intracellularly within the first 2 h p.i. before bacterial degradation occurs [117]. Moreover, it has been demonstrated that *S. aur*eus persists in human primary ECs for up to seven days p.i. with a significant bacterial degradation over time [32]. These observations are consistent with the results obtained here. Overall, HCAEC reduced the number of intracellular bacteria. Nevertheless, a low number of bacteria persisted intracellularly, which may serve as a reservoir for chronic infections.

Furthermore, the specific outcome of a bacterial invasion depends on the interplay between bacterial and cellular factors [32, 118]. Regarding ECs, two plausible situations could be possible: first, *S. aureus* might be able to invade intact endothelium via cell surface-bound fibronectin [119]; second, a lesion of the endothelial monolayer leads to an increased fibronectin exposure which may allow *S. aureus*, circulating in the blood, to invade the cells [120]. The ability to bind fibronectin correlates with the invasiveness of *S. aureus*. This fact is ascertained by 22 bacterial isolates from patients infected with invasive *S. aureus* strains which have a higher amount of fibronectin binding proteins (FnBPs) compared to 19 non-invasive strains [121]. The proteome of host cells revealed no regulation of fibronectin in infected cells, which appears to determine the invasiveness of the bacteria. The proteome analysis of cultured *S. aureus* strains demonstrated that T-72949 had a higher abundance of adhesion proteins, including fibronectin binding protein B, and thus might be more invasive compared to HG001 (Table S2). This would allow the endocarditis strain to internalize into HCAEC to a greater extent before bacterial clearance is initiated by the host cell.

4.1.2 Proteome adaptation of host cells to infection with two different *S. aureus* strains

In this study, the response of HCAEC to an infection with control strain HG001 and endocarditis strain T-72949 revealed varying proteome patterns depending on the infecting strain. A higher number of proteins was significantly changed in GFP_{pos} cells compared to GFP_{neg} cells (Figure 3.3). Furthermore, slightly more proteins were altered in abundance in HCAEC infected with T-72949 than in cells infected with

HG001 compared to mock cells. This observation suggests that an infection with strain T-72949 corresponds more specifically to the selected cell line compared to an infection with strain HG001. Additionally, an infection of HCAEC with T-72949 also led to a higher abundance of proteins changed in GFP_{neg} cells compared to cells infected with HG001 (Figure 3.3). This effect may indicate an enhanced cross talk between cells after an infection with T-72949. A previous study with human alveolar epithelial A549 cells infected with HG001 identified an intersection of 737 proteins in GFP_{pos} and GFP_{neg} cells. At 6.5 h p.i. more proteins displayed different abundances in GFP_{pos} cells (121 proteins: 75 upregulated/ 46 downregulated) compared to GFP_{neg} cells (99 proteins: 57 proteins upregulated/ 42 proteins downregulated) [1]. This observation supports the results of the present study by underlining the fact that in GFP_{pos} cells more proteins are changed in abundance compared to GFP_{neg} cells.

The first specific proteome analysis focused on the five most regulated pathways in HCAEC after bacterial infection in GFP_{pos} host cells compared to GFP_{neg} host cells and indicated the relevance of eukaryotic translation initiation factor 2 (EIF2), EIF4, mammalian target of rapamycin (mTOR), sirtuin and Rho GDP-dissociation inhibitor (RhoGDI) signaling (Figure 3.4). All of these proteins are directly or indirectly involved in the integrated stress response, which is a highly conserved intracellular signaling network. This process is essential for the cell to deal with different pathological and environmental conditions and helps to maintain cellular homeostasis [122]. The five most regulated pathways were all elevated, except for RhoGDI signaling.

In the present study, elevated protein levels related to EIF2-signaling in early stages after infection (T-72949: 1.5 h p.i., HG001: 6.5 h p.i.) were observed. Diverse types of cellular stress lead to a transient reduction in protein synthesis. EIF2 is one component of translational response in ECs [123]. It plays an essential role in the initiation of messenger ribonucleic acid (mRNA) translation and the recognition of the AUG start codon [124]. In mammalian cells, EIF2 signaling occurs after an infection with bacteria and is part of the general antibacterial defense system [125]. EIF2 signaling facilitates the translation of proteins that are involved in the cellular recovery and the attenuation of bacterial invasion. Stress-induced activation of EIF2

kinases, followed by an EIF2 phosphorylation leads to a translation of specific mRNAs, which encode for proteins that contribute to cellular recovery [123]. There is also evidence that a deficient EIF2 signaling increases the susceptibility to bacterial invasion [125]. Studies on viral infections, which represent one type of cellular stress, showed that the EIF2 protein kinase R (PKR) is activated by virus-derived double-stranded RNA. This results in a reduced translation of cellular and viral mRNAs and consequently a reduced viral replication. Therefore, some viruses express PKR inhibitors to enable virus replication [126]. PKR is also a key mediator of bacterially induced apoptosis. Thus, bacteria would also benefit from the expression of PKR inhibitors [127]. This suggests that antiviral and antibacterial responses to specific signaling pathways, such as EIF2, may overlap to ensure the survival of the pathogen [125]. A higher abundance of proteins of EIF2 signaling, as one of the results of the present study, allow the translation of proteins that are involved in cellular recovery as well as to reduce the level of bacterial invasion. Therefore, a cellular answer to the bacterial internalization and the activation of parts of the integrated stress response can be concluded which is advantageous for the cell.

Moreover, EIF4 and mTOR signaling, which are closely interacting, were among the top five regulated signaling pathways. There are two relevant mTOR complexes in the mTOR signaling pathway which have entirely different functions. MTORC1 is involved in protein synthesis and mTORC2 controls actin cytoskeleton organization [128]. Translation of mRNA is repressed by mTOR by activating P70S6 kinase and by inactivating the eukaryotic initiation factor 4E [129]. An activation of mTOR signaling promotes cell growth and proliferation [130]. However, cellular stress, which can be sensed by e.g., p53, leads to an inhibition of mTOR signaling. Translation and ribosome biogenesis are then downregulated and autophagy is upregulated [131]. These findings are in accordance with the results of the present study. After bacterial internalization, the higher abundance of proteins of EIF4 and mTOR signaling is beneficial for the host because downregulating general translation processes and activating autophagy inhibits bacterial replication and spreading. A previous study on fibroblasts also revealed that different factors (serum, insulin, amino acids) that activate mTOR signaling also affect the actin cytoskeleton. Interestingly, the initiation of the reorganization of the actin cytoskeleton by mTOR is passed on through Rho

GTPases [128]. A linkage of these signaling pathways reveals the importance in the cellular response to a bacterial infection which is represented in the top five affected signaling pathways.

Additionally, we observed a lower abundance of proteins of RhoGDI-mediated signaling. Guanine nucleotide dissociation inhibitors are regulators of Rho proteins and modulate the activation state of RhoGTPases, which are key regulators of the state of actin cytoskeleton organization [132, 133]. A selective inhibition of Rho proteins, via RhoGDI, results in a loss of actin stress fibers, a reduction of F-actin content and an increased cell surface area. This process mediates changes in the permeability of ECs [134] and might allow *S. aureus* to invade the ECs to a greater extent. Thus, an inhibited RhoGDI-mediated signaling might be advantageous for the bacteria because higher internalization rates would ensure bacterial survival.

4.1.3 Analysis of specific pathways of host cells after an infection with two different *S. aureus* strains

Selected pathways related to bacterial recognition (integrin, ILK), cytokine production, and infection-related cellular processes (actin cytoskeleton, apoptosis) were examined to investigate the cellular fate of *S. aureus* (Figure 3.5) [100-102].

Bacterial recognition/invasion: A higher abundance of proteins involved in integrin signaling and ILK-signaling confirmed the internalization of *S. aureus* [101]. Thereby, integrin $\alpha_5\beta_1$ interacts with FnBPs through soluble or cellular fibronectin which results in an uptake of *S. aureus* after cytoskeletal rearrangements. The integrin-linked kinase (ILK) is associated with integrins and positively influences the bacterial invasion [118, 135, 136]. A previous study with epithelial cells infected with *S. aureus* postulated ILK as a universal link between integrins and various bacterial pathogens. Experiments conducted therein showed that the inhibition of ILK reduces the bacterial invasion up to 80% [101].

Cytokine production/immune response: Proteins of cytokine signaling were higher in abundance. Cytokines, such as proinflammatory cytokine interleukin-8 (IL-8), are important soluble mediators which realize the communication between cells [135]. The expression and secretion of IL-8 as a response to a *S. aureus* infection can recruit

inflammatory cells to the site of infection and thus activate the innate immune response [137]. A prior study showed that human umbilical vein endothelial cells produce IL-8 after *S. aureus* infection. However, the release of IL-8 varies according to the virulence of the infecting *S. aureus* strain. Non-invasive bacteria cannot induce IL-8 production, and a correlation between the number of intracellular bacteria and the amount of cytokine release exists [138]. Our findings could demonstrate a higher abundance of proteins of IL-8 signaling after infection with T-72949 which underlines the invasive character of the endocarditis isolate compared to the control strain. In this context, infection with T-72949 would probably induce neutrophil migration mediated through activated ECs to prevent bacterial spreading [139].

Cellular processes: A higher abundance of proteins of actin cytoskeleton signaling was measured after an infection with both *S. aureus* strains. A study with epithelial cells infected with *S. aureus* revealed that the inhibition of F-actin microfilament polymerization significantly reduced bacterial invasion [140]. Therefore, it is advantageous for *S. aureus* to activate signaling pathways of the actin cytoskeleton since cytoskeletal rearrangements are necessary to enable the bacterial uptake [101]. In addition, a lower abundance of proteins involved in apoptosis signaling were identified. Various bacterial toxins can induce apoptosis during infection. In early stages of infection, this may enable an injury or even disruption of the endothelial barrier without causing an inflammatory response. Besides this, the host organism may benefit from induced cellular apoptosis to limit bacterial proliferation [141-143]. An inhibition of apoptosis signaling after *S. aureus* infection, which was the case in the present internalization experiment, may thus allow bacterial survival and persistence within the cell.

In summary, the analysis of signaling pathways revealed positive effects for host cell defense and also for bacterial invasion and persistence. Additionally, in cells infected with endocarditis strain T-72949 more proteins were changed in abundance at early time points p.i. (1.5 h p.i.) compared to cells infected with strain HG001. This might indicate an improved adaption of endocarditis strain T-72949 to the specific cell type (HCAEC). The analysis of the proteome provides insights regarding the underlying mechanisms of bacterial invasion and the cellular response. Especially a higher

abundance of adhesion proteins was present in T-72949 compared to HG001 (Table S2). This may allow T-72949 to internalize ECs faster and to translate proteins more effectively, which could be crucial for bacterial replication.

4.2 Effect of *S. aureus*-derived PGN on HCAEC

Stimulation of HCAEC with *S. aureus*-derived PGN was used as a cell model for bacterial internalization experiments described above. PGN is a cell wall component of Gram-positive bacteria which triggers a pro-inflammatory response in various cell types, including ECs [103]. Besides static experiments, a more physiological approach was performed by culturing HCAEC under flow conditions similar to those in recirculation areas of cardiac implants [49]. Mechanical signals (e.g., flow) influence cell properties, such as proliferation and migration which are also altered in many diseases, resulting in cellular dysfunction and further disease progression [48]. Different cellular parameters, which are important in the context of a bacterial infection, were analysed in the present work. PGN affected cell stiffness, wound healing, and platelet aggregation in comparison to non-stimulated cells. For platelet aggregation the effect of PGN-treatment was statistically significant. Regarding cell stiffness, cell migration and wound healing, no significant effect of PGN-treatment could be observed which may indicate that more bacterial characteristics are required to cause effects on the host defense mechanisms [144].

4.2.1 Cell stiffness

The internalization experiments revealed a correlation of bacterial infection and changes in the actin cytoskeleton signaling which was associated with bacterial invasion. Therefore, cell stiffness was analysed as a first cellular parameter. PGN-treatment led to a reduction of cell stiffness under non-physiological flow (Figure 3.9 A).

Barrier function, anti-thrombotic and anti-inflammatory activity are the most important properties of ECs, which are all influenced by changes in the stiffness of the endothelium. ECs are able to adapt their mechanical characteristics to force changes in the bloodstream [60]. There is further evidence that EC stiffness is a key factor for endothelial function or dysfunction, and changes in mechanical properties can be considered as the origin of cardiovascular diseases [58]. An important factor in this

context is NO which is synthesized by eNOS. NO is an endothelium-derived relaxing factor which diffuses to adjacent smooth muscle cells and leads to vasorelaxation [60, 145]. The stiffness of the apical endothelial cortex directly correlates with eNOS function. Soft ECs release higher levels of NO in comparison to stiff cells. Hence, mechanics and cellular function are linked to each other, and the endothelial stiffness can be used as an indicator for endothelial function [59, 60, 66]. Moreover, integrins anchor actin stress fibers to the plasma membrane which function as a mechanical linkage between the cytoskeleton and the ECM [146]. The stiffness of the ECM can be sensed by cells and influence cellular parameters such as migration [48, 147]. A critical process is a persistent stiffening of ECs leading to endothelial dysfunction and vascular pathologies [48, 60].

Under flow conditions the Young´s Modulus of HCAEC increased significantly compared to static control samples. In contrast, PGN-treatment abrogated this cellular stiffening. A comparative study between Gram-negative bacteria (*E. coli*) and Gram-positive bacteria (*S. aureus*) could show that *S. aureus* internalization in epithelial cells is enabled through an interaction and rearrangement of the actin cytoskeleton. Furthermore, the inflammation and immune response is weaker compared to *E. coli* which allows *S. aureus* to develop a chronic infection [148]. A previous study with macrophages infected with *Salmonella* sp. revealed that an increased cellular stiffness correlates with a reduced bacterial uptake, a lower production of antimicrobial molecules and an arrested cellular migration. These processes limit bacterial replication within the cells and prevent further spreading in tissues [105]. The ability of PGN to reduce the cellular stiffness has several advantages for bacteria. First, a soft EC might enable an increased bacterial uptake and could promote the development of a chronic *S. aureus* infection. Secondly, an improved migration could be achieved which would be beneficial for bacterial spreading. Thus, cell migration is the next analysed parameter.

4.2.2 Cell migration and wound healing

In the present study wound healing experiments suggested that under flow conditions PGN might have a negative effect on wound healing (Figure 3.11 B).

An injury of the endothelial monolayer, e.g., after TAVI, requires endothelial repair [18, 19]. A previous study revealed negative effects such as a delay in re-endothelialization and impaired endothelial function after implantation which may be linked to thrombosis and adverse effects on the clinical outcome [20]. A compromised wound healing can also be postulated for *S. aureus* infections [72]. A study with methicillin resistant *S. aureus* showed a delayed wound healing for up to six months in patients with major amputation, due to a chronic bacterial infection [149]. *In vitro* and *in vivo* studies identified bacterial-derived proteins, which are able to inhibit wound healing. Especially the bacterial extracellular adherence protein (Eap) plays a role in *S. aureus* pathogenesis in non-healing wounds [150]. An experimental setup with mice demonstrated a significant delay in wound healing of the skin in the presence of a *S. aureus* infection. After only 2 days, clear differences could be determined between the wound with a bacterial infection and the non-infected wounds. The use of an Eap-deficient strain resulted in a reversion of the *S. aureus*-mediated wound healing delay. Further analysis indicated that Eap is able to inhibit wound closure by preventing the recruitment of inflammatory cells and by blocking EC migration [72].

Our analysis of the bacterial proteome demonstrated a higher protein abundance of Eap in cultured bacterial strain T-72949 compared to strain HG001 (Table S2). This manifestation may allow the endocarditis strain to inhibit wound healing for prolonged periods of time, thus providing more time for infection to develop. The results of wound healing experiments suggest that stimulation with PGN delays wound healing, in comparison with non-stimulated samples under shear stress. This delay is similar to the shown effects of Eap and can be critical because endothelial dysfunction promotes pro-thrombotic and pro-inflammatory conditions [151]. In conclusion, strategies which improve endothelial function and result in an accelerated wound healing are important to improve the outcome of patients with a *S. aureus* infection.

4.2.3 Gene and protein expression

Gene and protein expression analyses focused on IL6 which is induced by PGN, stimulates an immune response [103], and increases cell permeability [106]. Furthermore, eNOS, a marker of endothelial homeostasis was examined [107] (Figure 3.12).

In vitro, PGN increased IL6 mRNA expression and IL6 release. This effect was more pronounced under static conditions since the higher residence time of PGN may trigger a more pronounced cellular response. Furthermore, a flow-induced increase in IL6 gene expression was determined. On protein level the increase of IL6-concentration for static and flow samples could be confirmed in the cell supernatant (Figure 3.13). This observation is consistent with a study that described that non-physiological flow should be considered as a potent trigger of cytokine production [152]. The capability of ECs to produce and release IL6 *in vitro* in response to an infection with *S. aureus* is described in the literature. The stimulation of ECs with *S. aureus* α-toxin (~80-fold increase compared to control samples) and enterotoxin A (~40-fold increase compared to control samples) significantly increases the IL6 concentration in the supernatant [153, 154]. Furthermore, IL6 expression is detectable in ECs in infected tissues, which indicates that besides leukocytes, ECs also contribute to increased cytokine levels [155]. A previous study also elevated the serum levels of the inflammatory marker IL6 in patients with IE. They demonstrated that the IL6 concentration is significantly enhanced in patients with IE compared to a control group [156]. All these findings point out that PGN is sufficient to trigger the same inflammatory effect as a bacterial infection.

In the present study PGN-treatment also reduced eNOS expression in comparison to non-stimulated static samples on gene expression level. A flow-induced decrease was present on gene expression level and on protein level. Previous experiments in our working group revealed that recirculation areas contribute to the manifestation of an inflammatory phenotype (dissertation of Lasse Korff). This observation could be confirmed by the present eNOS analyses.

For ECs it is essential to produce NO by eNOS to maintain cellular homeostasis. An interference of this ability contributes to the pathogenesis of vascular disease. Various

physiological (e.g., shear stress) and pathophysiological stimuli (e.g., tumor necrosis factor-α) are described that modify eNOS expression by altered eNOS mRNA levels, including alterations of eNOS gene transcription and changes in eNOS mRNA processing and stability [157, 158]. *S. aureus* is also capable to downregulate eNOS expression which enhances *S. aureus* infection [159]. A further study revealed that *S. aureus* endotoxin shortens the half-life of the eNOS messenger RNA and reduces eNOS protein expression. This effect is caused by the binding of cytosolic proteins to a cytidine-rich region within the 3´-untranslated region of eNOS mRNA. This interaction is associated with eNOS mRNA destabilization and a downregulation of eNOS protein expression [160]. Another study adds the fact that eNOS mRNA destabilization can also be achieved by cytokines, such as tumor necrosis factor-α [161].

The results of the present study underline the fact that PGN reflects the effects of a *S. aureus* infection *in vitro* in ECs or even *in vivo* results of patients. Nevertheless, it should be kept in mind that non-physiological flow also triggers effects similar to an inflammatory response and might therefore be considered as a critical parameter in the context of IE.

4.2.4 Platelet aggregation

The present study demonstrated that PGN-stimulation of platelets is sufficient to induce platelet aggregation (Figure 3.16).

In a previous study, it was shown that the formation of platelet aggregates correlates with a low blood flow velocity [162]. Pathological blood flow, which occurs in recirculation and stagnation areas, induces platelet aggregation in blood vessels. The low shear stress in combination with a long particle residence time supports this process (Figure 4.1) [163].

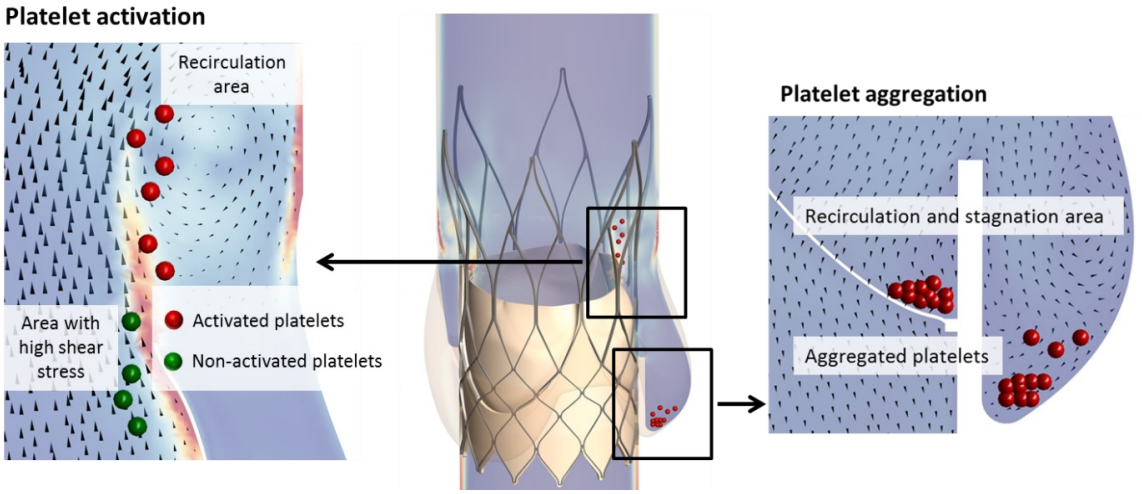

Figure 4.1 Hemodynamic flow conditions after TAVI correlates with the problem of platelet activation (left site of the figure) and subsequent platelet aggregation (right side of the figure) in recirculation and stagnation areas. Areas with low velocities enhance the formation of platelet aggregates [provided by Finja Borowski, Institute for ImplantTechnology and Biomaterials].

Platelets are a key factor of the immune system and secret antimicrobial peptides (platelet microbicidal proteins or thrombin-induced platelet microbicidal proteins) upon activation, which contain a local infection. An *in vitro* resistance of *S. aureus* to these antimicrobial peptides correlates with a more severe disease state [164, 165]. Moreover, the *S. aureus*-to-platelet ratio directly correlates with the extent and velocity of platelet aggregation which influence the severity of a disease [166]. The interaction of *S. aureus* and platelets plays an essential role in the pathogenesis of IE [24]. Numerous proteins secreted by *S. aureus* bind to platelets and induce platelet aggregation. Prothrombin is bound by vWF- factor-binding protein. After a conformational change fibrinogen is converted into fibrin. Platelet aggregation and activation then ease the interaction of *S. aureus* and platelets [24, 110, 111]. Besides *S. aureus*, *Streptococcus sanguinis*, and *Streptococcus gordonii* are also able to activate circulating platelets with serious consequences for the host. A bacterial infection of the heart valves results in the formation of a bacteria-platelet-thrombus which can lead to valve failure, stroke, pulmonary embolism, or heart attack [164, 165].

Targeting platelets in the context of IE can be helpful to reduce the risk of thrombosis. But it must be kept in mind that the ideal anti-platelet agent should not affect the overall platelet function [110]. Dabigatran, a direct thrombin inhibitor, which blocks

the conversion of fibrinogen to fibrin may be a promising adjunctive therapy in IE. Applying dabigatran to rats with an aortic valve infective endocarditis reduced the valve vegetation size, the bacterial load in aortic valves and the inflammation by expressing lower levels of pro-inflammatory markers (e.g., IL6) in comparison to control samples [167]. Nevertheless, a pharmacological manipulation can cause severe complications, such as a high bleeding risk. Therefore, additional research is essential to get a deeper knowledge of the correlation between infection and coagulation. Designing a more targeted treatment option may then improve the clinical outcome of IE patients [10].

In summary, it can be stated that a formation of aggregates may improve bacterial spreading through the blood stream and may allow the adhesion to pro-thrombotic surfaces, e.g., to dysfunctional endothelium. Additionally, a protective microenvironment formed by platelets, shields the pathogen from immune mechanisms in the blood which increases the chance of bacterial survival [24]. Because pharmacological treatment of coagulation processes is not an appropriate option at this time, a fast re-endothelialization involving the anti-thrombogenic and anti-infective barrier function of the cells must be kept in focus [74].

Conclusion and outlook

The important barrier function of ECs to blood flow is realized by a number of mechanosensitive structures on the cell surface. These transfer mechanical stimuli into intracellular signals and thus modulate cell function. Hemodynamic changes influence the endothelial phenotype and thus have the potential to modulate the pathophysiology of cardiovascular diseases. Therefore, the role of ECs is becoming more prominent in the context of IE.

In the present work, the influence of a *S. aureus* infection on HCAEC regarding bacterial internalization, cellular migration and thrombogenicity was investigated. Both employed *S. aureus* strains (T-72949 and HG001) were able to infect HCAEC but the time point of infection occurred earlier with endocarditis strain T-72949 compared to HG001. This effect, in combination with findings from the proteome analyses (higher abundance of fibronectin binding protein B), indicates a better adaptation of T-72949 to the specific cell type. Additionally, the analysis of signaling pathways revealed positive effects for host cell defense (higher abundance of cytokines) and also for bacterial invasion (higher abundance of integrin-linked kinase) and persistence (down-regulation of apoptosis). Further experiments showed that PGN can induce similar effects already known from *S. aureus* infections. PGN reduced cellular stiffening of endothelial cells under disturbed flow and delayed wound healing which facilitates bacterial internalization in endothelial cells. Gene and protein expression analyses underlined the fact that PGN triggered an immune response and also negatively influenced endothelial homeostasis which may contribute to the development of IE. Platelet aggregation was also induced by PGN which may assist in bacterial adherence to dysfunctional endothelium.

The extensive proteome dataset generated in this project will be a useful source of information for future investigations to reveal further molecular mechanisms of endocarditis and potential therapeutic targets. In this work, mainly the host response was extensively studied, but the dataset also allows an analysis of the adaptation of the pathogen.

While internalization experiments were only performed under static conditions, it limits the generalizability of the results in the context of areas with disturbed flow after insertion of cardiac implants. Nevertheless, this approach provides new insights into general mechanisms of an endocarditis isolate to internalize endothelial cells of the coronary artery and simultaneously reveals cellular defense mechanisms. In order to extend the results of the static tests, experiments with flow chambers should be carried out. This investigation would provide more details about the formation of bacterial biofilms, which play an essential role in the development of IE. Furthermore, the question arises how HCAEC from diseased donors would react to a bacterial infection. This additional setup could be used to test new therapeutic approaches. Under the present laboratory equipment and the associated classification into safety levels only PGN-treatment was possible as an alternative to bacterial infection to analyse further cellular parameters. It would be a further gain in knowledge if individual PGN experiments could be repeated with the bacterial infection of HCAEC to confirm the present results. Nonetheless, the systematic analysis of infectious links with bacterial components and ECs allows the use of a variety of methods that can contribute to the understanding of endocarditis.

Although intensive research has been carried out, the pathogenesis of IE has not yet been fully understood. Systematic research expands the available knowledge and contributes to a better prevention of this fatal disease. The importance of ECs is increasingly coming into focus and should therefore be considered as a highly promising therapeutic target. Thus, future therapeutic approaches that attempt to achieve a healthy EC function, may finally reduce the incidence of IE.

Appendix

I Supplemental data

Table S1 Minimum number of wells, which were detached for host cell and pathogen analysis for each time point post infection.

Time point post infection	host cell analysis	pathogen analysis
1.5 h	11	6
3.5 h	10	5
6.5 h	15	7
10.5 h	15	13
24 h	15	13

Table S2 Overview of selected bacterial proteins with changes in protein abundance in bacteria culture of *S. aureus* strain T-72949/HG001

			Cultured bacteria T-72949/HG001		
Description	**Symbol**	**Function**	**signal log2 ratio**	**raw p value**	**adjusted p value**
Fibronectin binding protein B	FnbB	adhesion	1,53125	2,3357E-06	0,00029
Surface protein SasD	SasD	adhesion	2,61959	0,03004	0,21481
MHC class II analog protein	Eap/Map	adhesion	2,57445	0,90565	1
Adenosine synthase A	AdsA	adhesion	2,12487	0,00038	0,01484

Table S3 Time-dependent changes in protein abundance after infection of HCAEC by *S. aureus* strain T-72949 or HG001. Ratios of normalized protein intensities were calculated between 1.5 h and 6.5 h post infection for GFPneg, GFPpos and mock cells. Proteins which were identified with more than two peptides were considered.

The data of table S3 were used for IPA analysis and can be found on the enclosed CD.

I Supplemental data

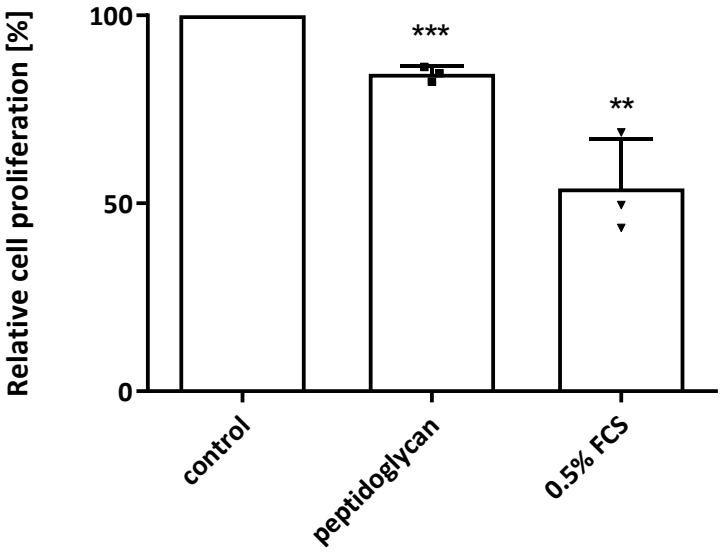

Figure S1 Effect of PGN on cell proliferation measured with BrdU ELISA: human coronary artery endothelial cells (HCAEC) were stimulated with 10 µg/ml PGN for 12 h. Cell proliferation was determined with the BrdU ELISA. The mean of at least three independent experiments ± SD is presented in the graphs (**p<0.01, *** p<0.001).

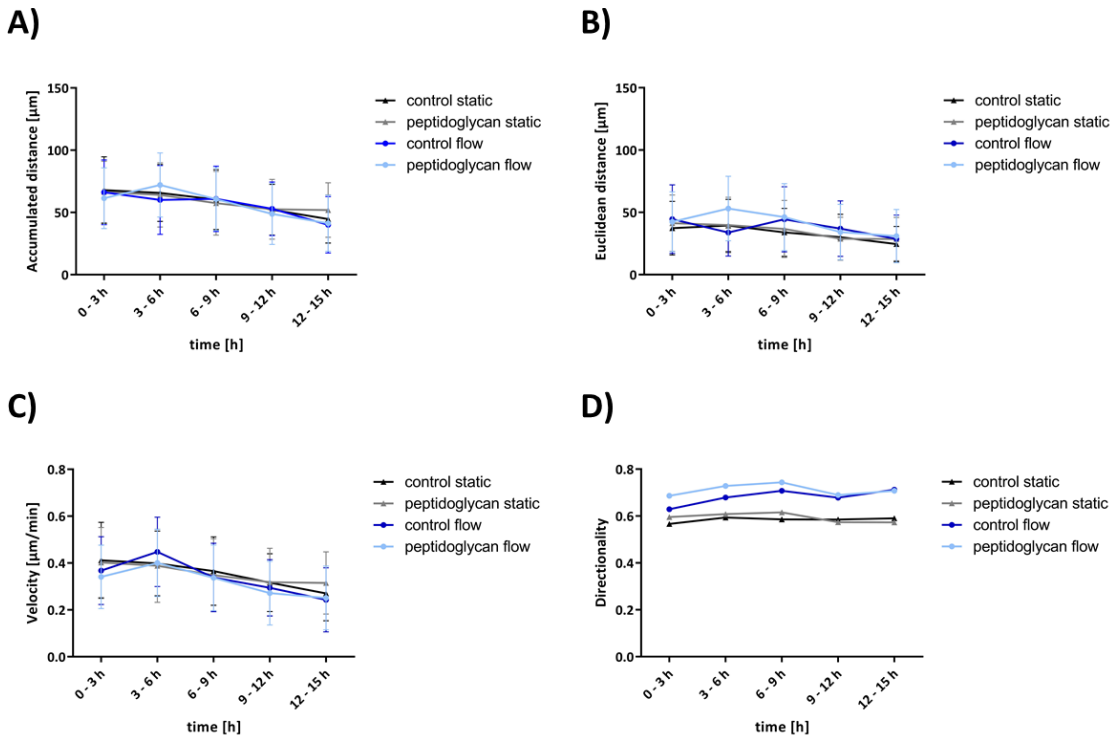

Figure S2 Effect of PGN on cell migration – time analysis: Presented are the A) accumulated distance, B) Euclidean distance, C) velocity and D) directionality broken down in time interval of 3 h. The mean of five independent experiments ± Min to Max is presented in the graphs.

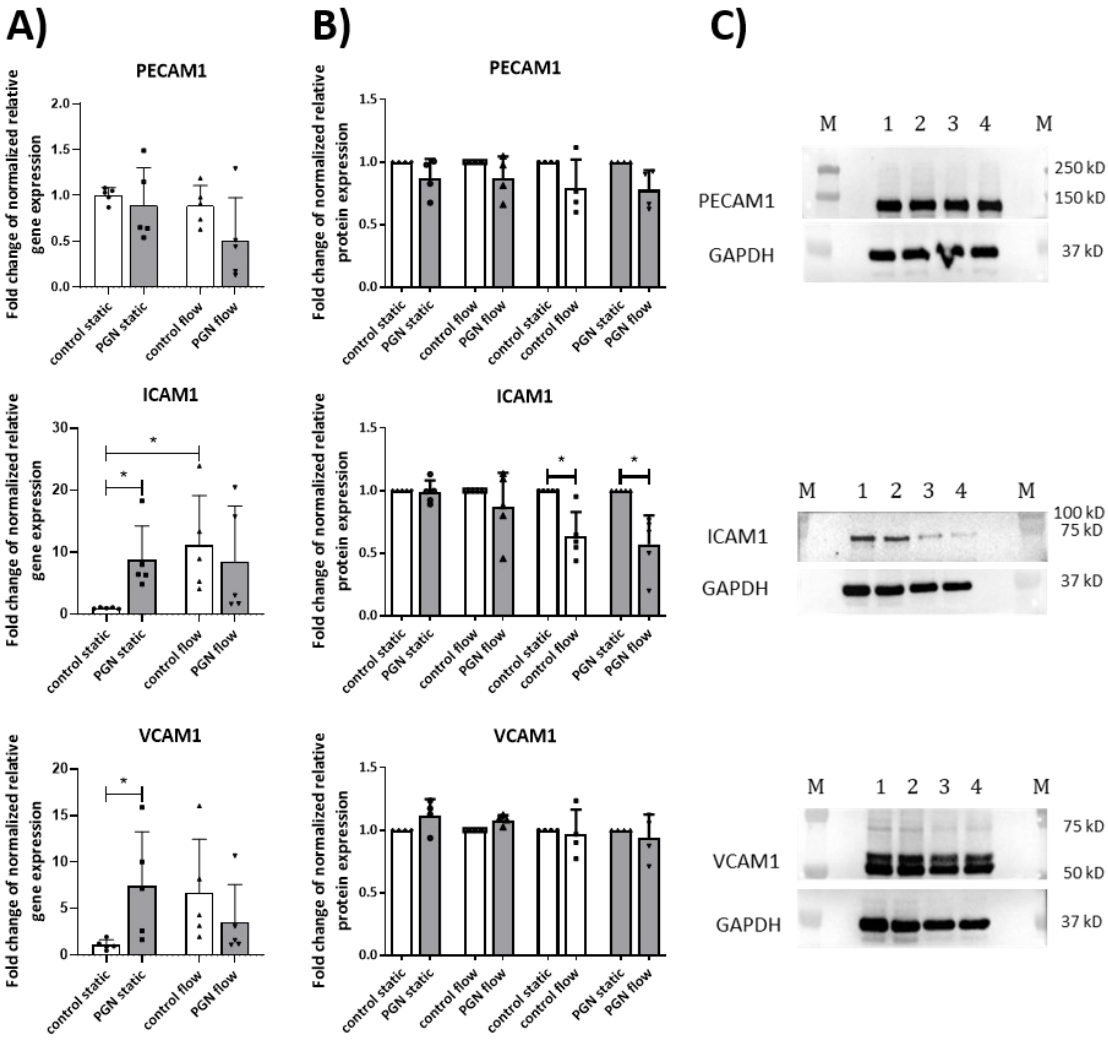

Figure S3 Effect of PGN on gene expression and protein expression of further endothelial factors: HCAEC were stimulated with 10 µg/ml PGN for 12 h. Presented are the A) gene expression, B) protein expression and C) representative Western Blot results (M: colorimetric marker, 1: control static, 2: PGN static, 3: control flow, 4: PGN flow). On gene expression level ICAM1 increased in static PGN-stimulated samples in comparison to static non-stimulated samples and under shear stress in non-stimulated samples in comparison to the static control. On protein level a flow-induced reduction of ICAM1 was detected in non-stimulated and PGN-stimulated samples. In static samples PGN led to an increase of VCAM1 on gene expression level. The mean of at least four independent experiments ± SD is presented in the graphs (*p<0.05).

I Supplemental data

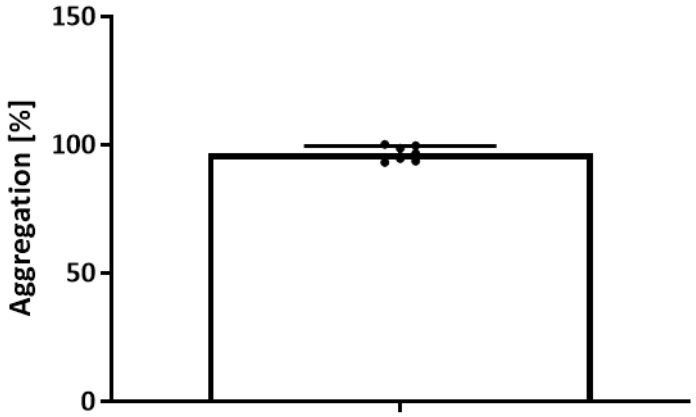

Figure S4 Platelet aggregation measured with aggregometer: Platelet aggregation was determined with the Chrono-log Model 700. The mean of four independent experiments ± SD is presented in the graph.

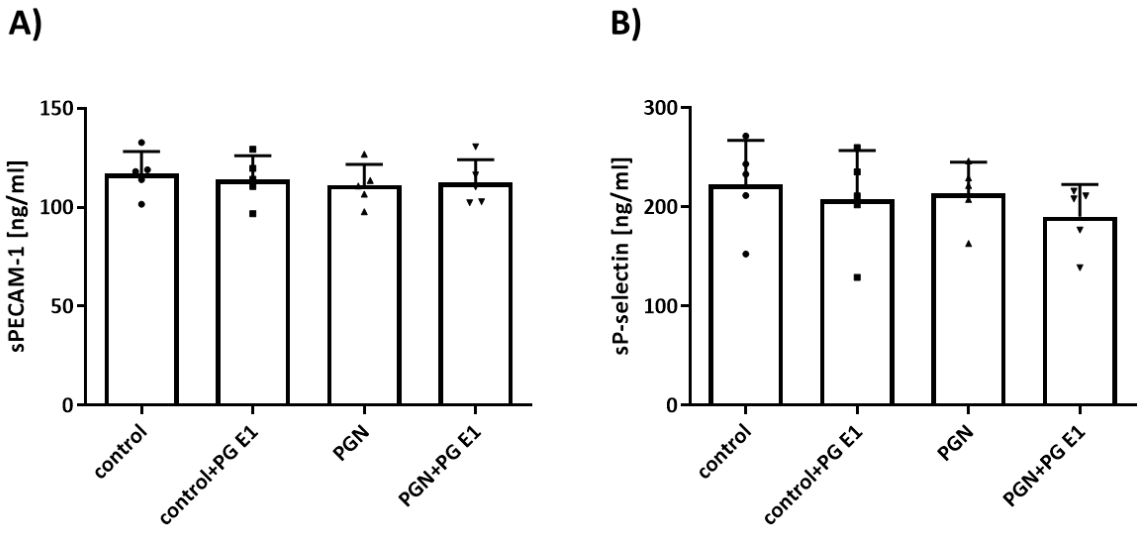

Figure S5 A) sPECAM-1 concentration and B) sP-selectin concentration in supernatants of platelet adhesion experiments. The mean of four independent experiments ± SD is presented in the graphs.

II Literature index

1. Surmann K, Simon M, Hildebrandt P, Pfortner H, Michalik S, Stentzel S, Steil L, Dhople VM, Bernhardt J, Schluter R *et al*: **A proteomic perspective of the interplay of Staphylococcus aureus and human alveolar epithelial cells during infection**. *J Proteomics* 2015, **128**:203-217.
2. https://ibidi.com/img/cms/products/instruments/I_1090X_PumpSystem/IN_1090X_pump_system.pdf
3. https://www.provitro.com/fcs_1c.pdf
4. https://www.agilent.com/en/technology/cellular-impedance
5. https://www.cellbiolabs.com/brdu-cell-proliferation-elisa-kit
6. Chang K-C, Chiang Y-W, Yang C-H, Liou J-W: **Atomic force microscopy in biology and biomedicine**. *Tzu Chi Med J* 2012, **24**:162-169.
7. Chiu JJ, Chien S: **Effects of disturbed flow on vascular endothelium: pathophysiological basis and clinical perspectives**. *Physiol Rev* 2011, **91**(1):327-387.
8. Vedula SR, Ravasio A, Lim CT, Ladoux B: **Collective cell migration: a mechanistic perspective**. *Physiology (Bethesda)* 2013, **28**(6):370-379.
9. Chorianopoulos E, Bea F, Katus HA, Frey N: **The role of endothelial cell biology in endocarditis**. *Cell Tissue Res* 2009, **335**(1):153-163.
10. Liesenborghs L, Meyers S, Vanassche T, Verhamme P: **Coagulation: At the heart of infective endocarditis**. *J Thromb Haemost* 2020, **18**(5):995-1008.
11. McDonald JR: **Acute infective endocarditis**. *Infect Dis Clin North Am* 2009, **23**(3):643-664.
12. Andersen MH, Holle SLK, Klein CF, Bruun NE, Arpi M, Bundgaard H, Tonder N, Iversen KK: **Risk for infective endocarditis in bacteremia with Gram positive cocci**. *Infection* 2020, **48**(6):905-912.
13. Tleyjeh I, Abdulhak A: **Epidemiology and global burden of infective endocarditis**. In., edn.; 2018: 325-328.
14. Salvador VB, Chapagain B, Joshi A, Brennessel DJ: **Clinical Risk Factors for Infective Endocarditis in Staphylococcus aureus Bacteremia**. *Tex Heart Inst J* 2017, **44**(1):10-15.
15. O'Brien L, Kerrigan SW, Kaw G, Hogan M, Penades J, Litt D, Fitzgerald DJ, Foster TJ, Cox D: **Multiple mechanisms for the activation of human platelet aggregation by Staphylococcus aureus: roles for the clumping factors ClfA and ClfB, the serine-aspartate repeat protein SdrE and protein A**. *Mol Microbiol* 2002, **44**(4):1033-1044.
16. Darouiche RO: **Treatment of infections associated with surgical implants**. *N Engl J Med* 2004, **350**(14):1422-1429.
17. Sohns JM, Bavendiek U, Ross TL, Bengel FM: **Targeting Cardiovascular Implant Infection: Multimodality and Molecular Imaging**. *Circ Cardiovasc Imaging* 2017, **10**(12).
18. Cornelissen A, Vogt FJ: **The effects of stenting on coronary endothelium from a molecular biological view: Time for improvement?** *J Cell Mol Med* 2019, **23**(1):39-46.
19. Fyfe AI, Rosenthal A, Gotlieb AI: **Immunosuppressive agents and endothelial repair. Prednisolone delays migration and cytoskeletal rearrangement in wounded porcine aortic monolayers**. *Arterioscler Thromb Vasc Biol* 1995, **15**(8):1166-1171.

20. Inoue T, Croce K, Morooka T, Sakuma M, Node K, Simon DI: **Vascular inflammation and repair: implications for re-endothelialization, restenosis, and stent thrombosis**. *JACC Cardiovasc Interv* 2011, **4**(10):1057-1066.
21. Tan FPP, Xu XY, Torii R, Wood NB, Delahunty N, Mullen M, Moat N, Mohiaddin R: **Comparison of Aortic Flow Patterns Before and After Transcatheter Aortic Valve Implantation**. *Cardiovascular Engineering and Technology* 2012, **3**(1):123-135.
22. Ducci A, Pirisi F, Tzamtzis S, Burriesci G: **Transcatheter aortic valves produce unphysiological flows which may contribute to thromboembolic events: An in-vitro study**. *J Biomech* 2016, **49**(16):4080-4089.
23. Ducci A, Tzamtzis S, Mullen MJ, Burriesci G: **Hemodynamics in the Valsalva sinuses after transcatheter aortic valve implantation (TAVI)**. *J Heart Valve Dis* 2013, **22**(5):688-696.
24. Vanassche T, Kauskot A, Verhaegen J, Peetermans WE, van Ryn J, Schneewind O, Hoylaerts MF, Verhamme P: **Fibrin formation by staphylothrombin facilitates Staphylococcus aureus-induced platelet aggregation**. *Thromb Haemost* 2012, **107**(6):1107-1121.
25. Kwiecinski JM, Horswill AR: **Staphylococcus aureus bloodstream infections: pathogenesis and regulatory mechanisms**. *Curr Opin Microbiol* 2020, **53**:51-60.
26. Bouchiat C, Moreau K, Devillard S, Rasigade JP, Mosnier A, Geissmann T, Bes M, Tristan A, Lina G, Laurent F *et al*: **Staphylococcus aureus infective endocarditis versus bacteremia strains: Subtle genetic differences at stake**. *Infect Genet Evol* 2015, **36**:524-530.
27. Garzoni C, Francois P, Huyghe A, Couzinet S, Tapparel C, Charbonnier Y, Renzoni A, Lucchini S, Lew DP, Vaudaux P *et al*: **A global view of Staphylococcus aureus whole genome expression upon internalization in human epithelial cells**. *BMC Genomics* 2007, **8**:171.
28. Ziebandt AK, Kusch H, Degner M, Jaglitz S, Sibbald MJ, Arends JP, Chlebowicz MA, Albrecht D, Pantucek R, Doskar J *et al*: **Proteomics uncovers extreme heterogeneity in the Staphylococcus aureus exoproteome due to genomic plasticity and variant gene regulation**. *Proteomics* 2010, **10**(8):1634-1644.
29. Soderquist B, Sundqvist KG, Vikerfors T: **Adhesion molecules (E-selectin, intercellular adhesion molecule-1 (ICAM-1) and vascular cell adhesion molecule-1 (VCAM-1)) in sera from patients with Staphylococcus aureus bacteraemia with or without endocarditis**. *Clin Exp Immunol* 1999, **118**(3):408-411.
30. Golias C, Tsoutsi E, Matziridis A, Makridis P, Batistatou A, Charalabopoulos K: **Review. Leukocyte and endothelial cell adhesion molecules in inflammation focusing on inflammatory heart disease**. *In Vivo* 2007, **21**(5):757-769.
31. Eisenreich W, Heesemann J, Rudel T, Goebel W: **Metabolic host responses to infection by intracellular bacterial pathogens**. *Front Cell Infect Microbiol* 2013, **3**:24.
32. Strobel M, Pfortner H, Tuchscherr L, Volker U, Schmidt F, Kramko N, Schnittler HJ, Fraunholz MJ, Loffler B, Peters G *et al*: **Post-invasion events after infection with Staphylococcus aureus are strongly dependent on both the**

host cell type and the infecting S. aureus strain. *Clin Microbiol Infect* 2016, **22**(9):799-809.

33. Surmann K, Michalik S, Hildebrandt P, Gierok P, Depke M, Brinkmann L, Bernhardt J, Salazar MG, Sun Z, Shteynberg D *et al*: **Comparative proteome analysis reveals conserved and specific adaptation patterns of Staphylococcus aureus after internalization by different types of human non-professional phagocytic host cells**. *Front Microbiol* 2014, **5**:392.
34. Liesenborghs L, Meyers S, Lox M, Criel M, Claes J, Peetermans M, Trenson S, Vande Velde G, Vanden Berghe P, Baatsen P *et al*: **Staphylococcus aureus endocarditis: distinct mechanisms of bacterial adhesion to damaged and inflamed heart valves**. *Eur Heart J* 2019, **40**(39):3248-3259.
35. Bouis D, Hospers GA, Meijer C, Molema G, Mulder NH: **Endothelium in vitro: a review of human vascular endothelial cell lines for blood vessel-related research**. *Angiogenesis* 2001, **4**(2):91-102.
36. Florey: **The endothelial cell**. *Br Med J* 1966, **2**(5512):487-490.
37. Jaffe EA: **Cell biology of endothelial cells**. *Hum Pathol* 1987, **18**(3):234-239.
38. Wolinsky H: **A proposal linking clearance of circulating lipoproteins to tissue metabolic activity as a basis for understanding atherogenesis**. *Circ Res* 1980, **47**(3):301-311.
39. Janssens SP, Simouchi A, Quertermous T, Bloch DB, Bloch KD: **Cloning and expression of a cDNA encoding human endothelium-derived relating factor/nitric oxide synthase**. *J Biol Chem* 1992, **267**(31):22694.
40. Jehle AB, Li Y, Stechschulte AC, Stechschulte DJ, Dileepan KN: **Endotoxin and mast cell granule proteases synergistically activate human coronary artery endothelial cells to generate interleukin-6 and interleukin-8**. *J Interferon Cytokine Res* 2000, **20**(4):361-368.
41. Widmer RJ, Lerman A: **Endothelial dysfunction and cardiovascular disease**. *Glob Cardiol Sci Pract* 2014, **2014**(3):291-308.
42. Clarkson P, Celermajer DS, Powe AJ, Donald AE, Henry RM, Deanfield JE: **Endothelium-dependent dilatation is impaired in young healthy subjects with a family history of premature coronary disease**. *Circulation* 1997, **96**(10):3378-3383.
43. Kaye DM, Ahlers BA, Autelitano DJ, Chin-Dusting JP: **In vivo and in vitro evidence for impaired arginine transport in human heart failure**. *Circulation* 2000, **102**(22):2707-2712.
44. Widmer RJ, Lerman LO, Lerman A: **Low-flow motion in the vascular ocean**. *Circ Cardiovasc Interv* 2012, **5**(5):617-619.
45. Davies PF: **Hemodynamic shear stress and the endothelium in cardiovascular pathophysiology**. *Nat Clin Pract Cardiovasc Med* 2009, **6**(1):16-26.
46. Malek AM, Alper SL, Izumo S: **Hemodynamic shear stress and its role in atherosclerosis**. *JAMA* 1999, **282**(21):2035-2042.
47. Hahn C, Schwartz MA: **Mechanotransduction in vascular physiology and atherogenesis**. *Nat Rev Mol Cell Biol* 2009, **10**(1):53-62.
48. Mason BN CJ, Reinhart-King CA: **Matrix Stiffness: A Regulator of Cellular Behavior and Tissue Formation**. In: *Engineering Biomaterials for Regenerative Medicine: Novel Technologies for Clinical Applications.* edn. Edited by SK B. New York: Springer New York; 2012: 19-37.

49. Aird WC: **Phenotypic heterogeneity of the endothelium: I. Structure, function, and mechanisms**. *Circ Res* 2007, **100**(2):158-173.
50. Aird WC: **Phenotypic heterogeneity of the endothelium: II. Representative vascular beds**. *Circ Res* 2007, **100**(2):174-190.
51. Peng Z, Shu B, Zhang Y, Wang M: **Endothelial Response to Pathophysiological Stress**. *Arterioscler Thromb Vasc Biol* 2019, **39**(11):e233-e243.
52. Gimbrone MA, Jr., Garcia-Cardena G: **Vascular endothelium, hemodynamics, and the pathobiology of atherosclerosis**. *Cardiovasc Pathol* 2013, **22**(1):9-15.
53. Kliche K, Jeggle P, Pavenstadt H, Oberleithner H: **Role of cellular mechanics in the function and life span of vascular endothelium**. *Pflugers Arch* 2011, **462**(2):209-217.
54. Gimbrone MA, Jr., Garcia-Cardena G: **Endothelial Cell Dysfunction and the Pathobiology of Atherosclerosis**. *Circ Res* 2016, **118**(4):620-636.
55. Singh AB, Harris RC: **Autocrine, paracrine and juxtacrine signaling by EGFR ligands**. *Cell Signal* 2005, **17**(10):1183-1193.
56. Briones MA, Phillips DJ, Renshaw MA, Hooper WC: **Expression of chemokine by human coronary-artery and umbilical-vein endothelial cells and its regulation by inflammatory cytokines**. *Coron Artery Dis* 2001, **12**(3):179-186.
57. Cahill PA, Redmond EM: **Vascular endothelium - Gatekeeper of vessel health**. *Atherosclerosis* 2016, **248**:97-109.
58. Lenders M, Hofschroer V, Schmitz B, Kasprzak B, Rohlmann A, Missler M, Pavenstadt H, Oberleithner H, Brand SM, Kusche-Vihrog K *et al*: **Differential response to endothelial epithelial sodium channel inhibition ex vivo correlates with arterial stiffness in humans**. *J Hypertens* 2015, **33**(12):2455-2462.
59. Fels J, Jeggle P, Kusche-Vihrog K, Oberleithner H: **Cortical actin nanodynamics determines nitric oxide release in vascular endothelium**. *PLoS One* 2012, **7**(7):e41520.
60. Fels J, Kusche-Vihrog K: **Endothelial Nanomechanics in the Context of Endothelial (Dys)function and Inflammation**. *Antioxid Redox Signal* 2019, **30**(7):945-959.
61. Oberleithner H, Callies C, Kusche-Vihrog K, Schillers H, Shahin V, Riethmuller C, Macgregor GA, de Wardener HE: **Potassium softens vascular endothelium and increases nitric oxide release**. *Proc Natl Acad Sci U S A* 2009, **106**(8):2829-2834.
62. Duprez DA: **Arterial stiffness and endothelial function: key players in vascular health**. *Hypertension* 2010, **55**(3):612-613.
63. Park S, Lakatta EG: **Role of inflammation in the pathogenesis of arterial stiffness**. *Yonsei Med J* 2012, **53**(2):258-261.
64. Weiss TW, Arnesen H, Seljeflot I: **Components of the interleukin-6 transsignalling system are associated with the metabolic syndrome, endothelial dysfunction and arterial stiffness**. *Metabolism* 2013, **62**(7):1008-1013.
65. Della Corte V, Tuttolomondo A, Pecoraro R, Di Raimondo D, Vassallo V, Pinto A: **Inflammation, Endothelial Dysfunction and Arterial Stiffness as**

Therapeutic Targets in Cardiovascular Medicine. *Curr Pharm Des* 2016, **22**(30):4658-4668.

66. Fels J, Callies C, Kusche-Vihrog K, Oberleithner H: **Nitric oxide release follows endothelial nanomechanics and not vice versa**. *Pflugers Arch* 2010, **460**(5):915-923.
67. Li S, Huang NF, Hsu S: **Mechanotransduction in endothelial cell migration**. *J Cell Biochem* 2005, **96**(6):1110-1126.
68. Lamalice L, Le Boeuf F, Huot J: **Endothelial cell migration during angiogenesis**. *Circ Res* 2007, **100**(6):782-794.
69. Wen JH, Choi O, Taylor-Weiner H, Fuhrmann A, Karpiak JV, Almutairi A, Engler AJ: **Haptotaxis is cell type specific and limited by substrate adhesiveness**. *Cell Mol Bioeng* 2015, **8**(4):530-542.
70. Chang AH, Raftrey BC, D'Amato G, Surya VN, Poduri A, Chen HI, Goldstone AB, Woo J, Fuller GG, Dunn AR *et al*: **DACH1 stimulates shear stress-guided endothelial cell migration and coronary artery growth through the CXCL12-CXCR4 signaling axis**. *Genes Dev* 2017, **31**(13):1308-1324.
71. Jufri NF, Mohamedali A, Avolio A, Baker MS: **Mechanical stretch: physiological and pathological implications for human vascular endothelial cells**. *Vasc Cell* 2015, **7**:8.
72. Athanasopoulos AN, Economopoulou M, Orlova VV, Sobke A, Schneider D, Weber H, Augustin HG, Eming SA, Schubert U, Linn T *et al*: **The extracellular adherence protein (Eap) of Staphylococcus aureus inhibits wound healing by interfering with host defense and repair mechanisms**. *Blood* 2006, **107**(7):2720-2727.
73. Khan A, Aslam A, Satti KN, Ashiq S: **Infective endocarditis post-transcatheter aortic valve implantation (TAVI), microbiological profile and clinical outcomes: A systematic review**. *PLoS One* 2020, **15**(1):e0225077.
74. Xia LZ, Tao J, Chen YJ, Liang LL, Luo GF, Cai ZM, Wang Z: **Factors Affecting the Re-Endothelialization of Endothelial Progenitor Cell**. *DNA Cell Biol* 2021, **40**(7):1009-1025.
75. Jackson SP: **Arterial thrombosis--insidious, unpredictable and deadly**. *Nat Med* 2011, **17**(11):1423-1436.
76. Gkaliagkousi E, Ferro A: **Nitric oxide signalling in the regulation of cardiovascular and platelet function**. *Front Biosci (Landmark Ed)* 2011, **16**:1873-1897.
77. Esmon CT: **Thrombomodulin as a model of molecular mechanisms that modulate protease specificity and function at the vessel surface**. *FASEB J* 1995, **9**(10):946-955.
78. Cheng Y, Austin SC, Rocca B, Koller BH, Coffman TM, Grosser T, Lawson JA, FitzGerald GA: **Role of prostacyclin in the cardiovascular response to thromboxane A2**. *Science* 2002, **296**(5567):539-541.
79. Jin RC, Voetsch B, Loscalzo J: **Endogenous mechanisms of inhibition of platelet function**. *Microcirculation* 2005, **12**(3):247-258.
80. Huck V, Schneider MF, Gorzelanny C, Schneider SW: **The various states of von Willebrand factor and their function in physiology and pathophysiology**. *Thromb Haemost* 2014, **111**(4):598-609.

81. Rana A, Westein E, Niego B, Hagemeyer CE: **Shear-Dependent Platelet Aggregation: Mechanisms and Therapeutic Opportunities**. *Front Cardiovasc Med* 2019, **6**:141.
82. Liesenborghs L, Verhamme P, Vanassche T: **Staphylococcus aureus, master manipulator of the human hemostatic system**. *J Thromb Haemost* 2018, **16**(3):441-454.
83. Claes J, Vanassche T, Peetermans M, Liesenborghs L, Vandenbriele C, Vanhoorelbeke K, Missiakas D, Schneewind O, Hoylaerts MF, Heying R *et al*: **Adhesion of Staphylococcus aureus to the vessel wall under flow is mediated by von Willebrand factor-binding protein**. *Blood* 2014, **124**(10):1669-1676.
84. Pappelbaum KI, Gorzelanny C, Grassle S, Suckau J, Laschke MW, Bischoff M, Bauer C, Schorpp-Kistner M, Weidenmaier C, Schneppenheim R *et al*: **Ultralarge von Willebrand factor fibers mediate luminal Staphylococcus aureus adhesion to an intact endothelial cell layer under shear stress**. *Circulation* 2013, **128**(1):50-59.
85. Fleming I, Kwak B, Meens M: **The endothelial cell**. *The ESC textbook of vascular biology* 2017:73-90.
86. Sumpio BE, Riley JT, Dardik A: **Cells in focus: endothelial cell**. *The international journal of biochemistry & cell biology* 2002, **34**(12):1508-1512.
87. Hoerr V, Franz M, Pletz MW, Diab M, Niemann S, Faber C, Doenst T, Schulze PC, Deinhardt-Emmer S, Loffler B: **S. aureus endocarditis: Clinical aspects and experimental approaches**. *Int J Med Microbiol* 2018, **308**(6):640-652.
88. Fowler VG, Jr., Miro JM, Hoen B, Cabell CH, Abrutyn E, Rubinstein E, Corey GR, Spelman D, Bradley SF, Barsic B *et al*: **Staphylococcus aureus endocarditis: a consequence of medical progress**. *JAMA* 2005, **293**(24):3012-3021.
89. Palma Medina LM, Becker AK, Michalik S, Yedavally H, Raineri EJM, Hildebrandt P, Gesell Salazar M, Surmann K, Pfortner H, Mekonnen SA *et al*: **Metabolic Cross-talk Between Human Bronchial Epithelial Cells and Internalized Staphylococcus aureus as a Driver for Infection**. *Mol Cell Proteomics* 2019, **18**(5):892-908.
90. Nagel DA: **Untersuchungen zum Einfluss der Rho-Aktivität auf die Expression SaeRS-abhängiger Virulenzfaktoren in *Staphylococcus aureus***. *Dissertation.* University of Greifswald; 2018.
91. Hildebrandt P, Surmann K, Salazar MG, Normann N, Volker U, Schmidt F: **Alternative fluorescent labeling strategies for characterizing gram-positive pathogenic bacteria: Flow cytometry supported counting, sorting, and proteome analysis of Staphylococcus aureus retrieved from infected host cells**. *Cytometry A* 2016, **89**(10):932-940.
92. Blankenburg S, Hentschker C, Nagel A, Hildebrandt P, Michalik S, Dittmar D, Surmann K, Volker U: **Improving Proteome Coverage for Small Sample Amounts: An Advanced Method for Proteomics Approaches with Low Bacterial Cell Numbers**. *Proteomics* 2019, **19**(23):e1900192.
93. Butt HJ, Jaschke M: **Calculation of Thermal Noise in Atomic-Force Microscopy**. *Nanotechnology* 1995, **6**(1):1-7.
94. Glaubitz M, Medvedev N, Pussak D, Hartmann L, Schmidt S, Helm CA, Delcea M: **A novel contact model for AFM indentation experiments on soft spherical cell-like particles**. *Soft Matter* 2014, **10**(35):6732-6741.

95. Oldenburg J, Maletzki L, Strohbach A, Belle P, Siewert S, Busch R, Felix SB, Schmitz KP, Stiehm M: **Methodology for comprehensive cell-level analysis of wound healing experiments using deep learning in MATLAB**. *BMC Mol Cell Biol* 2021, **22**(1):32.
96. Holland PM, Abramson RD, Watson R, Gelfand DH: **Detection of specific polymerase chain reaction product by utilizing the 5'----3' exonuclease activity of Thermus aquaticus DNA polymerase**. *Proc Natl Acad Sci U S A* 1991, **88**(16):7276-7280.
97. Arya M, Shergill IS, Williamson M, Gommersall L, Arya N, Patel HR: **Basic principles of real-time quantitative PCR**. *Expert Rev Mol Diagn* 2005, **5**(2):209-219.
98. Grumann D, Ruotsalainen E, Kolata J, Kuusela P, Jarvinen A, Kontinen VP, Broker BM, Holtfreter S: **Characterization of infecting strains and superantigen-neutralizing antibodies in Staphylococcus aureus bacteremia**. *Clin Vaccine Immunol* 2011, **18**(3):487-493.
99. Herbert S, Ziebandt AK, Ohlsen K, Schäfer T, Hecker M, Albrecht D, Novick R, Götz F: **Repair of global regulators in Staphylococcus aureus 8325 and comparative analysis with other clinical isolates**. *Infect Immun* 2010, **78**(6):2877-2889.
100. Fraunholz M, Sinha B: **Intracellular Staphylococcus aureus: live-in and let die**. *Front Cell Infect Microbiol* 2012, **2**:43.
101. Wang B, Yurecko RS, Dedhar S, Cleary PP: **Integrin-linked kinase is an essential link between integrins and uptake of bacterial pathogens by epithelial cells**. *Cell Microbiol* 2006, **8**(2):257-266.
102. Yao L, Bengualid V, Lowy FD, Gibbons JJ, Hatcher VB, Berman JW: **Internalization of Staphylococcus aureus by endothelial cells induces cytokine gene expression**. *Infect Immun* 1995, **63**(5):1835-1839.
103. Robertson J, Lang S, Lambert PA, Martin PE: **Peptidoglycan derived from Staphylococcus epidermidis induces Connexin43 hemichannel activity with consequences on the innate immune response in endothelial cells**. *Biochem J* 2010, **432**(1):133-143.
104. Strohbach A, Pennewitz M, Glaubitz M, Palankar R, Gross S, Lorenz F, Materzok I, Rong A, Busch MC, Felix SB *et al*: **The apelin receptor influences biomechanical and morphological properties of endothelial cells**. *J Cell Physiol* 2018, **233**(8):6250-6261.
105. Man SM, Ekpenyong A, Tourlomousis P, Achouri S, Cammarota E, Hughes K, Rizzo A, Ng G, Wright JA, Cicuta P *et al*: **Actin polymerization as a key innate immune effector mechanism to control Salmonella infection**. *Proc Natl Acad Sci U S A* 2014, **111**(49):17588-17593.
106. Maruo N, Morita I, Shirao M, Murota S: **IL-6 increases endothelial permeability in vitro**. *Endocrinology* 1992, **131**(2):710-714.
107. Heiss C, Rodriguez-Mateos A, Kelm M: **Central role of eNOS in the maintenance of endothelial homeostasis**. *Antioxid Redox Signal* 2015, **22**(14):1230-1242.
108. Hiroi Y, Guo Z, Li Y, Beggs AH, Liao JK: **Dynamic regulation of endothelial NOS mediated by competitive interaction with alpha-actinin-4 and calmodulin**. *FASEB J* 2008, **22**(5):1450-1457.

109. Prasain N, Stevens T: **The actin cytoskeleton in endothelial cell phenotypes**. *Microvasc Res* 2009, **77**(1):53-63.
110. Kerrigan SW, Cox D: **Platelet-bacterial interactions**. *Cell Mol Life Sci* 2010, **67**(4):513-523.
111. Kroh HK, Panizzi P, Bock PE: **Von Willebrand factor-binding protein is a hysteretic conformational activator of prothrombin**. *Proc Natl Acad Sci U S A* 2009, **106**(19):7786-7791.
112. Raineri EJM, Yedavally H, Salvati A, van Dijl JM: **Time-resolved analysis of Staphylococcus aureus invading the endothelial barrier**. *Virulence* 2020, **11**(1):1623-1639.
113. McGill SN, Ahmed NA, Christou NV: **Endothelial cells: role in infection and inflammation**. *World J Surg* 1998, **22**(2):171-178.
114. Kahl BC, Goulian M, van Wamel W, Herrmann M, Simon SM, Kaplan G, Peters G, Cheung AL: **Staphylococcus aureus RN6390 replicates and induces apoptosis in a pulmonary epithelial cell line**. *Infect Immun* 2000, **68**(9):5385-5392.
115. Richter E, Harms M, Ventz K, Nolker R, Fraunholz MJ, Mostertz J, Hochgrafe F: **Quantitative Proteomics Reveals the Dynamics of Protein Phosphorylation in Human Bronchial Epithelial Cells during Internalization, Phagosomal Escape, and Intracellular Replication of Staphylococcus aureus**. *J Proteome Res* 2016, **15**(12):4369-4386.
116. Tuchscherr L, Medina E, Hussain M, Volker W, Heitmann V, Niemann S, Holzinger D, Roth J, Proctor RA, Becker K *et al*: **Staphylococcus aureus phenotype switching: an effective bacterial strategy to escape host immune response and establish a chronic infection**. *EMBO Mol Med* 2011, **3**(3):129-141.
117. Oviedo-Boyso J, Cardoso-Correa BI, Cajero-Juarez M, Bravo-Patino A, Valdez-Alarcon JJ, Baizabal-Aguirre VM: **The capacity of bovine endothelial cells to eliminate intracellular Staphylococcus aureus and Staphylococcus epidermidis is increased by the proinflammatory cytokines TNF-alpha and IL-1beta**. *FEMS Immunol Med Microbiol* 2008, **54**(1):53-59.
118. Sinha B, Francois PP, Nusse O, Foti M, Hartford OM, Vaudaux P, Foster TJ, Lew DP, Herrmann M, Krause KH: **Fibronectin-binding protein acts as Staphylococcus aureus invasin via fibronectin bridging to integrin alpha5beta1**. *Cell Microbiol* 1999, **1**(2):101-117.
119. D FTOC: **Host-pathogen protein-protein interactions in *Staphylococcus***. *J Lab Clin Med* 1997, **104**(4):455-469.
120. Smeltzer MS, Gillaspy AF, Pratt FL, Jr., Thames MD, Iandolo JJ: **Prevalence and chromosomal map location of Staphylococcus aureus adhesin genes**. *Gene* 1997, **196**(1-2):249-259.
121. Proctor RA, Christman G, Mosher DF: **Fibronectin-induced agglutination of Staphylococcus aureus correlates with invasiveness**. *J Lab Clin Med* 1984, **104**(4):455-469.
122. Costa-Mattioli M, Walter P: **The integrated stress response: From mechanism to disease**. *Science* 2020, **368**(6489).
123. Sonenberg N, Hinnebusch AG: **Regulation of translation initiation in eukaryotes: mechanisms and biological targets**. *Cell* 2009, **136**(4):731-745.

124. Pakos-Zebrucka K, Koryga I, Mnich K, Ljujic M, Samali A, Gorman AM: **The integrated stress response**. *EMBO Rep* 2016, **17**(10):1374-1395.
125. Shrestha N, Bahnan W, Wiley DJ, Barber G, Fields KA, Schesser K: **Eukaryotic initiation factor 2 (eIF2) signaling regulates proinflammatory cytokine expression and bacterial invasion**. *J Biol Chem* 2012, **287**(34):28738-28744.
126. Garcia MA, Meurs EF, Esteban M: **The dsRNA protein kinase PKR: virus and cell control**. *Biochimie* 2007, **89**(6-7):799-811.
127. Hsu LC, Park JM, Zhang K, Luo JL, Maeda S, Kaufman RJ, Eckmann L, Guiney DG, Karin M: **The protein kinase PKR is required for macrophage apoptosis after activation of Toll-like receptor 4**. *Nature* 2004, **428**(6980):341-345.
128. Jacinto E, Loewith R, Schmidt A, Lin S, Ruegg MA, Hall A, Hall MN: **Mammalian TOR complex 2 controls the actin cytoskeleton and is rapamycin insensitive**. *Nat Cell Biol* 2004, **6**(11):1122-1128.
129. Yentrapalli R, Azimzadeh O, Sriharshan A, Malinowsky K, Merl J, Wojcik A, Harms-Ringdahl M, Atkinson MJ, Becker KF, Haghdoost S *et al*: **The PI3K/Akt/mTOR pathway is implicated in the premature senescence of primary human endothelial cells exposed to chronic radiation**. *PLoS One* 2013, **8**(8):e70024.
130. Hannan KM, Brandenburger Y, Jenkins A, Sharkey K, Cavanaugh A, Rothblum L, Moss T, Poortinga G, McArthur GA, Pearson RB *et al*: **mTOR-dependent regulation of ribosomal gene transcription requires S6K1 and is mediated by phosphorylation of the carboxy-terminal activation domain of the nucleolar transcription factor UBF**. *Mol Cell Biol* 2003, **23**(23):8862-8877.
131. Feng Z, Zhang H, Levine AJ, Jin S: **The coordinate regulation of the p53 and mTOR pathways in cells**. *Proc Natl Acad Sci U S A* 2005, **102**(23):8204-8209.
132. Gorovoy M, Neamu R, Niu J, Vogel S, Predescu D, Miyoshi J, Takai Y, Kini V, Mehta D, Malik AB *et al*: **RhoGDI-1 modulation of the activity of monomeric RhoGTPase RhoA regulates endothelial barrier function in mouse lungs**. *Circ Res* 2007, **101**(1):50-58.
133. Ridley AJ: **Rho family proteins: coordinating cell responses**. *Trends Cell Biol* 2001, **11**(12):471-477.
134. Carbajal JM, Schaeffer RC, Jr.: **RhoA inactivation enhances endothelial barrier function**. *Am J Physiol* 1999, **277**(5 Pt 1):C955-964.
135. Albelda SM, Buck CA: **Integrins and other cell adhesion molecules**. *FASEB J* 1990, **4**(11):2868-2880.
136. Sinha B, Francois P, Que YA, Hussain M, Heilmann C, Moreillon P, Lew D, Krause KH, Peters G, Herrmann M: **Heterologously expressed Staphylococcus aureus fibronectin-binding proteins are sufficient for invasion of host cells**. *Infect Immun* 2000, **68**(12):6871-6878.
137. Kumar A, Zhang J, Yu FS: **Innate immune response of corneal epithelial cells to Staphylococcus aureus infection: role of peptidoglycan in stimulating proinflammatory cytokine secretion**. *Invest Ophthalmol Vis Sci* 2004, **45**(10):3513-3522.
138. Tajima A, Seki K, Shinji H, Masuda S: **Inhibition of interleukin-8 production in human endothelial cells by Staphylococcus aureus supernatant**. *Clin Exp Immunol* 2007, **147**(1):148-154.

139. Tajima A, Iwase T, Shinji H, Seki K, Mizunoe Y: **Inhibition of endothelial interleukin-8 production and neutrophil transmigration by Staphylococcus aureus beta-hemolysin**. *Infect Immun* 2009, **77**(1):327-334.
140. Almeida RA, Matthews KR, Cifrian E, Guidry AJ, Oliver SP: **Staphylococcus aureus invasion of bovine mammary epithelial cells**. *J Dairy Sci* 1996, **79**(6):1021-1026.
141. Menzies BE, Kourteva I: **Staphylococcus aureus alpha-toxin induces apoptosis in endothelial cells**. *FEMS Immunol Med Microbiol* 2000, **29**(1):39-45.
142. Ulett GC, Adderson EE: **Regulation of Apoptosis by Gram-Positive Bacteria: Mechanistic Diversity and Consequences for Immunity**. *Curr Immunol Rev* 2006, **2**(2):119-141.
143. Zhang X, Hu X, Rao X: **Apoptosis induced by Staphylococcus aureus toxins**. *Microbiol Res* 2017, **205**:19-24.
144. Kuhn S, Slavetinsky CJ, Peschel A: **Synthesis and function of phospholipids in Staphylococcus aureus**. *Int J Med Microbiol* 2015, **305**(2):196-202.
145. Husain M, Moss J: **Endothelium-dependent vascular smooth muscle control**. *J Clin Anesth* 1988, **1**(2):135-145.
146. Geiger B, Spatz JP, Bershadsky AD: **Environmental sensing through focal adhesions**. *Nat Rev Mol Cell Biol* 2009, **10**(1):21-33.
147. Bastounis EE, Yeh YT, Theriot JA: **Matrix stiffness modulates infection of endothelial cells by Listeria monocytogenes via expression of cell surface vimentin**. *Mol Biol Cell* 2018, **29**(13):1571-1589.
148. Gunther J, Petzl W, Bauer I, Ponsuksili S, Zerbe H, Schuberth HJ, Brunner RM, Seyfert HM: **Differentiating Staphylococcus aureus from Escherichia coli mastitis: S. aureus triggers unbalanced immune-dampening and host cell invasion immediately after udder infection**. *Sci Rep* 2017, **7**(1):4811.
149. Grimble SA, Magee TR, Galland RB: **Methicillin resistant Staphylococcus aureus in patients undergoing major amputation**. *Eur J Vasc Endovasc Surg* 2001, **22**(3):215-218.
150. Chavakis T, Wiechmann K, Preissner KT, Herrmann M: **Staphylococcus aureus interactions with the endothelium: the role of bacterial "secretable expanded repertoire adhesive molecules" (SERAM) in disturbing host defense systems**. *Thromb Haemost* 2005, **94**(2):278-285.
151. Verma S, Anderson TJ: **Fundamentals of endothelial function for the clinical cardiologist**. *Circulation* 2002, **105**(5):546-549.
152. Duvigneau JC, Hartl RT, Teinfalt M, Gemeiner M: **Delay in processing porcine whole blood affects cytokine expression**. *J Immunol Methods* 2003, **272**(1-2):11-21.
153. Calandra T, Gerain J, Heumann D, Baumgartner JD, Glauser MP: **High circulating levels of interleukin-6 in patients with septic shock: evolution during sepsis, prognostic value, and interplay with other cytokines. The Swiss-Dutch J5 Immunoglobulin Study Group**. *Am J Med* 1991, **91**(1):23-29.
154. Soderquist B, Kallman J, Holmberg H, Vikerfors T, Kihlstrom E: **Secretion of IL-6, IL-8 and G-CSF by human endothelial cells in vitro in response to Staphylococcus aureus and staphylococcal exotoxins**. *APMIS* 1998, **106**(12):1157-1164.

155. Yao L, Berman JW, Factor SM, Lowy FD: **Correlation of histopathologic and bacteriologic changes with cytokine expression in an experimental murine model of bacteremic Staphylococcus aureus infection**. *Infect Immun* 1997, **65**(9):3889-3895.
156. Watkin RW, Harper LV, Vernallis AB, Lang S, Lambert PA, Ranasinghe AM, Elliott TS: **Pro-inflammatory cytokines IL6, TNF-alpha, IL1beta, procalcitonin, lipopolysaccharide binding protein and C-reactive protein in infective endocarditis**. *J Infect* 2007, **55**(3):220-225.
157. Rossig L, Li H, Fisslthaler B, Urbich C, Fleming I, Forstermann U, Zeiher AM, Dimmeler S: **Inhibitors of histone deacetylation downregulate the expression of endothelial nitric oxide synthase and compromise endothelial cell function in vasorelaxation and angiogenesis**. *Circ Res* 2002, **91**(9):837-844.
158. Searles CD: **Transcriptional and posttranscriptional regulation of endothelial nitric oxide synthase expression**. *Am J Physiol Cell Physiol* 2006, **291**(5):C803-816.
159. Ma X, Xia W, Zong Y, Jiang C, Shan H, Lin Y, Yin F, Wang N, Zhou L, Wen G *et al*: **Tumor necrosis factor-alpha promotes Staphylococcus aureus-induced osteomyelitis through downregulating endothelial nitric oxide synthase**. *J Microbiol Immunol Infect* 2020.
160. Arriero MM, de La Pinta JC, Escribano M, Celdran A, Munoz-Alameda L, Garcia-Canete J, Jimenez AM, Casado S, Farre J, Lopez-Farre A: **Aspirin prevents Escherichia coli lipopolysaccharide- and Staphylococcus aureus-induced downregulation of endothelial nitric oxide synthase expression in guinea pig pericardial tissue**. *Circ Res* 2002, **90**(6):719-727.
161. Alonso J, Sanchez de Miguel L, Monton M, Casado S, Lopez-Farre A: **Endothelial cytosolic proteins bind to the 3' untranslated region of endothelial nitric oxide synthase mRNA: regulation by tumor necrosis factor alpha**. *Mol Cell Biol* 1997, **17**(10):5719-5726.
162. Begent N, Born GV: **Growth rate in vivo of platelet thrombi, produced by iontophoresis of ADP, as a function of mean blood flow velocity**. *Nature* 1970, **227**(5261):926-930.
163. Ha H, Lee SJ: **Hemodynamic features and platelet aggregation in a stenosed microchannel**. *Microvasc Res* 2013, **90**:96-105.
164. Cox D, Kerrigan SW, Watson SP: **Platelets and the innate immune system: mechanisms of bacterial-induced platelet activation**. *J Thromb Haemost* 2011, **9**(6):1097-1107.
165. Fowler VG, Jr., McIntyre LM, Yeaman MR, Peterson GE, Barth Reller L, Corey GR, Wray D, Bayer AS: **In vitro resistance to thrombin-induced platelet microbicidal protein in isolates of Staphylococcus aureus from endocarditis patients correlates with an intravascular device source**. *J Infect Dis* 2000, **182**(4):1251-1254.
166. Yeaman MR: **Platelets in defense against bacterial pathogens**. *Cell Mol Life Sci* 2010, **67**(4):525-544.

167. Lerche CJ, Christophersen LJ, Goetze JP, Nielsen PR, Thomsen K, Enevold C, Hoiby N, Jensen PO, Bundgaard H, Moser C: **Adjunctive dabigatran therapy improves outcome of experimental left-sided Staphylococcus aureus endocarditis**. *PLoS One* 2019, **14**(4):e0215333.

III Index of figures

1.1 Hemodynamic flow conditions after transcatheter aortic valve implantation (TAVI) 3

1.2 Pathophysiological role of endothelial cells (ECs) in endocarditis 4

1.3 Effects of different flow patterns and associated shear stresses on endothelial cells 7

1.4 Mechanism of single cell migration 11

1.5 Analogous mechanisms of platelet adhesion and bacterial adhesion to injured endothelium 13

2.1 Experimental time-course for internalization experiments 29

2.2 Principle of cell proliferation ELISA 34

2.3 Principle of xCelligence to measure the cell index (CI) 35

2.4 Detection scheme for atomic force microscopy (AFM) 37

2.5 Assembly of the flow chamber system (provitro) 38

2.6 Ibidi perfusion set 40

3.1 Effect of an *S. aureus* infection on human coronary artery endothelial cells (HCAEC) 52

3.2 Fluorescence microscopy of human coronary artery endothelial cells (HCAEC) infected with *S. aureus* strain HG001 and endocarditis strain T-72949 53

3.3 Classification of proteins expressed in human coronary artery endothelial cells (HCAEC) after bacterial infection 55

3.4 Regulated pathways in human coronary artery endothelial cells (HCAEC) after bacterial infection 56

3.5 A selection of regulated pathways of proteins expressed in human coronary artery endothelial cells (HCAEC) after bacterial infection 57

3.6 Cytotoxicity test of peptidoglycan (PGN) 58

3.7 PGN stimulation and its effects on IL-6 59

3.8 PGN stimulation and its effects on IL-6 in a time lapse experiment 59

3.9 Effect of PGN on cell stiffness 61

3.10 Effect of PGN on cell migration 62

3.11 Effect of PGN on wound healing 63

3.12 Effect of PGN on gene expression and protein expression 65

3.13 Effect of PGN on IL6-concentration in cell supernatant 66

3.14 Fluorescence microscopy of human coronary artery endothelial cells (HCAEC) under static and flow conditions (1.5 dyn/cm^2) 67

3.15 Effect of PGN on platelets 68

3.16 Quantitative analysis of the effect of PGN on platelets 69

4.1 Hemodynamic flow conditions after TAVR correlates with the problem of platelet activation and subsequent platelet aggregation in the recirculation and stagnation areas 82

S1 Effect of PGN on cell proliferation measured with BrdU ELISA 88

S2 Effect of PGN on cell migration – time analysis 88

S3 Effect of PGN on gene expression and protein expression of further endothelial factors 89

S4 Platelet aggregation measured with aggregometer 90

S5 sPECAM-1 concentration and sP-selectin concentration in supernatants of platelet adhesion experiments 90

IV Index of tables

2.1.1 Chemicals 17

2.1.2 Antibodies 18

2.1.3 Enzymes and inhibitors 19

2.1.4 Cell lines 19

2.1.5 Media 19

2.1.6 Bacteria 19

2.1.7 Plasmid 20

2.1.8 Assays and Kits 20

2.1.9 Marker 21

2.1.10 Buffers 21

2.1.11 Consumable materials 22

2.1.12 Devices 23

2.1.13 Software 25

2.2.1 Reagent volumes for a 50 µl cDNA reaction 42

2.2.2 Cycling parameters for cDNA synthesis 42

2.2.3 Applied TaqMan® primers 44

2.2.4 Reagent volumes for a 10 µl RT-qPCR reaction 44

2.2.5 Cycling parameters for TaqMan®-RT-qPCR 45

S1 Minimum number of wells, which were detached for host cell and pathogen analysis for each time point post infection 87

S2 Overview of selected bacterial proteins with changes in protein abundance in bacteria culture of *S. aureus* strain T-72949/HG001 87

S3 Time-dependent changes in protein abundance after infection of HCAEC by *S. aureus* strain T-72949 or HG001. Ratios of normalized protein intensities were calculated between 1.5 h and 6.5 h post infection for GFPneg, GFPpos and mock cells. Proteins which were identified with more than two peptides were considered CD

V List of abbreviations

°C	degree Celsius
%	percent
~	approximately
µl	microliter
β-ME	beta-mercaptoethanol
ABC buffer	ammonium bicarbonate buffer
ACTN4	α-actinin 4
AFM	atomic force microscopy
APS	ammonium persulfate
AW	absorption wavelength
BrdU	5-bromo-2'-deoxyuridine
cDNA	complementary DNA
CI	cell index
CI	confidence interval
CO_2	carbon dioxide
CT	threshold cycle
DES	drug eluting stents
DIA	data independent acquisition
DNA	deoxyribonucleic acid
DNase	deoxyribonuclease
DTT	dithiothreithol
dyn/cm^2	dyne per square centimetre
EAP	extracellular adherence protein
EC	endothelial cell
e.g.	exempli gratia; for example

V List of abbreviations

EIF2	eukaryotic translation initiation factor 2
EIF4	eukaryotic translation initiation factor 4
ELISA	enzyme-linked immune sorbent assay
eNOS	endothelial nitric oxide synthase
EW	excitation wavelength
FAM	6-carboxyfluorescein
FACS	Fluorescence activated cell sorting
FRET	Förster resonance energy transfer
FnBPs	fibronectin binding proteins
g	gravity
GAPDH	glyceraldehyde-3-phosphate dehydrogenase
GFP	green fluorescent protein
h	hour
HBSS	Hank's Balanced Salt Solution
HCAEC	human coronary artery endothelial cell
IAA	iodoacetamide
IE	infective endocarditis
IL 6	interleukin 6
ILK	integrin-linked kinase
k	spring constant
mg	milligram
min	minute
ml	millilitre
mm	millimeter
MOI	multiplicity of infection
mRNA	messenger ribonucleic acid

V List of abbreviations

mTOR	mammalian target of rapamycin
nm	nanometer
NO	nitric oxide
NTC	no template control
OD	optical density
PBS	phosphate buffered saline
PCR	polymerase chain reaction
Pen/Strep	Penicillin/Streptomycin
PGN	peptidoglycan
p.i.	post infection
PI	propidium iodide
PKR	protein kinase R
POD	peroxidase
PPP	platelet poor plasma
PRP	platelet rich plasma
PS	phosphatidylserine
RhoGDI	Rho GDP-dissociation inhibitor
RNA	ribonucleic acid
RNase	ribonuclease
rpm	revolutions per minute
RT	reverse transcriptase
RT-DC	real-time deformability cytometry
RT-PCR	reverse transcription polymerase chain reaction
S. aureus	*Staphylococcus aureus*
SD	standard deviation

V List of abbreviations

SDS-PAGE	sodium dodecyl sulphate polyacrylamide gel electrophoresis
SEM	scanning electron microscopy
SEM	standard error of the mean
TAMRA	6-carboxytetramethylrhodamine
TAVI	transcatheter aortic valve implantation
TEMED	N,N,N',N'-tetramethylethylenediamine
TSB	tryptic soy broth
VCAM1	vascular cell adhesion molecule 1
vWF	von Willebrand Factor

VI Acknowledgements

I would like to take this opportunity to thank all of those who have supported me and who have contributed to the successful completion of this work.

My first thanks go to Prof. Dr. Stephan B. Felix from the Department of Internal Medicine B for the opportunity to write the dissertation and to Prof. Dr. Katharina Riedel from the Department of Microbial Physiology and Molecular Biology for the successful collaboration, the constant interest in the progress of my work and its review. This work was under the supervision of PD Dr. med. Raila Busch and Dr. Anne Strohbach in the Department of Cardiovascular Cell Research. At this point I would like to thank both of them for giving me the opportunity to do my doctorate and for supervising and reviewing my work.

I would like to express my sincere thanks to Dr. Kristin Surmann and all other colleagues who were involved for the constant excellent cooperation and assistance in processing and performing the internalization experiments at the Institute for Functional Genomics under the direction of Prof. Dr. Uwe Völker. I would also like to thank Dr. Michael Stiehm and his working group from the Institute for Biomedical Engineering for their great collaboration and support. Additionally, I would like to express my special thanks to the entire working group of Prof. Dr. Oliver Otto. Thanks to your willingness to help me with the AFM experiments, I was always able to look at the lengthy measurements and evaluations of the analyses with a smile on my face.

Furthermore, I would like to especially thank Alex, Ines, Caterina, Niklas, Elisa, Luca, Daniel, Lasse and all the other colleagues of the Cardiology Research Group for the interesting discussions and great working atmosphere. Thanks to you, there were many moments in which you cheered me up and distracted me from difficulties of the laboratory work. I would also like to sincerely thank Roswitha Dressler, Brita Püschel and Lucy Dietzsch for their great technical support in the daily laboratory routine and their assistance in all matters.

My special thanks go to my family, Luiz and Mila Luana and my friends who always supported and motivated me at the right times with convincing words. Without you, I would not have been able to overcome all the difficult phases and the everyday life with you has provided numerous distractions and unforgettable moments. Thank you from the bottom of my heart!